UNIVERSIDADE FEDERAL DO PARANÁ

LUIZ EDUARDO NOCHI DE CASTRO

USE OF BREWER INDUSTRY RESIDUE IN THE DEVELOPMENT OF CLEAN TECHNOLOGIES AND APPLICATION IN AN INDUSTRIAL ENVIRONMENT

PALOTINA

2021

LUIZ EDUARDO NOCHI DE CASTRO

USE OF BREWER INDUSTRY RESIDUE IN THE DEVELOPMENT OF CLEAN TECHNOLOGIES AND APPLICATION IN AN INDUSTRIAL ENVIRONMENT

Dissertação apresentada ao curso de Pós-Graduação em Biotecnologia, Setor Palotina, Universidade Federal do Paraná, como requisito parcial à obtenção do título de Mestre em Biotecnologia.

Orientador(a): Prof(a). Dr(a). Leda M. S. Colpini

PALOTINA

2021

Dados Internacionais de Catalogação na Publicação (CIP)

Castro, Luiz Eduardo Nochi de
C355 Use of brewer industry residue in the development of clean technologies and application in an industrial environment / Luiz Eduardo Nochi de Castro – Palotina, 2021.
106f.

Orientadora: Leda M. S. Colpini
Dissertação (mestrado) – Universidade Federal do Paraná, Setor Palotina, Programa de Pós-graduação em Biotecnologia.

1.Desenvolvimento sustentável. 2. Meio ambiente. 3.Bagaço de malte. 4.Gestão de resíduos. 5. Tratamento de efluentes. 6. Economia circular. I. Colpini, Leda M. S. II. Universidade Federal do Paraná. III. Título.

CDU 602

Ficha catalográfica elaborada por Liliane Cristina Soares Sousa – CRB 9/1736

MINISTÉRIO DA EDUCAÇÃO
SETOR PALOTINA
UNIVERSIDADE FEDERAL DO PARANÁ
PRÓ-REITORIA DE PESQUISA E PÓS-GRADUAÇÃO
PROGRAMA DE PÓS-GRADUAÇÃO BIOTECNOLOGIA - 40001016083P6

TERMO DE APROVAÇÃO

Os membros da Banca Examinadora designada pelo Colegiado do Programa de Pós-Graduação em BIOTECNOLOGIA da Universidade Federal do Paraná foram convocados para realizar a arguição da Dissertação de Mestrado de **LUIZ EDUARDO NOCHI DE CASTRO** intitulada: **Use of brewer industry residue in the development of clean technologies and application in an industrial environment**, sob orientação da Profa. Dra. LEDA MARIA SARAGIOTTO COLPINI, que após terem inquirido o aluno e realizada a avaliação do trabalho, são de parecer pela sua APROVAÇÃO no rito de defesa.
A outorga do título de mestre está sujeita à homologação pelo colegiado, ao atendimento de todas as indicações e correções solicitadas pela banca e ao pleno atendimento das demandas regimentais do Programa de Pós-Graduação.

PALOTINA, 19 de Março de 2021.

Assinatura Eletrônica
20/03/2021 14:47:19.0
LEDA MARIA SARAGIOTTO COLPINI
Presidente da Banca Examinadora (UNIVERSIDADE FEDERAL DO PARANÁ)

Assinatura Eletrônica
19/03/2021 23:48:06.0
LINDOMAR JOSE CALUMBY ALBUQUERQUE
Avaliador Externo (UNIVERSIDADE FEDERAL DO ABC)

Assinatura Eletrônica
22/03/2021 08:24:25.0
GIANE GONÇALVES LENZI
Avaliador Externo (UNIVERSIDADE TECNOLÓGICA FEDERAL DO PARANÁ)

A minha avó Vanda, gostaria que estivesse aqui para compartilharmos mais essa vitória, agora o que me resta são as lembranças e a saudade,

Te amo...

AGRADECIMENTOS

A minha mãe Denise, pelo amor e apoio incondicionais durante todo esse percurso. Sem você nada disso teria sido possível e não poderia ser mais grato por tê-la como mãe e amiga.

A minha orientadora de Leda, não existem palavras suficientes para expressar o tamanho carinho e apreço que tenho por você, um exemplo de profissional e docente e que me ensinou tanto sobre a vida acadêmica nesses últimos 7 anos. Eu não seria o pesquisador que sou hoje sem você, obrigado por me ensinar tudo o que sei sobre ciência. O nosso relacionamento é um dos mais especiais que qualquer aluno poderia pedir, muito obrigado por ser essa mãezona.

Ao restante da minha família, obrigado por todo apoio e amor durante mais essa etapa na minha vida, vocês são incríveis.

As meninas da Rep 48, Débora, Larissa, Laryssa, Nathália e Rosana, obrigado por cada momento compartilhado, cada memória, cada riso, dentro e fora do lab. Vocês são incríveis e eu amo muito.

A todos os meus amigos, não vou conseguir citar todos aqui, mas saibam que vocês ocupam um lugar especial no meu coração e eu não poderia ser mais grato por todos vocês.

A UFPR Campus Jandaia, por propiciar todo o apoio estrutural, técnico e pessoal para realização de todos os experimentos desse projeto, em especial aos professores Fábio, Leomara, Maycon e Padilha.

A todos os meus colegas e docentes do Programa de Biotecnologia da UFPR Setor Palotina, obrigado por cada ensinamento e momento compartilhado.

A Coordenação de Aperfeiçoamento de Pessoal de Nível Superior (Capes), o financiamento do projeto através da bolsa foi um ponto importantíssimo para a realização desse trabalho, o meu muito obrigado.

“Amar os outros é a única salvação individual que conheço:
ninguém estará perdido se der amor e às vezes receber amor em troca...”
(Clarice Lispector, A Descoberta do Mundo,1968)

RESUMO

O processo de industrialização no mundo ocorreu em várias etapas e promoveu avanços tecnológicos indispensáveis aos dias de hoje, mas junto com esse desenvolvimento desenfreado, a degradação do meio ambiente também ocorreu em uma velocidade alta, resultando em uma grande poluição do ar e da água. Foi necessário que medidas fossem tomadas para tentar conter a evolução desse processo de degradação, em grande parte devido aos resíduos gerados pelas indústrias. A gestão ambiental passou a ser foco de pesquisas científicas e o desenvolvimento de tecnologias limpas foi iniciado e tem suas aplicações nos mais diversos campos, como por exemplo na geração de energia limpa. Diante deste fato, o objetivo deste trabalho foi utilizar o bagaço de malte, para a produção de tecnologias limpas e aplicação em um ambiente industrial. Para isso, diversas técnicas foram utilizadas para determinar os parâmetros físicos, químicos, morfológicos, estruturais e superficiais desse resíduo, a fim de determinar seu uso na geração de novas tecnologias limpas e produtos de valor agregado. Foi possível aproveitar o bagaço de malte, na geração de tecnologias limpas, como a produção de vapor e energia elétrica por meio de um sistema de cogeração utilizando a biomassa sólida na combustão direta em uma caldeira, com uma economia de aproximadamente 85% no volume total de combustíveis, o que representa aproximadamente 3,8 milhões de dólares anualmente. Além disso, foi realizada a síntese do carvão ativado utilizando as cinzas residuais do processo de queima e a aplicação do material adsorvente no tratamento do efluente alimentício, azul indigotina, esse material adsorvente pode ser produzido a um valor de aproximadamente 9,35 dólares o kilograma e utilizado para tratar em torno de 5.500 L de efluente.

Palavras-chave: desenvolvimento sustentável, meio ambiente, bagaço de malte, gestão de resíduos, tratamento de efluentes, economia circular.

ABSTRACT

The process of industrialization in the world occurred in several stages and promoted technological advances indispensable for today, but together with this unrestrained development, the degradation of the environment also occurred at a high rate, resulting in great air and water pollution. It was necessary that measures were taken to try to contain the progress of this degradative process, largely due to the effluents generated by the industries. The management of these residues became the focus of scientific research and the development of clean technologies was initiated and has its applications in the most diverse fields, such as in the generation of clean energy. In view of this fact, the aim of this work was to use brewers' spent grains (BSG), for the production of clean technologies and application in an industrial environment. For this, several techniques were used to determine the physical, chemical, morphological, structural and surface parameters of this residue in order to determine its use in the generation of new clean technologies and value-added products. It was possible to reuse the BSG in the generation of clean technologies, such as the production of steam and electric energy through a cogeneration system using the solid biomass in direct combustion in a boiler, with a saving of approximately 85% in the total volume of fuels, which represents approximately 3.8 million dollars annually. In addition, the synthesis of activated carbon was performed using the residual ash from the burning process and the application of the adsorbent material in the treatment of the food effluent, Indigo Carmine, this adsorbent material can be produced at a value of approximately 9.35 dollars per kilogram and used to treat around 5,500 L of effluent.

Keywords: sustainable development, environment, brewers spent grain, waste management, effluent treatment, circular economy.

SUMÁRIO

1 STATE OF ART

In the middle of the 18th century, the world underwent one of its greatest transformations, more precisely between the years 1760 and 1850; the so-called Industrial Revolution took place, the first of the other three that would still come during the course of humanity until today. From that point in history, capitalism was consolidated as the current economic system (HOBSBAWM and WRIGLEY,1999).

The 1st industrial revolution marked the end of manufacturing and the beginning of machining, initially in the textile industries of England, but which would spread throughout Western Europe. Also during this period the first change in the energy matrix of the world occurred, the energy stopped being generated by man and started to be produced by fuels, more specifically coal, which resulted in the invention of the steam engine and the locomotive, a new mean for transportation (HOBSBAWM, 2000; STEARNS, 2013).

From the middle of the 19th century until the middle of the 20th century, the 2nd industrial revolution took the lead and the industrialization process spread to Eastern Europe and reached countries like Japan and the United States. During this stage, the energy matrix was expanded and petroleum began to be used as an energy source, which led to the development of new technology, the combustion engine. Electricity started to be widely used in industries and iron started to be replaced by steel, causing the rapid expansion of the metallurgical industry (LEVIN, 2010; STEARNS, 2013).

With the end of the Second World War, in the middle of the 20th century, the 3rd industrial revolution, also known as the Techno-scientific Revolution, began. During this period, not only did the industrial sector have a considerable advance, but there was also a boost in scientific advancement, in the development of new areas such as, biotechnology, robotics, genetics, telecommunications, electronics, transportation, among others. The transformation ceased to be simply of the means of production, but started to consider social and environmental relations (RIFKIN, 2011).

However, with all the impulse that industrial revolutions provoked for the development of the industrial sector around the world, the negative effects also began to accumulate, the first and most significant was the disposal of human labor in general, to be replaced by machines, leaving workers in precarious working conditions, which

leads to precarious living conditions, low wages and not to mention the exploitation of child labor. The polarization of capitalism pushed countries to adopt this monetary system, called Laissez-Faire Capitalism, even if they had the minimum socio-political structure, since until the 80s some countries were still colonies of European countries. This late emancipation meant that countries had little to no time to develop and were left to fend for themselves after centuries being relentlessly explored whether its population or its natural resources, as is the case of Brazil and countless other countries (HORRELL and HUMPHRIES, 1995; LEVY-LEBOYERD, 2014).

In addition to this social aspect, the industrial revolution also had a huge negative impact on the environment, with the introduction of more and more devices powered by the combustion of fossil fuels, the greater was the emission of greenhouse gases, such as CO_2 and SO_x, causing an uncontrollably increase in the pollution of air during the last centuries, leading to the development of phenomena such as the greenhouse effect, heat islands, acid rain, among others (CANDELONE et al., 1995).

Besides to air pollution, the industrialization process in general intensified the pollution of water bodies, when industries deliberately discarded their residues and effluents in rivers and lakes (BARCA, 2011). A famous case of water pollution due to industrialization is the Cuyahoga River in the state of Ohio in the United States, where in 1969 after chemical waste disposal it caught fire and the waterway became a symbol of how industrial pollution was destroying America's natural resources (BLAKEMORE, 2019).

In 2007, CNN reported that “up to 500 million tons of heavy metals, solvents and toxic sludge slip into the global water supply every year” (OLIVER, 2007). In the developing world, according to UNESCO, up to 70% of industrial waste is simply dumped untreated into rivers and lakes (WWAP, 2017).China is a great example of this, according to Greenpeace, about 70 percent of China's lakes and rivers are now polluted with industrial waste, leaving 300 million people 'forced to depend on polluted water sources' (GREEPEACE, 2014).

All these negative impacts on the environment, open a window of opportunity for science, allied to governments and civil society, to take measures to contain the progress of these pollutions, especially in the last decades. An environmental agenda has been taken into account by most of the countries through conferences and decrees

that have the intention of curbing and reducing the emission of these pollutants to nature.

As, for example, the Stockholm Conference in Sweden in 1972, where the Declaration of the United Nations Conference on the Human Environment was drafted, the first document of international law to recognize the human right to a quality environment, one that allows man to live with dignity (BRISMAN, 2011). In 1992, the Rio-92 conference created Agenda 21, a document that established the importance of each country to commit to thinking, globally and locally, on how governments, companies, non-governmental organizations and all sectors of society could cooperate in the study of solutions to socio-environmental problems (LAGO, 2007). At the end of the 1990s, during the Kyoto Convention, the Kyoto Protocol was written, an international treaty with stricter commitments to reduce the emission of gases that produce the greenhouse effect, which is the cause of current global warming (RICHARDSON, 1998).

After all these worldwide efforts to understand and take into account environmental problems and their causes, science began to play a leading role in the remediation of these degrading causes of the environment, through numerous researches in the most diverse sectors of biodiversity, energy, air pollution, water pollution, among others (O'RIORDAN, 2000). Being the focus of this work, address how industries have taken measures to contain damage to the environment and ways to remedy or reduce the generation of pollutants generated by their processes.

The manufacturing industry is the one that biggest responsible for environmental pollution. To reduce carbon emissions in the industry, green/clean manufacturing has been adopted as a way to produce low carbon emissions through the efficient use of energy and control of pollutants, which is an important solution for sustainability issues (SHI et al., 2019).

There is a necessary urge to restructure industrial systems to improve sustainability through more efficient use of resources and reducing the volume of waste generation (PROMENTILLA et al., 2018). The cleaner production concept promotes recycling, reuse and reduction at source as preventive measures to achieve sustainable development (ALMEIDA et al., 2015). These measures can be collectively classified as clean technologies (CT). The evaluation of these CT options requires the

simultaneous consideration of several and often conflicting criteria that cover the economic, environmental and social dimensions (PROMENTILLA et al.,2018).

Low carbon manufacturing most of the time requires investments in CT, the cost of investing is generally substantial and causes entrepreneurs to end up ignoring environmental issues and treat the waste management stage as a burden and an unnecessary cost, leading to the incorrect and often illegal disposal of these effluents in the environment (SHI et al., 2019).

A study conducted in Brazil shows that the absence of policies to encourage the adoption of high-cost clean technologies is the most important restrictive factor (SILVA et al., 2017). Consequently, considerable regulation, policies and tools, such as subsidies, cap-and-trade mechanisms, fines and environmental taxes, were planned to encourage or stipulate companies' investment in clean technologies (DONG al., 2014). The environmental/emission tax is one of the most effective regulations applied by some countries (DRAKE et al., 2015). Faced with the environmental tax, companies have reasons to invest in the implementation of clean technologies to control carbon emissions by credit/tax reduction. From the consumer point of view, with increased consciousness of environmental protection questions, customers are more inclined to green products and are willing to pay more for the same product (LIU et al., 2012). In the case of Brazil, industries adopt the ISO 14001 certificate as a differential in their products. This certification assures the consumer that the entire production process has undergone an extensive study of environmental monitoring and ensures that the process and the product respect the principles of environmental management (JABBOUR et al., 2014).

Within the entire industrial process and the principles of environmental management, waste control is one of the most important stages during the current manufacturing process, since with a high number of industries, a high volume of waste, whether solid or liquid, is produced (PETEK and GLAVIC, 1996). It is imperative that these effluents receive the proper treatment so that they can return to nature without causing any damage (CASTRO et al., 2019). Several techniques are used for the treatment of effluents, such as primary treatments of flocculation, coagulation, sedimentation and decantation; secondary treatments such as stabilization ponds, aerated ponds, reactors with activated sludge and other types of bioreactors; in

addition to emerging techniques, such as advanced oxidative processes, adsorption and reverse osmosis (CASTRO et al., 2020).

Among all these innumerable techniques, CT becomes an important ally in these pollutant reductions, reuse, and recycling processes. Recent studies have shown the development of CT using industrial effluents, such as Marousek and collaborators (2015) who used silage from the processing of corn, in the production of biogas through anaerobic fermentation, this biogas can be used for the production of heat and/or energy, avoiding the use of fuels based on fossil fuels. Zahan and collaborators (2018) reported the use of palm oil and its by-product in the production of biodiesel, a form of fuel that can replace petroleum-based fuel, leading to a decrease in the emissions of harmful pollutants and greenhouse gases. Zhou et al. (2017), on the other hand, shed light on the use of rare earth elements such as Ce, La, Gd, Au, and Ag in the development of clean technologies such as wind power turbines, electric vehicles, energy-efficient lighting, and catalytic converters.

The potential for exploring the use of waste for the production of clean technologies and its use in an industrial environment is high and the trend is that more and more scientists continue to research and develop knowledge that can be applied effectively in society, causing a positive impact on the environment, so that the next generations can enjoy the planet just as the past generations did, but with a better environmental and collective awareness, with a consumption directed to the minimization of residues and consequently greater preservation of the environment.

2 AIMS

2.1 RESEARCH AIM

In view of what was exposed previously, the aim of this work was to use brewers' spent grains, a brewer industry residue, for the production of clean technologies and application in an industrial environment.

2.1.1 Research Objective

- Carry out a complete characterization of the brewers' spent grains, determining its parameters: physical, chemical, thermal, morphological, structural and surface.
- Provide the characterization data for the brewers' spent grain for use as a database.
- Study the possible use of brewers' spent grains as a solid fuel for energy generation in an industrial cogeneration system.
- Perform synthesis and characterization of activated carbons obtained from residual ashes of brewers spent grains burning process.
- Investigate the use of the activated carbon in absorptive processes of food dye Indigo Carmine.
- Examine the technical-economic use of the activated carbon obtained in an industrial environmental.

REFERENCES

ALMEIDA, C. M. V. B.; AGOSTINHO, F.; GIANNETTI, B. F.; HUISINGH, D. Integrating cleaner production into sustainability strategies: an introduction to this special volume. **Journal of Cleaner Production**, v. 96, p. 1–9, 2015.

BARCA, S. Energy, property, and the industrial revolution narrative. **Ecological Economics**, v. 70, n. 7, p. 1309–1315, 2011.

BLAKEMORE, E. The Shocking River Fire That Fueled the Creation of the EPA. Available in: <https://www.history.com/news/epa-earth-day-cleveland-cuyahoga-river-fire-clean-water-act>.

BRISMAN, A. Stockholm Conference, 1972. **Encyclopedia of Global Justice**, p. 1039–1040, 2011. Available in: <https://link.springer.com/referenceworkentry/10.1007%2F978-1-4020-9160-5_655>.

CANDELONE, J.-P.; HONG, S.; PELLONE, C.; BOUTRON, C. F. Post-Industrial Revolution changes in large-scale atmospheric pollution of the northern hemisphere by heavy metals as documented in central Greenland snow and ice. **Journal of Geophysical Research**, v. 100, n. D8, p. 16605, 1995.

CASTRO, L. E. N.; MEURER, E. C.; ALVES, H. J.; et al. Photocatalytic Degradation of Textile dye Orange-122 Via Electrospray Mass Spectrometry. **Brazilian Archives of Biology and Technology**, v. 63, 2020.

CASTRO, L. E. N.; SANTOS, J. V. F.; FAGNANI, K. C.; ALVES, H. J.; COLPINI, L. M. S. Evaluation of the effect of different treatment methods on sugarcane vinasse remediation. **Journal of Environmental Science and Health, Part B**, v. 54, n. 9, p. 791–800, 2019.

DONG, C.; SHEN, B.; CHOW, P.-S.; YANG, L.; NG, C. T. Sustainability investment under cap-and-trade regulation. **Annals of Operations Research**, v. 240, n. 2, p. 509–531, 2014.

DRAKE, D. F.; KLEINDORFER, P. R.; VAN WASSENHOVE, L. N. Technology Choice and Capacity Portfolios under Emissions Regulation. **Production and Operations Management**, v. 25, n. 6, p. 1006–1025, 2015.

GARCIA-HERRERO, I.; MARGALLO, M.; ONANDÍA, R.; ALDACO, R.; IRABIEN, A. Connecting wastes to resources for clean technologies in the chlor-alkali industry: a life cycle approach. **Clean Technologies and Environmental Policy**, v. 20, n. 2, p. 229–242, 2017.

GREENPEACE INTERNATIONAL. A Monstrous Mess: toxic water pollution in China. Available in: <https://www.greenpeace.org/international/story/6846/a-monstrous-mess-toxic-water-pollution-in-china/>.

HOBSBAWM, E. J. **The age of revolution : Europe 1789-1848**. London: Phoenix, 2000.

HOBSBAWM, E. J.; WRIGLEY, C. **Industry and empire : from 1750 to the present day**. New York: New Press, 1999.

HORRELL, S.; HUMPHRIES, J. “The Exploitation of Little Children”: Child Labor and the Family Economy in the Industrial Revolution. **Explorations in Economic History**, v. 32, n. 4, p. 485–516, 1995.

JABBOUR, A. B. L. DE S.; JABBOUR, C. J. C.; LATAN, H.; TEIXEIRA, A. A.; DE OLIVEIRA, J. H. C. Quality management, environmental management maturity, green supply chain practices and green performance of Brazilian companies with ISO 14001 certification: Direct and indirect effects. **Transportation Research Part E: Logistics and Transportation Review**, v. 67, p. 39–51, 2014.

LAGO, A. A. C. **Estocolmo, Rio, Joanesburgo: o Brasil e as Três Conferências Ambientais das Nações Unidas**. Brasilia (Df): Fundação Alexandre De Gusmão, 2007.

LEVIN, M. R. **Urban modernity : cultural innovation in the Second Industrial Revolution**. Cambridge, Mass.: Mit Press, 2010.

LEVY-LEBOYERD, M. **Disparities in economic development since the industrial revolution.** Palgrave Macmillan, 2014.

LIU, Z. (LEO); ANDERSON, T. D.; CRUZ, J. M. Consumer environmental awareness and competition in two-stage supply chains. **European Journal of Operational Research**, v. 218, n. 3, p. 602–613, 2012.

MAROUŠEK, J.; HAŠKOVÁ, S.; ZEMAN, R.; VÁCHAL, J.; VANÍČKOVÁ, R. Processing of residues from biogas plants for energy purposes. **Clean Technologies and Environmental Policy**, v. 17, n. 3, p. 797–801, 2014.

O’RIORDAN, T. **Environmental science for environmental management**. London: Prentice Hall, 2000.

OLIVER, R. All About: Water and Health. Available in: <http://edition.cnn.com/2007/WORLD/asiapcf/12/17/eco.about.water/>.

PETEK, J.; GLAVIČP. An integral approach to waste minimization in process industries. **Resources, Conservation and Recycling**, v. 17, n. 3, p. 169–188, 1996.

PROMENTILLA, M. A. B.; JANAIRO, J. I. B.; YU, D. E. C.; et al. A stochastic fuzzy multi-criteria decision-making model for optimal selection of clean technologies. **Journal of Cleaner Production**, v. 183, p. 1289–1299, 2018.

RICHARDSON, B. J. Kyoto Protocol to the United Nations Framework Convention on Climate Change. **New Zealand Journal of Environmental Law**, v. 2, p. 249, 1998.

RIFKIN, J. **The third industrial revolution : how lateral power is inspiring a generation and transforming the world**. Basingstoke: Palgrave Macmillan, 2011.

SHI, X.; DONG, C.; ZHANG, C.; ZHANG, X. Who should invest in clean technologies in a supply chain with competition? **Journal of Cleaner Production**, v. 215, p. 689–700, 2019.

SILVA, A. C.; MÉXAS, M. P.; QUELHAS, O. L. G. Restrictive factors in implementation of clean technologies in red ceramic industries. **Journal of Cleaner Production**, v. 168, p. 441–451, 2017.

STEARNS, P. N. **The industrial revolution in world history**. Boulder, Colo.: Westview Press, 2013.

WORLD WATER ASSESSMENT PROGRAMME (UNITED NATIONS. **Wastewater : the untapped resource : the United Nations world water development report 2017**. Paris: United Nations Education, Scientivic And Cultural Organization, 2017.

ZHOU, B.; LI, Z.; CHEN, C. Global Potential of Rare Earth Resources and Rare Earth Demand from Clean Technologies. **Minerals**, v. 7, n. 11, p. 203, 2017.

CHAPTER I

All-around characterization of brewers' spent grain

ABSTRACT

In this work was to carry out a complete characterization of the brewers' spent grains (BSG), determining its parameters: physical, chemical, thermal, morphological, structural and surface, serving as a database for this specific material. The parameters of moisture, ash, protein, fat, reducing and non-reducing sugars, starch, crude fiber, acid and neutral detergent fiber, cellulose, lignin, hemicellulose, titratable acidity, pH, crude energy, N_2 adsorption/desorption isotherms, Fourier transform infrared spectroscopy, scanning electron microscopy, thermogravimetric analysis and differential exploratory calorimetry analysis were determined. All the results obtained are consistent with the literature for those parameters. In addition to bringing results that are not commonly found in other works, which can bring positive impact to the scientific community, when other authors can consult this study to obtain the data they need for the production of their works in the most diverse fields of science.

Keywords: malt bagasse, physical analysis, chemical analysis, thermal analysis, structural analysis, morphological analysis.

Manuscript elaborated and formatted according to the guidelines of scientific publication, submitted to the journal *Food Chemistry: X*. Available at: <http://bit.ly/foodchemistryx>

1 INTRODUCTION

Barley (*Hordeum vulgare L.*) is one of the most cultivated cereals in the world, which is a source of important nutrients for both humans and domestic animals. In the last decade, approximately 156 million tons of grain were harvested annually worldwide (Serna-Diaz et al., 2020). Around 90% of barley grains are currently used for animal feed and for the production of alcoholic beverages (Yu et al., 2018).

Historically, most of the production of barley has been used mainly for beer production, since the Second World War its production has increased annually until nowadays, where in 2018 the world production was estimated in 190 billion liters of beer (Izydorczyk and Dexter, 2016; Barth-Hass, 2019). Beer is the alcoholic beverage that is obtained from four ingredients: malt, hops, yeast and water; it is found in the most diverse types such as, ale, stout, lager and porter and it is one of the oldest and most famous beverages in the world (Ryan, 2014; Mangang et al., 2016).

Barley becomes an effective part as an ingredient in beer production during the malting process, where the malt is originated. (Capece et al., 2018; Pascari et al., 2018). During malting, the barley grain undergoes an enzymatic activation process with the intention of leaving the starch present in the grains available for the mash process, where the starch is broken down into smaller sugars (Kok et al., 2019; Ispiryan et al., 2021).

The malting process is divided into, maceration, germination and drying and after this process the malt is ready for beer production (Geißinger et al., 2019), which is divided into three major stages: mashing, boiling and fermentation (Almeida et al., 2018). After the mashing step, the wort is filtered where all the particles present are naturally sedimented, resulting from the agglutination of the husks with residues from the process, generating the brewers' spent grains (Juchen et al., 2018; Rojas-Chamorro et al., 2020).

Brewers' spent grains are the main residue generated by the brewer industry and is produced on a large scale and at a low cost (Nocente et al., 2019; Saba et al., 2019). Around 85% of all residues generated in the manufacture of beer, corresponds to BSG, which is currently destined for animal feed to local farmers (Buffington, 2014; Gupta et al., 2010). According to Ministry of Agriculture, Livestock and Supply (MAPA), in 2018 Brazil was responsible for generated around 3 million tons of BSG (Brazil, 2019).

With this high amount of by-product produced, its disposal can become problematic and often harmful to the environment, if it ends up being disposal as garbage in landfills (Buffington, 2014). In addition, BSG storage is often not viable, especially in a large industry with a very high generation flow that does not have enough physical space to store waste (Lynch et al., 2016).

Therefore, it is necessary to find possible applications for the use of BSG, whether in nutritional applications for humans and/or animals, for energy generation or as a source of extraction of macromolecules (Cordeiro et al., 2012; Nocente et al., 2019). However, regardless of which application is decided to perform with the material, it is essential that it be characterized, determining its physical, chemical and thermal composition, among others. These parameters will serve as a basis for further studies and have as much scientific relevance as the application itself.

For this reason, the objective of this work was to carry out a complete characterization of the brewers' spent grains, determining its parameters: physical, chemical, thermal, morphological, structural and surface, serving as a database for this specific material.

2 MATERIALS AND METHODS

2.1 SAMPLE PREPARATION

The samples of brewers' spent grain (approximately 30 kg), were kindly provided by a craft beer producers in the north region of the state of Paraná, Brazil and immediately stored after collection at 4 ºC until use. Prior to use, the samples of BSG were placed on the workbench and divided into quarters, two quarters were separated for use and the other two dried in a convection oven at 60 ºC for 12 h, this procedure was repeated until there was a visual reduction of 80% of the initial mass. Then, the samples were washed until the residual liquid did not show color, subsequently, stored in plastic bags, vacuum sealed, labeled and frozen until use. The raw and dry BSG are shown in Fig. 1.

FIGURE 1 - BSG SAMPLES

2.2 SAMPLE CHARACTERIZATION

2.2.1 Physical parameters

Titratable acidity was determined using titrimetric method as described by AOAC (2000). pH was measured using a digital pH meter (Lucadema, LUCA 210) calibrated with buffers at pH 4 and 7 and hygroscopicity was determined using Cai and Corke adapted method (2000), at temperatures of 10, 25 and 35 ºC in relative humidity of 11, 43, 75 and 98%, using saturated solutions of LiCl, K_2CO_3, NaCl and K_2SO_4, respectively. The energy generated from BSG were determined in according to ASTM D5865, with a bomb calorimeter (IKA C5000), previously calibrated with benzoic acid.

2.2.2 Chemical parameters

Moisture content was determined by gravimetric method using an oven at 105ºC, ash content was also determined by gravimetric method using a muffle furnace at 550 ºC, crude protein content was determined by the micro-Kjeldahl method and fat content was determined by refluxing hot extraction using ethyl ether, all methodologies was described by AOAC (2000). Reducing and non-reducing sugars were determined by the method described by Somogyi-Nelson (Nelson, 1944). Starch content was

determined using the spectrophotometric method described by Aued-Pimentel and collaborators (1990). Crude fiber was determined by Weende method (AOAC, 1996) and neutral-detergent fiber and acid-detergent fiber were determined by Van Soest method (1967 and 1990). Finally, the contents of cellulose, hemicellulose and lignin were determined by the methodology proposed by Van Soest and Wine (1968).

2.2.3 Thermal parameters

Thermogravimetric analysis was performed in a thermal analyzer (STA6000 - PerkinElmer) with 6 milligrams of BSG that were inserted in a platinum sample holder. Nitrogen was the carrier gas at a flow rate of 20 mL min^{-1} and a temperature of 50 - 900 ºC with a ratio of 10 ºC min^{-1}. The differential exploratory calorimetry analysis was performed in a calorimeter (DSC 8500 Perkin Elmer) together with ultramicrobalance (AD-6 Perkin Elmer) with a 50 µL aluminum pan at range of 20 - 150 ºC with a constant rate of 10 ºC min^{-1} and with nitrogen gas at a flow rate of 50 mL min^{-1}.

2.2.4 Morphological, structural and superficial

The morphology was observed on scanning electron microscopy (SEM) with energy dispersive spectroscopy (VEGA3 - Tescan) equipped with an energy dispersive X-ray microsound (EDS) Penta FET Precision by Oxford Instruments, using on double-sided carbon tape and metallized with a thin layer of gold (5 nm, 35 mA). The materials structures were studied by Fourier transform infrared spectroscopy (FTIR) measuring diffuse reflectance from 4,500-10,000 cm^{-1} (Bruker - Tensor 37) with a resolution of 4 cm^{-1} and accumulating 128 scans in duplicate. The material surface was studied using N_2 adsorption/desorption isotherms that were measured in a sorption analyzer (NOVA 2000e - Quantachrome Instruments). The surface area, volume and pore diameter were calculated using the Brunauer-Emmertt-Teller (BET) method and pore size distributions with the Barret-Joyner-Hallenda (BJH) method.

2.3 STATISTICAL ANALYSIS

The results were expressed as mean ± standard deviation, where all parameters were determined in triplicate.

3 RESULTS AND DISCUSSION

3.1 PHYSICAL PARAMETERS DETERMINATION

Table 1 shows the results obtained for the determination of physical parameters for the BSG sample. It was possible to observe that the pH of the BSG sample was approximately 5.5, a value that was already expected since the pH of the wort in beer production varies around 5.1 to 5.6, an optimum pH range for the hydrolytic enzymes present in the mixture can act on the break of sugars and in the production of ethanol (Bamforth and Thomas, 2009).

The titratable acidity value of the BSG was approximately 2.3 mL of NaOH g^{-1} of sample, a relatively low value that was expected due to the nature of the sample, which has a small amount of acidic species in its composition, since a large part of its compounds are extracted in the production of beer. Some compounds such as amino acids, fatty acids and phenolic acids may be responsible for this low value in the acidity of the residue, even after all the processing of the malt (Kunze et al., 2019).

The energy generation value of the dry BSG sample was approximately 4,825 kcal kg^{-1}, a value considerably high and comparable to that of other materials used for energy generation such as eucalyptus wood chips, which has a calorific value of approximately 4,552 kcal kg^{-1}, this indicates that BSG could be used for power generation through direct combustion (Castro et al., 2019).

Other works in the literature have also reported similar results for the physical characterization of BSG, Mathias et al (2015) found pH values of 5.41 and titratable acidity of 3.60% when working with BSG. As for the energy parameter, Cordeiro et al (2012) found a value of ranging from 4,701 to 5,028 kcal kg^{-1} and Liñan-Montes et al (2013) found a value approximately of 4,555 kcal kg^{-1}, both working with dry BSG.

TABLE 1 - PHYSICAL PARAMETERS OF BSG SAMPLES.

Parameters		**Values**
pH		5.49 ± 0.11
Titratable acidity (mL of NaOH g^{-1} of wet sample)		2.29 ± 0.16
Energy (kcal kg^{-1} of dry sample)		4,825.00 ± 40.00
Hygroscopicity analysis		
Room temperature (ºC)	**Relative humidity (%)**	**$\dot{H}$* (g of moisture 100 g^{-1} of dry sample)**

10	11	27.22 ± 0.11
	43	29.72 ± 0.09
	75	33.79 ± 0.33
	98	43.40 ± 0.71
25	11	26.72 ± 0.13
	43	29.12 ± 0.07
	75	33.33 ± 0.24
	98	39.84 ± 0.10
35	11	26.47 ± 0.09
	43	27.03 ± 0.32
	75	31.06 ± 0.26
	98	37.53 ± 0.01

*Ḣ indicates the hygroscopicity value obtained for the dry BSG samples.

The hygroscopicity values for the BSG sample ranged from 26.47-43.40 g of moisture g g^{-1} of sample. It was possible to notice that with the increase in the relative humidity of the environment, the greater was the hygroscopicity value, since there is a greater presence of water molecules in the air and, consequently, increasing the capacity in which the BSG samples can absorb this moisture.

It was also possible to observe that with the increase of the room temperature, there is a decrease in the hygroscopicity value of the samples, this fact may be related to the influence of the temperature in the process of mass transfer between the water molecules present in the air with the porous structure of the material, the tendency is that with a higher temperature less moisture molecules are available for the BSG sample to absorb, causing a slight decrease in the hygroscopicity value.

3.2 CHEMICAL PARAMETERS DETERMINATION

Table 2 shows the results obtained for the determination of the chemical parameters of the BSG sample.

TABLE 2 - CHEMICAL PARAMETERS OF BSG SAMPLES.

Parameters	**Values (g 100 g^{-1} of dry sample)**
Moisture	77.86 ± 0.53
Ash	2.34 ± 0.07
Protein	18.14 ± 0.25

Fat	1.61 ± 0.10
Reducing sugar	2.64 ± 0.11
Non-reducing sugar	0.46 ± 0.05
Starch	26.64 ± 1.65
Crude fiber	21.59 ± 1.60
Neutral-detergent fiber	36.78 ± 2.47
Acid-detergent fiber	12.79 ± 1.01
Cellulose	23.99 ± 1.63
Lignin	3.35 ± 0.45
Hemicellulose*	9.44 ± 0.75

*Value determined by difference.

The moisture and ash content found for the brewers' spent grain are similar with the literature data. Mathias et al (2015) found values of 82.6% and 3.8% for moisture and ash, respectively. While Mussatto et al (2006) evaluated the ash content of BSG in 2.4% and Onofre and collaborators (2018) reported values for moisture of 78.2% and ashes of 3.76%. These variations are normal since parameters such as geographic location, type of seed, soil composition, amount of rain, can influence the chemical composition of barley and consequently the BSG. In addition, it is known that the type of water used in the beer production process can influence the mineral composition of the brewers' spent grain (Clerck, 1962).

It is worth mentioning that the moisture content is directly related to the hygroscopicity measure, as the moisture content of the BSG samples was high, it is expected that the hygroscopicity would also be high, since the sample vaporization water tends to return to the dry substrate when the relative humidity of the environment is high, mainly by mass transfer mechanisms by diffusion (Incropera, 2007; Juarez-Enriquez et al., 2017).

The determination of ash content is also an important parameter to be observed, since in applications such as civil construction in the production of Portland cement or synthesis of zeolitic materials, the composition of the ash is one of the main factors to be taken into account (Bukhari et al., 2017; Zgureva et al., 2020a). In addition, in the use of BSG as a fuel for power generation, the amount of ash produced after burning can influence the dimensioning of the power generation system, in addition to the generation of high amounts of residual ash, which can present a risk to the environment, due to incorrect disposal (Baek et al., 2018; Zgureva et al., 2020b).

The protein content of this work was similar to those reported in the literature when dry BSG samples were studied. Zhang and Wang (2016) found a protein content of approximately 23%, while Kezerle et al (2018) reported a value of 21% and Mussatto et al (2006) a value for the protein content of 24%. As for the fat content, the values varied with the results found in other studies in the literature, such as the result found by Liñan-Montes et al (2013) reported a fat content of approximately 7.74% for BSG samples and Vanreppelen et al (2014) found a value of approximately 8.17%, this high fat value may be related to the presence of to higher quantity of hemicelluloses, starch, and sugars in its structure of the BSG samples.

However, for the contents of reducing and non-reducing sugars and starch, no values were found in the literature, most because of the low amount of studies that carried out an in-depth study of the carbohydrate contents of this material, probably due to the fact that these sugars in most are extracted during the mashing process, leaving very small amounts to be quantified. Even so, Mathias and collaborators (2015), through the DNS method was able to report a value of approximately 0.65% of glucose-reducing sugars.

However, for the fibrous fraction, the contents of crude fiber, acid and neutral detergent fiber of this work were similar to those in the literature; Liñan-Montes et al (2013) reported values of 23.11%, 59.73% and 25.50% for crude fiber, neutral-detergent fiber and acid-detergent fiber, respectively. This high content of lignocellulosic fibers can be of great value to the food supplements industry, with the intention of extracting dietary fibers for use in human supplementation (Lynch et al., 2016). Another application for materials with a high fiber content is the production of composites with rubber to reinforce tires (Zedler et al., 2018).

Finally, for the cellulosic fraction, the contents of cellulose and lignin were close to those found in the literature. Liñan-Montes et al (2013) reported values of 22.46% and 3.04% for cellulose and lignin, respectively, when working with dry brewers spent grains. Kezerle et al (2018) report a value for cellulose of 22% and Vanreppelen et al (2014) when working with BSG found values of 20.8% for cellulose content and 11.3% for lignin content.

However, for the contents of hemicellulose and neutral-detergent fiber, values similar to this study were not found in the literature available for BSG. This is due to the fact that the contents are related to each other, the neutral-detergent fiber is the sum of the cellulosic residues present in the sample, such as cellulose, lignin and

hemicellulose, however these values may vary depending on the parameters used during the production of the beer, as well as the way the barley grains are treated during the malting and in addition to regional characteristics of each country, such as soil and clime (Mongeau and Brassard, 1982).

3.3 THERMAL CHARACTERIZATION

Fig. 2 shows the results obtained for the thermal characterization of the BSG.

FIGURE 2 - THERMAL CHARACTERIZATION: a) TG AND b) DSC.

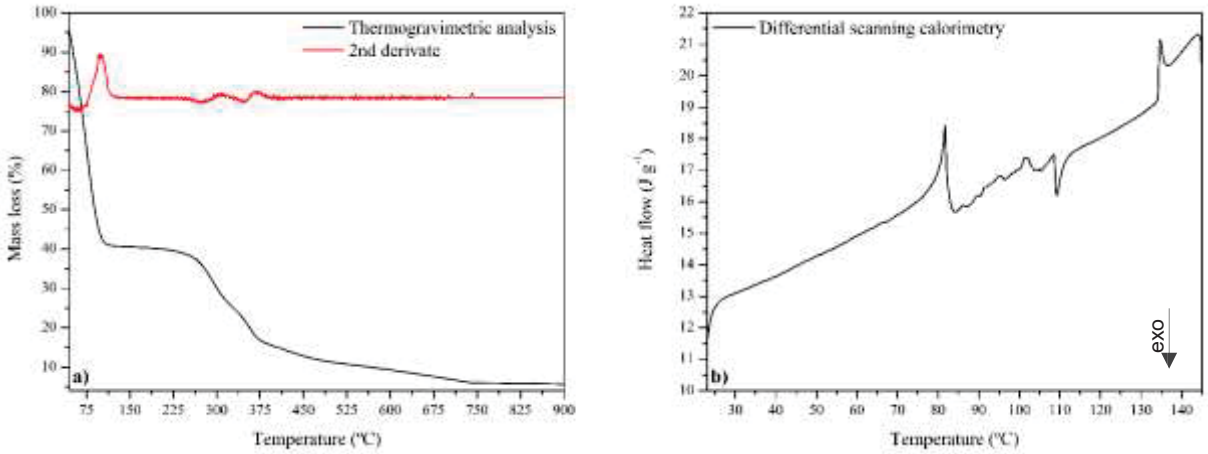

In Fig. 2 a) the TG curve of the brewers' spent grains presented two major mass loss steps. The first loss occurs from 50 to approximately 105 ºC, which is attributed to moisture elimination follow by a mass loss of approximately 60%. The second step occurs between 250 and 375 ºC and represents the release of extractive organic compounds, such as fats, waxes, alkaloids, glycosides, among others, resulting from the thermal degradation of cellulose, lignin and hemicellulose, resulting in a mass loss of approximately 80%. A lesser loss of mass occurs in the range between 450-750 ºC, and it is the residue of the total degradation process of the sample and reaches a final mass of approximately 5% of the initial mass and is composed of inorganic species in the form of oxides (Cordeiro et al., 2012).

In the DSC curve showed in Fig. 2 b) for the BSG sample is possible to observe three major peaks, the first one around 80 ºC is an exothermic peak possible related with the lignin glass-rubber transition with is similar to those reported for other lignocellulosic materials (Ibbett et al., 2011). The second peak around 110 ºC is related

to an endothermic event and is related to the dehydration process of the sample, which was also observed by the analysis of the TG curve. The third and final peak is related to an exothermic event in approximately 135 ºC, possible related to the glass-rubber transition of the hemicellulose present in the BSG sample (Olsson and Salmen, 1997).

3.4 MORPHOLOGICAL CHARACTERIZATION

Fig. 3 shows the SEM images obtained for the BSG sample.

FIGURE 3 - SEM IMAGES: a) 1,000X MAGNIFICATION AND b) 5,000X MAGNIFICATION.

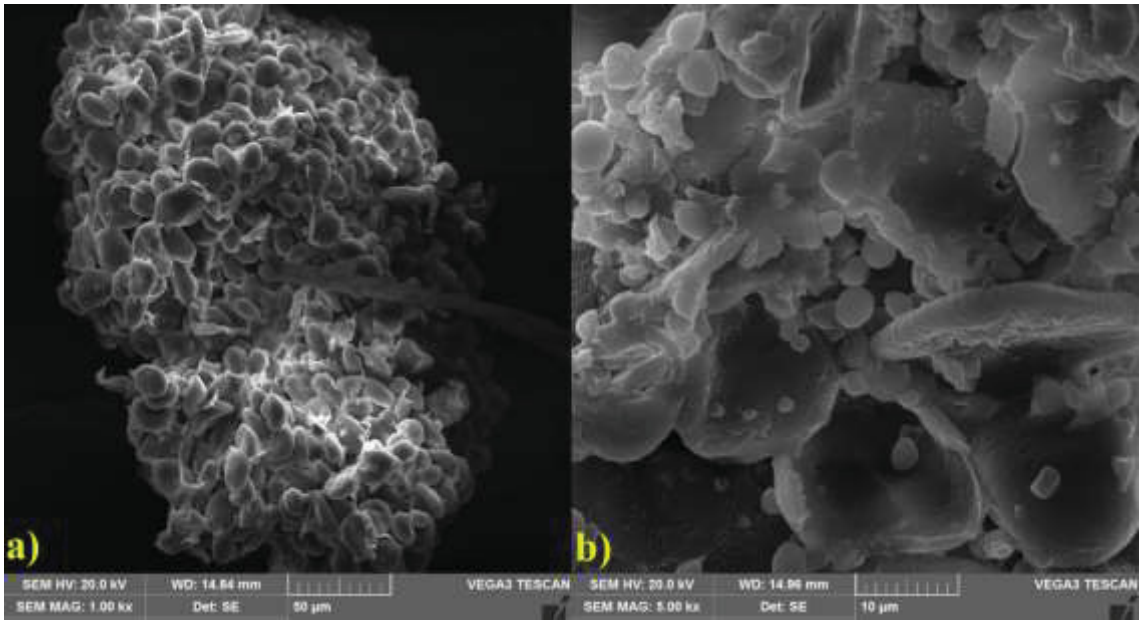

It was possible to observe that the BSG sample had a rough surface with laminar and granular particles, reasonably organized as shown in the 1,000x magnification. In addition to presenting a porous and granular surface when observed at 5,000x magnification.

This porous structure of the material, may be an indication that it can be used for the synthesis of porous materials, such as adsorbents or zeolites and consequently used in adsorption processes (Castro et al., 2019). Table 3 shows the results obtained for the analysis of EDS.

TABLE 3 - ELEMENTAL COMPOSITION OF BSG SAMPLE.

Sample	Element (%)					
	C	O	Si	Mg	K	Ca
BSG	82.65	16.02	0.12	0.29	0.06	0.86

It was possible to notice that the major element in the BSG composition was carbon with approximately 82.65%, followed by oxygen with approximately 16%. In view of the nature of the sample and the results obtained in the chemical characterization (Table 2) it was expected that carbon appear in greater quantity, since the carbohydrate content of BSG is high and the chemical structure of this macronutrients are mainly formed by bonds of C-H (Damodaran et al., 2008).

The elements in lower composition such as silicon (0.12%), magnesium (0.29%), potassium (0.06%) and calcium (0.86%) come from the nature of the barley grains used in the production of malt bagasse during the beer production process (Bamforth and Thomas, 2009; Husted et al., 2004).

3.5 STRUCTURAL CHARACTERIZATION

Fig. 4 shows the FTIR spectra for the BSG sample.

FIGURE 4 - NEAR INFRARED SPECTRUMS (NIR) OF THE BSG AND SECOND DERIVATE.

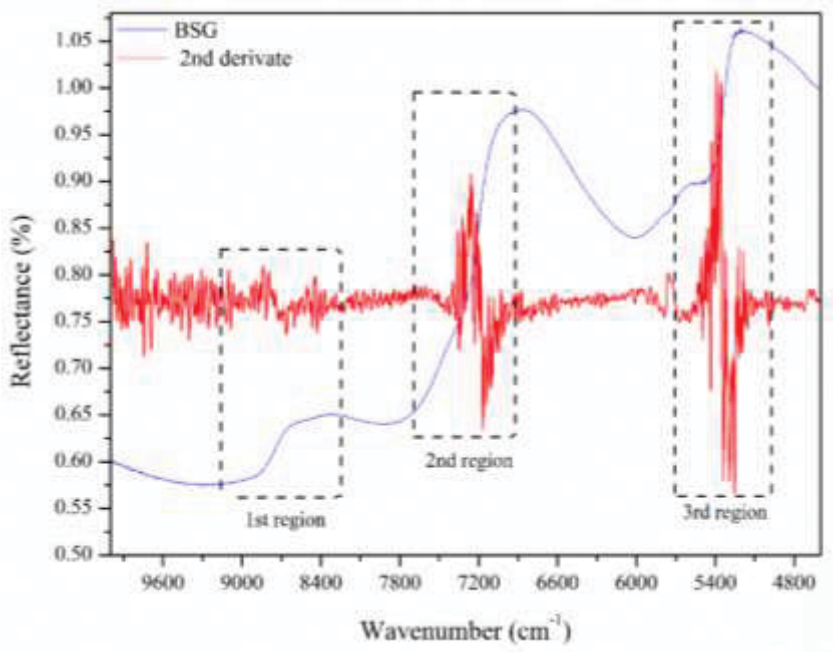

It was possible to observe through Fig 4 that the NIR spectrum was divided in three regions. In region 1, which contains the wavenumbers from 8,300 to 9,000 cm^{-1}, it was possible to identify characteristic vibration signals of the bonds -CH_3, -CH_2 and -CH in the second overtone region. In region 2, from the wavenumbers of 6,900 to 7,700 cm^{-1}, the same vibrations were observed; this can indicate the possible presence of cellulosic compounds, such as hemicellulose, lignin and cellulose (Li et al., 2015; McLellan et al., 1991). While for region 3, which ranges from 5,000 to 5,700 cm^{-1}, it was possible to identify characteristics of vibration between the –C-C and H_2O bonds in the combination region (Xiaobo et al., 2010).

3.6 SUPERFICIAL CHARACTERIZATION

The N_2 adsorption/desorption isotherms are shown in Fig. 5.

FIGURE 5 - BSG SURFACE CHARACTERIZATION: a) N_2 ISOTHERM AND b) PORE DIAMETER DISTRIBUTION.

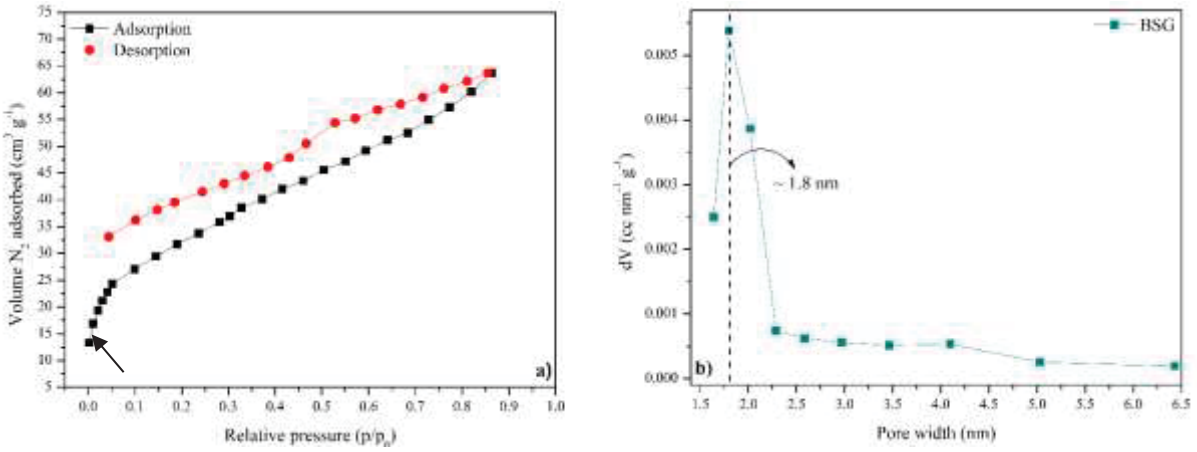

The isotherm presented in Fig. 5 a) resembled a Type IV isotherm according to IUPAC, characteristic of a microporous and mesoporous materials, the inflection point of the isotherm corresponds to the formation of the first adsorbed layer that covers the entire surface of the material (ALOthman, 2012; Sing, 1982). It was also possible to notice the presence of an H2 hysteresis gap according to IUPAC, which indicates the presence of ink-bottle-shaped type of pores (Cychosz and Thommes, 2018).

The pore distribution for the adsorbent are shown in Fig. 4 b), it was possible to observe that the pore size distribution is concentrated in the range of approximately

1.8 nm. Table 4 shows the BET surface area (S_o), mean pore diameter (d_p) and pore volumes (V_p) for the BSG sample.

TABLE 4 - SUPERFICIAL PROPERTIES OF THE BSG SAMPLE.

Adsorbent	S_o (m^2 g^{-1})	V_p (cm^3 g^{-1})	d_p (nm)
BSG	104.3	0.109	2.03

It was possible to observe that the BSG sample presented a high surface area and a mean pore diameter of 2.03 nm, which indicates that the material has a porous structure that fits in the mesoporosity range ($2 \leq d_p \leq 50$ nm), these results corroborate with those obtained in the isotherms of Fig. 5.

The data on the characterization of the brewers' spent grains surface are valuable for future studies, such as those related to the production of adsorbent materials, since the base material (BSG) naturally presents properties of a good adsorbent, such as a high surface area and the presence of a porous structure (Castro et al., 2019; Zgureva et al., 2020).

4 CONCLUSIONS

It can be concluded that the characterization of the brewers' spent grains sample were carried out efficiently, producing results consistent with the literature, for physical, chemical, thermal, morphological, structural and surface parameters. In addition to bringing results that are not commonly found in other works, which can bring positive impact to the scientific community, when other authors consult their databases to obtain these results and consequent production of their works in the most diverse fields of science.

REFERENCES

Almeida, F. S., Andrade Silva, C. A., Lima, S. M., Suarez, Y. R., & Cunha Andrade, L. H. (2018). Use of Fourier transform infrared spectroscopy to monitor sugars in the beer mashing process. *Food Chemistry*, *263*, 112–118. https://doi.org/10.1016/j.foodchem.2018.04.109

ALOthman, Z. (2012). A Review: Fundamental Aspects of Silicate Mesoporous Materials. *Materials*, *5*(12), 2874–2902. https://doi.org/10.3390/ma5122874

American Society For Testing And Materials (2019), ASTM D5865: Standard Test Method for Gross Calorific Value of Coal and Coke. West Conshohocken.

Association of Official Analytical Chemists, AOAC (1996). Fiber (crude) in animal feed and pet food: Gaithersburg, MD, USA. Methods 978.10-1979.

Association of Official Analytical Chemists, AOAC (2000). The Association of Official Analytical Chemists, Gaithersburg, MD, USA.

Aued-Pimentel, S., Alho, J., Vares, M., Maria, A., & Bacetti, L. (1990). Starch determination in sausages (hot dogs): comparison between the Fehling and Somogyi-Nelson methods and evaluation of methodology for starch extraction. *Revista Do Instituto Adolfo Lutz*, *50*, 251–256.

Baek, C., Seo, J., Choi, M., Cho, J., Ahn, J., & Cho, K. (2018). Utilization of CFBC Fly Ash as a Binder to Produce In-Furnace Desulfurization Sorbent. *Sustainability*, *10*(12), 4854. https://doi.org/10.3390/su10124854

Bamforth, C. W., & Thomas, D. (2009). *Beer: tap into the art and science of brewing*. New York, New York: Oxford University Press.

Barth-HaasGroup. (2019). The Barth Report. In (pp. 1–32). Retrieved from Joh. Barth & Sohn GmbH & Co KG website: https://www.barthhaas.com/fileadmin/user_upload/news/2019-07-23/barthreport20182019en.pdf

Buffington, J. (2014). The Economic Potential of Brewer's Spent Grain (BSG) as a Biomass Feedstock. *Advances in Chemical Engineering and Science*, *04*(03), 308–318. https://doi.org/10.4236/aces.2014.43034

Bukhari, S., & Rohani, S. (2017). Continuous Flow Synthesis of Zeolite-A from Coal Fly Ash Utilizing Microwave Irradiation with Recycled Liquid Stream. *American Journal of Environmental Sciences*, *13*(3), 233–244. https://doi.org/10.3844/ajessp.2017.233.244

Cai, Y. Z., & Corke, H. (2000). Production and Properties of Spray-dried Amaranthus Betacyanin Pigments. *Journal of Food Science*, *65*(7), 1248–1252. https://doi.org/10.1111/j.1365-2621.2000.tb10273.x

Capece, A., Romaniello, R., Siesto, G., & Romano, P. (2018). Conventional and Non-Conventional Yeasts in Beer Production. *Fermentation*, *4*(2), 38. https://doi.org/10.3390/fermentation4020038

Castro, L. E. N., Santos, J. V. F., Fagnani, K. C., Alves, H. J., & Colpini, L. M. S. (2019). Evaluation of the effect of different treatment methods on sugarcane vinasse remediation. *Journal of Environmental Science and Health, Part B*, *54*(9), 791–800. https://doi.org/10.1080/03601234.2019.1669981

Clerck, J. (1962). Cours de Brasserie. In *Google Books* (Vol. 1, pp. 478–481). Retrieved from

Cordeiro, L. G., El-Aouar, Â. A., & de Araújo, C. V. B. (2012). Energetic characterization of malt bagasse by calorimetry and thermal analysis. *Journal of Thermal Analysis and Calorimetry*, *112*(2), 713–717. https://doi.org/10.1007/s10973-012-2630-x

Cychosz, K. A., & Thommes, M. (2018). Progress in the Physisorption Characterization of Nanoporous Gas Storage Materials. *Engineering*, *4*(4), 559–566. https://doi.org/10.1016/j.eng.2018.06.001

Damodaran, S., Parkin, K. L., & Fennema, O. R. (2008). *Fennema's food chemistry* (4th ed.). Boca Raton: CRC Press.

Geißinger, C., Whitehead, I., Hofer, K., Heß, M., Habler, K., Becker, T., & Gastl, M. (2019). Influence of Fusarium avenaceum infections on barley malt: Monitoring changes in the albumin fraction of barley during the malting process. *International Journal of Food Microbiology*, *293*, 7–16. https://doi.org/10.1016/j.ijfoodmicro.2018.12.026

Gupta, M., Abu-Ghannam, N., & Gallaghar, E. (2010). Barley for Brewing: Characteristic Changes during Malting, Brewing and Applications of its By-Products. *Comprehensive Reviews in Food Science and Food Safety*, *9*(3), 318–328. https://doi.org/10.1111/j.1541-4337.2010.00112.x

Husted, S., Mikkelsen, B. F., Jensen, J., & Nielsen, N. E. (2004). Elemental fingerprint analysis of barley (Hordeum vulgare) using inductively coupled plasma mass spectrometry, isotope-ratio mass spectrometry, and multivariate statistics. *Analytical and Bioanalytical Chemistry*, *378*(1), 171–182. https://doi.org/10.1007/s00216-003-2219-0

Ibbett, R., Gaddipati, S., Davies, S., Hill, S., & Tucker, G. (2011). The mechanisms of hydrothermal deconstruction of lignocellulose: New insights from thermal–analytical and complementary studies. *Bioresource Technology*, *102*(19), 9272–9278. https://doi.org/10.1016/j.biortech.2011.06.044

Incropera, F. P. (2007). *Fundamentals of heat and mass transfer.* Hoboken, Nj: John Wiley.

Ispiryan, L., Kuktaite, R., Zannini, E., & Arendt, E. K. (2021). Fundamental study on changes in the FODMAP profile of cereals, pseudo-cereals, and pulses during the malting process. *Food Chemistry*, *343*, 128549. https://doi.org/10.1016/j.foodchem.2020.128549

Izydorczyk, M. S., & Dexter, J. E. (2016). Barley: Milling and Processing. *Reference Module in Food Science*. https://doi.org/10.1016/b978-0-08-100596-5.00154-2

Juarez-Enriquez, E., Olivas, G. I., Zamudio-Flores, P. B., Ortega-Rivas, E., Perez-Vega, S., & Sepulveda, D. R. (2017). Effect of water content on the flowability of hygroscopic powders. *Journal of Food Engineering*, *205*, 12–17. https://doi.org/10.1016/j.jfoodeng.2017.02.024

Juchen, P. T., Piffer, H. H., Veit, M. T., da Cunha Gonçalves, G., Palácio, S. M., & Zanette, J. C. (2018). Biosorption of reactive blue BF-5G dye by malt bagasse: kinetic and equilibrium studies. *Journal of Environmental Chemical Engineering*, *6*(6), 7111–7118. https://doi.org/10.1016/j.jece.2018.11.009

Kezerle, A., Velić, N., Hasenay, D., & Kovačević, D. (2018). Lignocellulosic Materials as Dye Adsorbents: Adsorption of Methylene Blue and Congo Red on Brewers' Spent Grain. *Croatica Chemica Acta*, *91*(1). https://doi.org/10.5562/cca3289

Kok, Y. J., Ye, L., Muller, J., Ow, D. S.-W., & Bi, X. (2019). Brewing with malted barley or raw barley: what makes the difference in the processes? *Applied Microbiology and Biotechnology*, *103*(3), 1059–1067. https://doi.org/10.1007/s00253-018-9537-9

Kunze, W., Hendel, O., Versuchs, U. Lehranstalt Für Brauerei Abt. Verlag. (2019). *Technology brewing and malting*. Editorial: Berlin Vlb Berlin.

Li, X., Sun, C., Zhou, B., & He, Y. (2015). Determination of Hemicellulose, Cellulose and Lignin in Moso Bamboo by Near Infrared Spectroscopy. *Scientific Reports*, *5*(1). https://doi.org/10.1038/srep17210

Liñán-Montes, A., de la Parra-Arciniega, S. M., Garza-González, M. T., García-Reyes, R. B., Soto-Regalado, E., & Cerino-Córdova, F. J. (2013). Characterization and thermal analysis of agave bagasse and malt spent grain. *Journal of Thermal Analysis and Calorimetry*, *115*(1), 751–758. https://doi.org/10.1007/s10973-013-3321-y

Lynch, K. M., Steffen, E. J., & Arendt, E. K. (2016). Brewers' spent grain: a review with an emphasis on food and health. *Journal of the Institute of Brewing*, *122*(4), 553–568. https://doi.org/10.1002/jib.363

Mangang, K. C. S., Das, A. J., & Deka, S. C. (2016). Shelf Life Improvement of Rice Beer by Incorporation of Albizia myriophylla Extracts. *Journal of Food Processing and Preservation*, *41*(4), e12990. https://doi.org/10.1111/jfpp.12990

Mathias, T. R. dos S., Alexandre, V. M. F., Cammarota, M. C., de Mello, P. P. M., & Sérvulo, E. F. C. (2015). Characterization and determination of brewer's solid wastes composition. *Journal of the Institute of Brewing*, *121*(3), 400–404. https://doi.org/10.1002/jib.229

McLellan, T. M., Aber, J. D., Martin, M. E., Melillo, J. M., & Nadelhoffer, K. J. (1991). Determination of nitrogen, lignin, and cellulose content of decomposing leaf material by near infrared reflectance spectroscopy. *Canadian Journal of Forest Research*, *21*(11), 1684–1688. https://doi.org/10.1139/x91-232

Ministério da Agricultura, Pecuária e Abastecimento. (2019). Anuário da Cerveja. In (pp. 1–16). Retrieved from MAPA website: https://www.gov.br/agricultura/pt-br/assuntos/inspecao/produtos-vegetal/publicacoes/anuario-da-cerveja-2019

Mongeau, R., & Brassard, R. (1982). Determination of Neutral Detergent Fiber in Breakfast Cereals: Pentose, Hemicellulose, Cellulose and Lignin Content. *Journal of Food Science*, *47*(2), 550–555. https://doi.org/10.1111/j.1365-2621.1982.tb10121.x

Mussatto, S. I., Dragone, G., & Roberto, I. C. (2006). Brewers' spent grain: generation, characteristics and potential applications. Journal of Cereal Science, 43(1), 1–14. https://doi.org/10.1016/j.jcs.2005.06.001

Nelson, N. (1944). A photometric adaptation of the Somogyi method for the determination of glucose. *Journal of Biological Chemistry*, *153*(2), 375–380. https://doi.org/10.1016/s0021-9258(18)71980-7

Nocente, F., Taddei, F., Galassi, E., & Gazza, L. (2019). Upcycling of brewers' spent grain by production of dry pasta with higher nutritional potential. *LWT*, *114*, 108421. https://doi.org/10.1016/j.lwt.2019.108421

Olsson, A., & Salmén, L. (1997). The effect of lignin structure on the viscoelastic properties of wood. *Nordic Pulp and Paper Research Journal*, *12*, 140–144.

Onofre, S. B., Bertoldo, I. C., Abatti, D., & Refosco, D. (2018). Physiochemical Characterization of the Brewers' Spent Grain from a Brewery Located in the Southwestern Region of Paraná - Brazil. *International Journal of Advanced Engineering Research and Science*, *5*(9), 18–21. https://doi.org/10.22161/ijaers.5.9.3

Pascari, X., Ramos, A. J., Marín, S., & Sanchís, V. (2018). Mycotoxins and beer. Impact of beer production process on mycotoxin contamination. A review. *Food Research International*, *103*, 121–129. https://doi.org/10.1016/j.foodres.2017.07.038

Rojas-Chamorro, J. A., Romero-García, J. M., Cara, C., Romero, I., & Castro, E. (2020). Improved ethanol production from the slurry of pretreated brewers' spent grain through different co-fermentation strategies. *Bioresource Technology*, *296*, 122367. https://doi.org/10.1016/j.biortech.2019.122367

Ryan, R. (2014). Safety of Food and Beverages: Alcoholic Beverages. *Encyclopedia of Food Safety*, 364–370. https://doi.org/10.1016/b978-0-12-378612-8.00432-7

Saba, S., Zara, G., Bianco, A., Garau, M., Bononi, M., Deroma, M., Budroni, M. (2019). Comparative analysis of vermicompost quality produced from brewers' spent grain and cow manure by the red earthworm Eisenia fetida. *Bioresource Technology*, *293*, 122019. https://doi.org/10.1016/j.biortech.2019.122019

Serna-Díaz, M. G., Mercado-Flores, Y., Jiménez-González, A., Anducho-Reyes, M. A., Medina-Marín, J., Seck Tuoh-Mora, J. C., & Téllez-Jurado, A. (2020). Use of barley straw as a support for the production of conidiospores of Trichoderma harzianum. *Biotechnology Reports*, *26*, e00445. https://doi.org/10.1016/j.btre.2020.e00445

Sing, K. S. W. (1982). Reporting physisorption data for gas/solid systems with special reference to the determination of surface area and porosity (Provisional). *Pure and Applied Chemistry*, *54*(11), 2201–2218. https://doi.org/10.1351/pac198254112201

Van Soest, P. J. (1967). Development of a Comprehensive System of Feed Analyses and its Application to Forages. *Journal of Animal Science*, *26*(1), 119–128. https://doi.org/10.2527/jas1967.261119x

Van Soest, P. J. (1990). Use of Detergents in the Analysis of Fibrous Feeds. II. A Rapid Method for the Determination of Fiber and Lignin. *Journal of AOAC INTERNATIONAL*, *73*(4), 491–497. https://doi.org/10.1093/jaoac/73.4.491

Van Soest, P. J., & Wine, R. H. (1968). Determination of Lignin and Cellulose in Acid-Detergent Fiber with Permanganate. *Journal of AOAC INTERNATIONAL*, *51*(4), 780–785. https://doi.org/10.1093/jaoac/51.4.780

Vanreppelen, K., Vanderheyden, S., Kuppens, T., Schreurs, S., Yperman, J., & Carleer, R. (2014). Activated carbon from pyrolysis of brewer's spent grain: Production and adsorption properties. *Waste Management & Research*, *32*(7), 634–645. https://doi.org/10.1177/0734242x14538306

Xiaobo, Z., Jiewen, Z., Povey, M. J. W., Holmes, M., & Hanpin, M. (2010). Variables selection methods in near-infrared spectroscopy. *Analytica Chimica Acta*, *667*(1-2), 14–32. https://doi.org/10.1016/j.aca.2010.03.048

Yu, W., Zou, W., Dhital, S., Wu, P., Gidley, M. J., Fox, G. P., & Gilbert, R. G. (2018). The adsorption of α-amylase on barley proteins affects the in vitro digestion of starch in barley flour. *Food Chemistry*, *241*, 493–501. https://doi.org/10.1016/j.foodchem.2017.09.021

Zedler, Ł., Colom, X., Saeb, M. R., & Formela, K. (2018). Preparation and characterization of natural rubber composites highly filled with brewers' spent grain/ground tire rubber hybrid reinforcement. *Composites Part B: Engineering*, *145*, 182–188. https://doi.org/10.1016/j.compositesb.2018.03.024

Zgureva, D., Stoyanova, V., Shoumkova, A., Boycheva, S., & Avdeev, G. (2020a). Quasi Natural Approach for Crystallization of Zeolites from Different Fly Ashes and Their Application as Adsorbent Media for Malachite Green Removal from Polluted Waters. *Crystals*, *10*(11), 1064. https://doi.org/10.3390/cryst10111064

Zgureva, D., Boycheva, S., Behunová, D., & Václavíková, M. (2020b). Smart- and Zero-Energy Utilization of Coal Ash from Thermal Power Plants in the Context of Circular Economy and Related to Soil Recovery. *Journal of Environmental Engineering*, *146*(8), 04020081. https://doi.org/10.1061/(asce)ee.1943-7870.0001752

Zhang, J., & Wang, Q. (2016). Sustainable mechanisms of biochar derived from brewers' spent grain and sewage sludge for ammonia–nitrogen capture. *Journal of Cleaner Production*, *112*, 3927–3934. https://doi.org/10.1016/j.jclepro.2015.07.096

CHAPTER II

Study of the use of waste from brewing industry as biomass and its application as a fuel for steam production in a cogeneration system

ABSTRACT

The present work aimed to study the use of brewers' spent grains (BSG) as a fuel for energy generation in an industrial cogeneration system, using wood chips as a control sample. The BSG were undergone analysis to determine the density, particle size, ultimate and immediate analysis, elemental ash composition and calorific power analysis. The results indicated that BSG has a moisture content of 77.68%, ash 0.52%, volatile material 95.94%, fixed carbon 3.57%, mean particle size of 0.28 mm, density of 113 kg m^3 and lower calorific value of 17.84 MJ kg^{-1}. Tests were carried out with different mixing ratios between the BSG and wood chip to evaluate its effects on the energy efficiency in the system. The 1:5 ratio of wood chips to BSG obtained the best characteristics to be used as fuel in a cogeneration system, with an ash content of 0.39%, volatile material 97.3% and lower calorific value of 17.71 MJ kg^{-1}. In addition, the ash generated in the burning does not contribute to degradation processes inside the boiler. The substitution of wood by BSG promoted an 82% reduction in the use of wood chips and generated savings of approximately 3.8 million US dollars annually.

Keywords: brewers spent grains, malt bagasse, food waste, circular economy, heat generation, bioenergy.

Manuscript elaborated and formatted according to the guidelines of scientific publication, submitted to the journal *Renewable Energy*. Available at: <http://bit.ly/RenewableEnergyy>

1 INTRODUCTION

Brewers' spent grains (BSG) are the main by-product generated during the industrialization of malted barley for beer production [1-2]. They represent approximately 85% of all residues generated during processing, it is estimated that for every 100 L of beer, approximately 20 kg of BSG is generated [3-4]. According to the Ministry of Agriculture, Livestock and Supply (MAPA), in 2018, Brazil was responsible for producing 14 billion liters of beer, which generated around 3 million tons of BSG [5]. While in the world, beer production was around 190 billion liters, with a generation of waste of around 40 million tons [6].

Currently a large part of this waste is destined for animal feed, which generates a low profit for the industry, around 40 USD per ton and the rest of the waste ends up being disposed of like garbage in landfills [7-8]. One of the difficulties in processing this residue is the moisture content (~ 80%) and rich polysaccharide and protein content, which makes this biomass susceptible to the growth of microorganisms and consequent deterioration [1,9]. In addition, transporting wet BSG is often costly, since the material has a higher density and occupies a larger space, which means that industries end up disposing of this waste to local farmers, however production ends up exceeding demand most of the time [4,8].

Recent work in the literature has pointed out alternative uses on a small scale for BSG, such as a source of sugars, protein and antioxidant, as a culture medium for microorganism cultivation, use as a nutritional source for human consumption in the formulation of foods such as cookies, bread and cakes [1, 4, 10-12]. Plus, the use of BSG as biomass for energy production through cogeneration technologies can be an attractive destination for the brewers themselves [13].

The development of technologies for the production of new renewable energy sources has become a relevant issue in recent years, considering that an energy matrix dependent on fossil fuels tends to collapse over time, since these fuels are not renewable, in addition to increasing impacts on the environment and the emission of greenhouse gases [14-16]. Thus, the use of biomass from lignocellulosic materials for energy generation is a technology that has been explored in recent years as an alternative to the use of fossil fuels [14, 17-18].

Brazil currently produces around 300 million tons of lignocellulosic waste annually, such as rice, coffee and soy husks, waste from forest harvests, among others

[19]. This high production impelled the industries to use their own residues for energy generation and in the development of technologies, an example is the sugar-alcohol mills, which uses sugarcane bagasse and straw as fuel for the boiler [20-21].

Usually, the use of biomass for energy production is the most widely used method in the world, being responsible for approximately 97% of all bioenergy generated [22-23]. In an industrial environment, solid biomass of different sizes can be burned in furnaces or boilers and the scale of the installations can vary between small to large scale with the power of generation varying between 500 and 3000 MW [24].

Two types of boilers are the most common, grate heating systems and fluidized bed combustion chambers, these systems offer great flexibility regarding the use of fuels and can be fed completely with solid biomass or by joint use with coal [25]. The direct combustion of biomass produces heat to meet the needs of the industry, or to produce high-pressure steam that is directed to turbines and consequently to electrical energy generation [22]. Biomass combustion plants that produce energy through steam turbo-generators have a conversion efficiency between 17 and 25%; however, the use of cogeneration systems can increase this efficiency up to 85% [26-27].

Cogeneration is the concurrent production of electricity and heat, through a system that uses biomass as fuel [22, 28]. By producing the two products in a combined manner, these systems present themselves as a solution for saving energy, through increasing energy efficiency and as a method of environmental preservation [29]. Biomass cogeneration is considered an effective method for reducing greenhouse gas emissions, due to low carbon dioxide emissions and in addition to using solid waste from industrial processes that would be disposed of in landfills, contaminating the environment and underground water bodies [29-31].

In view of this fact, BSG presents itself as a candidate to be used as solid biomass in the production of energy by direct combustion in cogeneration systems, once it has the favorable characteristics, such as high content of volatile material (~ 90%) and oxygen (~ 40%) and low content of fixed carbon (~ 3%), these parameters contribute to a better boiler combustion process [32-34]. Allied to this, studies in the literature indicate a high value of gross calorific value, around 20 MJ kg^{-1}, while other fuels such as wood chips and coal have approximately 15 and 23 MJ kg^{-1} respectively [35-37]. This makes BSG a plausible candidate for being a high efficiency fuel.

Thus, the objective of this work was to carry out a study as to the possible use of brewers' spent grains as a solid fuel for energy generation through the production of steam and application in an industrial cogeneration system.

2 MATERIALS AND METHODS

2.1 BIOMASS PREPARATION

BSG samples were gently provided by craft beer producers in the north region of the state of Paraná, Brazil, prior to use the BSG were quartered, opposite quarters were used for the analysis and the other separated. Then, the samples were washed until the residual liquid had light brown color to no color, stored in plastic bags, vacuum-sealed, and frozen until use and part of the BSG was dried in oven at 60 ºC for 12 h, to remove all moisture from the samples that would be used in the tests.

The wood chips used in the study were kindly donated by a dairy in the north region of the state of Paraná, Brazil, the wood comes from the processing of eucalyptus (*Eucalyptus grandis*), and the chips were cut until they had a uniform size of approximately 5 mm.

2.1.1 Preliminary evaluations

In order to evaluate the BSG capacity as a possible fuel for the direct combustion system, its gross and lower calorific value was determined, for both raw and dry sample as a mean to evaluate the effect of the presence of water on the heat generation. As a means of comparison, wood chips were used as a control sample throughout the study.

2.2 FUELS CHARACTERIZATION

2.2.1 Ultimate analysis

The ultimate analysis was performed in the dry BSG samples to determine the amount of carbon, hydrogen, nitrogen and sulfur, using an elemental analyzer PERKIN-ELMER CHNS 2400. The oxygen content was determined by the difference between the contents of the other elements.

2.2.2 Calorific value analysis

The gross calorific value for both BSG and wood chips were determined in triplicate according to ASTM D5865 [38] in a bomb calorimeter (IKA C5000), previously calibrated with benzoic acid and the lower calorific value was determinate by Equation 1 [39].

$$LCV = GCV - 2{,}260\ (0.09\ H + 0.01\ M) \quad (1)$$

where: LCV (kJ kg^{-1}) is the lower calorific value GCV (kJ kg^{-1}) gross calorific value, H (%) hydrogen content of the sample, M (%) moisture content of the sample.

2.2.3 Particle size analysis

The particle size analysis of the dry BSG sample was performed according to ASTM D4749-87 in triplicate [40]. The sieves were used with opening of mesh 1.40; 0.85; 0.5; 0.35; 0.25; 0.18; 0.15; 0.09; 0.075 mm. From this, it was estimated the mean diameter of each sieve (d_p), according to the equation defined by Foust et al. (Equation 2) [41] and, consecutively, it was estimated the mean particle size of the sample ($\overline{d_s}$), according to the Sauter diameter equation (Equation 3) [42].

$$\ln d_p = \frac{\ln e_s + \ln e_i}{2} \quad (2) \qquad \overline{d_s} = \frac{1}{\sum_{i=1}^{n}\left(\frac{\Delta x_i}{d_p}\right)} \quad (3)$$

where: d_p (mm) is the mean diameter of each sieve, e_s (mm) opening of the superior sieve, ei (mm) opening of the inferior sieve, $\overline{d_s}$ (mm) mean particle size of the sample, Δx_i retained mass fraction between sieves.

In addition to the mean particle size obtained by Equation 3, the granulometric data was subjected to two graphical methods for estimating the particle diameter, (a) mass distribution density (MDD) and (b) cumulative/augmentative distribution (CAD) [43-44].

2.2.4 Bulk and relative densities and porosity

The bulk and relative density and porosity of dry BSG were determined in triplicate according to ASTM E873-82, D792 and C1039, respectively [45-47]. To determine the mass of the samples, an ACZET-CY224C analytical balance (± 0.2 mg) was used.

2.2.5 Immediate analysis

The immediate analysis includes the determination of moisture, ash, volatile matter and fixed carbon content of the dry samples, were determined according to the standard ASTM E870 in triplicate [48].

2.2.6 Ash composition analysis

The properties and quantity of the biomass ash can cause operational problems in the boiler, such as fouling, corrosion and slagging. Thus, to determine the elemental composition of the ashes, the fuel was calcined in a muffle furnace at 600 ºC ± 25 ºC in triplicate until constant weight.

The elementary analysis of the ashes was performed using the energy dispersive X-ray spectroscopy (EDS) technique and was done in a Scanning Electron Microscope TESCAN VEGA3, where the samples were fixed to the surface of a double-face adhesive tape and coated with a gold layer (5 nm, 35 mA).

2.3 ECONOMICAL EVALUATION

An economic analysis of the use of BSG as a fuel in a cogeneration system was performed, based on the methodology of the Association for the Advancement of Cost Engineering [49]. The assumptions for scale-up production costs comparisons were made from the information presented in this study and considering only the use of BSG for steam generation.

2.4 STATISTICAL ANALYSIS

The results were expressed as mean ± standard deviation. The variables were tested statically by ANOVA at a significance level of 0.05 and for the mean comparison was performed the Tukey test.

3 RESULTS AND DISCUSSION

3.1 ULTIMATE ANALYSIS

The results for the elemental analysis of BSG sample are shown in Table 1.

TABLE 1 - ELEMENTAL ANALYSIS OF THE BSG SAMPLE.

Elemental analysis (%)	
C	45.16
O	44.14
N	7.12
H	3.58
S	-

The values for nitrogen, carbon and hydrogen content in the BSG sample are similar to the results found in the literature [50-52]. Additionally, the values for sulfur and oxygen are similar to those found in the literature [35, 52]. In addition, the high carbon content makes BSG a good fuel for use in direct combustion in the boiler [21]. Also, the high oxygen content in combination with the hydrogen content, favors the oxidation process in the exothermic reaction during the combustion of the fuel [53].

3.2 PRELIMINARY CALORIFIC POWER ASSESSMENT

Fig. 1 shows the results obtained for the BSG and wood chips calorific analysis.

FIGURE 1 - CALORIFIC VALUE OF BIOMASS.

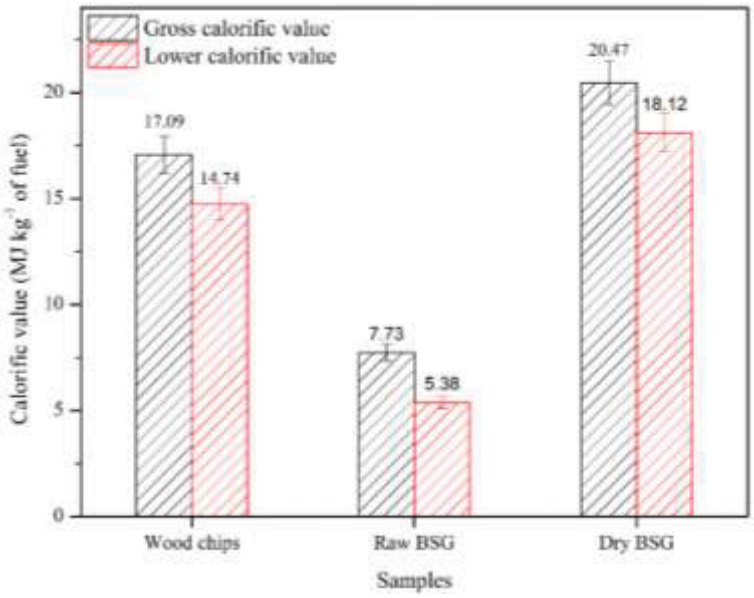

It was possible to observe that the presence of water in the BSG sample had a negative effect on the calorific value of the sample, decreasing its energy efficiency. For the dry sample, the GCV was approximately 20.47 MJ kg^{-1}, while for the raw sample this value was approximately 7.73 MJ kg^{-1}, a decrease of almost 62%. This decrease in the calorific value occurs, because during the burning of the fuel part of the generated energy is used in the vaporization of the water relative to the moisture content present in the sample [54-55]. Therefore, the higher the moisture content of the fuel, the lower its heating power and consequently its energy efficiency.

In the case of BSG, whose humidity is around 80%, the material must be dried before being used as biomass for direct combustion, since its calorific value is very high, surpassing even that of the wood chip used in this study, which has a value of approximately 17 MJ kg^{-1}, almost 20% less than that of dry BSG, which proves that this biomass studied can be used for energy generation through direct combustion in a boiler [32, 56].

Other authors reported values of calorific value similar to those found in this study, Sperandio et al. [50] when working with BSG, found values for the GCV of approximately 17 MJ kg^{-1} and for the LCV of approximately 14 MJ kg^{-1}. Whereas, Lorente et al. [57], found a value for GCV of approximately 20.95 MJ kg^{-1} and Dudek et al. [58] a value for LCV of approximately 17.74 MJ kg^{-1}.

Aware that the moisture of the fuel negatively affects the overall energy efficiency of the system, it is necessary to dry the material as illustrated above.

However, industrial drying processes are most often costly, as they require a high amount of energy, whether electric or in the form of steam, which means that biomass is often not dried and used the way it came, which leads to energy losses and consequently money. Thus, a drying kinetic study was carried out with BSG, the data was tested using the Page model and the results are shown in Fig. 2.

FIGURE 2 - DRYING KINETICS AND FITTING DATA USING PAGE MODEL: a) OVEN AT 60 ºC AND b) EXTERNAL ENVIRONMENT AT AN AVERAGE TEMPERATURE OF 27 ºC, AVERAGE WIND SPEED OF 8 km h^{-1}, AND AVERAGE HUMIDITY OF 73%.

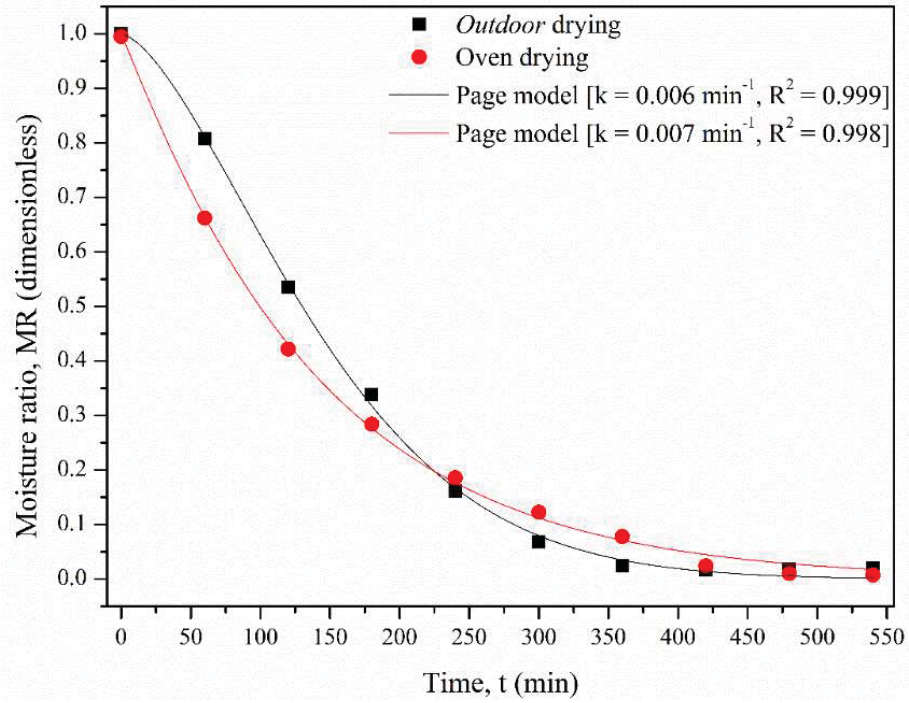

Observing the drying kinetics curves, it was possible to observe that for both situations the Page model adjusted to the data with a correlation coefficient $R^2 > 0.99$. In addition, the drying curve of the sample in the oven presented a drying coefficient (k) greater than the sample dried externally. This can be explained by observing the initial slope of both curves, for the oven curve in the initial minutes the kinetics is faster and remains constant throughout the entire period.

While for the external drying curve after time t = 240 min, the kinetic becomes faster until reaching equilibrium in 360 min, whereas for the oven dried sample, the equilibrium is only reached after 420 min, this difference in the equilibrium time can be explained by the presence of wind in the external environment, even with a temperature much lower than that of the oven. The presence of ventilation in the

external environment makes the heat exchange occur more efficiently, since in the oven the heat exchange is through conduction mechanisms, while for external drying we have the conduction and convection mechanisms [59].

In short, drying the BSG under the sun in an external environment proved to be as efficient as drying in an oven, but with the advantage of not needing electricity for the drying process or special equipment, being necessary to pay attention to the presence of foreign objects or pests during exposure to the external environment. This type of drying is already used in sugar and alcohol plants for the drying of sugarcane bagasse, which will later be used in cogeneration systems for the production of steam and electricity [20-21].

3.3 PARTICLE SIZE EVALUATION

As previously mentioned, the particle size tests were intended to determine the particle size distribution as well as to determine the mean particle size of the BSG samples. These characteristics are extremely important, as they give us information about the behavior of the fuel when it is burned, since the contact area is one of the variables that can accelerate the combustion reaction. In addition, the particle size must be taken into account when dimensioning a boiler, since it can become a limiting factor in the design, causing the particulate size to end up causing operational problems. Fig. 3 shows the graphical models obtained for the mass distribution of the BSG sample.

FIGURE 3 - GRAPHICAL DISTRIBUTION OF MASS FRACTIONS IN EACH SIEVE BY THE METHODS: A) MDD AND B) CAD.

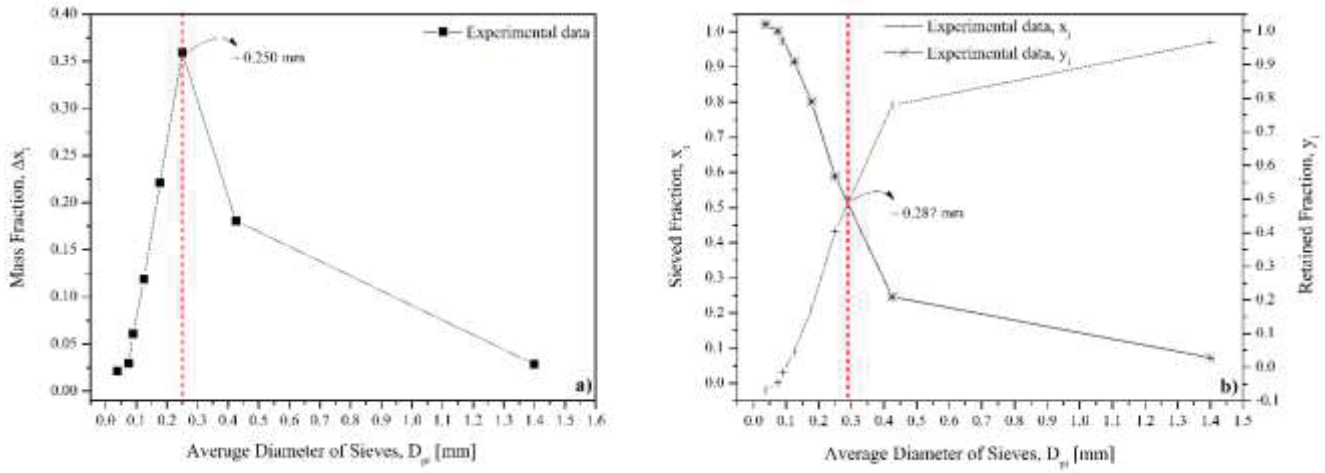

It was possible to observe from Fig. 3 a) that the range between 0.15 and 0.5 mm was the one that concentrated most of the sample's mass, approximately 70% of the total mass, with the peak of the greatest mass fraction being on 0.25 mm; graphically this indicates that the mean particle size has this diameter.

On the other hand, when looking at Fig. 3 b), by the intersection of the curves of retained mass fraction and sieved mass fraction, it was possible to observe that the mean particle size of the BSG was 0.287 mm, a value of approximately 13% higher than that obtained by the MDD model.

This difference in the mean particle size values through graphic techniques has been reported by other works in the literature, such as Jordan et al. [60], when evaluating the mean particle size of sugarcane bagasse, reached a variation of up to 10%.

However, the analytical method of determining the mean particle diameter using Equation 3 is a well-established and widely used method for determining the mean particle size and the result for the BSG sample is shown in Table 2.

TABLE 2 - MEAN PARTICLE SIZE VALUE OF BSG FOR DIFFERENT DETERMINATION METHODS.

Sample	**Methods***				
	Analytical (Sauter)	**MDD**	**Error (%)**	**CAD**	**Error (%)**
Particle size (mm)	0.281 ± 0.005^{a}	0.250 ± 0.012^{b}	12.40	0.287 ± 0.014^{a}	2.09

*Results are averages of three repetitions with deviation standard estimates. Same lower case letters do not differ between tests ($p \leq 0.05$) [ANOVA and Tukey test].

Observing Table 2, the mean particle size value determined by the analytical method was 0.281 mm, a value close to that obtained by the CAD graphic method of 0.287 mm. At a level of 5%, the value of the particle size between the analytical method and the CAD method did not show a significant statistically difference, with a standard error of approximately 2%, this indicates that the CAD graphic method was the one that best converged the result and adjusted the particle size distribution data in the best way.

Other works in the literature reported similar values of mean particle size of BSG, Ozturk et al. [12], found values between 0.212 and 0.425 mm, whereas Hejna et al. [61] reported values of approximately 0.275 mm. Variations between values are expected since the barley used for BSG production can vary from country to country, in addition to the time when planting is carried out, among other reasons.

3.4 DENSITY AND POROSITY DETERMINATION

Table 3 presents the values of bulk density, relative density and porosity obtained for a dry BSG sample.

TABLE 3 - DENSITIES AND POROSITY OBTAINED FOR THE DRY BSG SAMPLES.

Parameters	BSG
Bulk density (kg m^{-3})	113.00 ± 4.00
Relative density (kg m^{-3})	133.00 ± 3.00
Porosity	0.15 ± 0.01

It was possible to observe, that the BSG had a low bulk density, approximately 113 kg m^{-3}, a value close to that found in the literature, as by Cordeiro et al [33], who reported density values that varied from 117 to 121 kg m^{-3}. This low density value is an important variable to be taken into account when dimensioning the cogeneration system, since fuels with low density tend to fly into the boiler when air is injected into the system to feed the flame, causing operational problems such as incomplete fuel burning, plugging of valves and filters, among others.

Therefore, it is necessary to make some adaptations for the use of BSG as a fuel in the direct combustion process, such as the production of pellets or billets. In both processes, the density of the material is increased and high contact area is maintained, which facilitates the burning of biomass. In addition, the low porosity of the BSG (0.15, Table 3) makes the fuel compaction more efficient, due to the low amount of empty spaces in the material.

For a cogeneration system in operation, some adaptations can be made to use BSG as solid biomass, such as the use of a conveyor screw to feed the fuel from a high point in the boiler, this means that from the moment the BSG starts entering the system until it reaches the bottom of the boiler, the material will be burned in this path.

Another adaptation is the concomitant use of BSG biomass with other fuels, such as wood chips, the mixture of fuels increases the general density of the fuel and the burning can be carried out without many adaptations to the system, in addition to reducing the use of wood as a fuel, causing a positive impact on the environment.

Fagnani et al. [39], reported the concomitant use of flocculated sludge with wood chips to generate energy in a poultry slaughterhouse, through direct combustion

in a boiler. The mixture between the two fuels allowed both the saving of wood and a use for the sludge that until so it needed a separate treatment for disposal.

Therefore, a study was carried out using different mixtures between BSG and wood chips (Table 4) to evaluate the effect of the combination in main variables of this study and the possible use of the mixture in a cogeneration system.

TABLE 4 - MASS COMPOSITION OF THE BSG AND WOOD CHIPS SAMPLES USED IN THE TESTS.

Assays	**Mass proportions (%)**	
	BSG	**Wood chips**
1	80	20
2	60	40
3	40	60
4	20	80

3.5 IMMEDIATE ANALYSIS

Fig. 4 shows the results obtained for the immediate analysis of the BSG, wood chips and mixtures.

FIGURE 4 - IMMEDIATE ANALYSIS FOR THE SAMPLES.

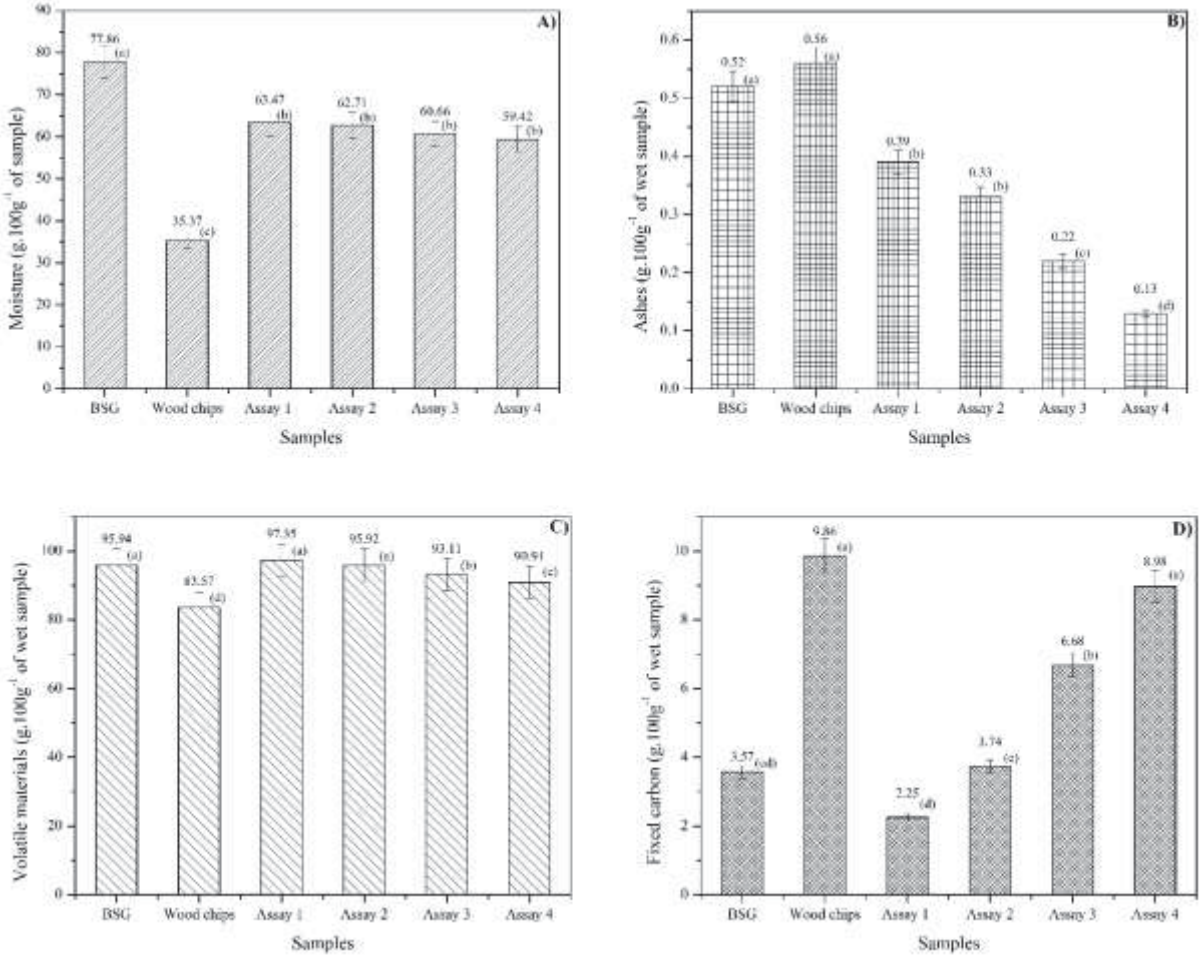

Results are averages of three repetitions with deviation standard estimates. Same lower case letters do not differ between tests ($p \leq 0.05$) [ANOVA and Tukey test].

Looking at Fig. 4 A), the moisture content of mixtures is lower than that BSG itself, this occurs since the wood chip has moisture almost three times lower than BSG causing the moisture in the mixtures to turn to be less, this reduction positively affects the efficiency of the boiler. It was also possible to observe that for the mixtures there was no statistically significant difference between the assays at a level of significance of 5%.

This reduction in the value of the parameter when compared to the BSG was repeated with the ash content, as shown in Figure 4 B). The value of ash content of the mixtures was also lower than that of wood chips, between Assay 1 and Assay 2, there was no significant statistical difference at a level of 5%. This reduction in ash content is an extremely important parameter since the ash directly affects the useful life of a cogeneration system, the accumulation of ash in the system can cause fouling and other problems inside the boiler, so fuels that generate a small amount of ash must

be chosen [21, 62]. In addition, the ash generated during burning is a waste that often does not have correct disposal and can become a problem for the environment [63-64].

In Fig. 4 C), the values for the volatile content did not show as much difference between the mixtures and the BSG, with only a significant increase in the volatile content concerning the wood chips. The volatile materials content of BSG and Assays 1 and 2 showed no significant statistical difference at a level of 5%. It is worth mentioning that the increase in the volatile material content of wood chips when mixed with BSG is an extremely important point, since the substitution of wood by biomass, in addition to saving the use of a substrate that is removed from nature, promotes better stability for the boiler.

Fig. 4 D) shows the data obtained for the fixed carbon content of the samples, there was a noticeable reduction in the value between the wood chip and Assay 1, this indicates the clear influence of the BSG in the mixture, promoting a reduction of approximately 77%. This decrease is important, since fuels with a high fixed carbon content tend to have their energy efficiency reduced [21].

In general, the mixture between BSG and wood chips had a positive influence on the variables studied in the immediate analysis, and it is worth highlighting Assay 1, where the mass ratio was 80% BSG to 20% wood chips, that had all the best results among the assays.

3.6 CALORIFIC VALUE EVALUATION TESTS

Fig. 5 shows the results obtained for the calorific value tests of the BSG, wood chips and mixtures.

FIGURE 5 - CALORIFIC VALUE ANALYSIS FOR THE SAMPLES.

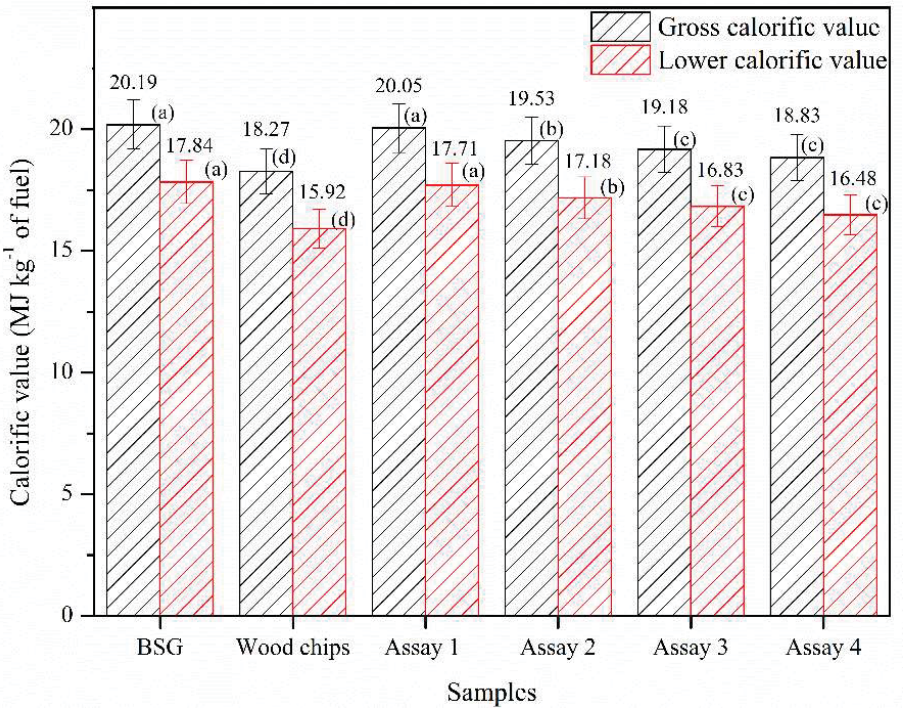

Results are averages of three repetitions with deviation standard estimates. Same lower case letters do not differ between tests ($p \leq 0.05$) [ANOVA and Tukey test].

It was possible to observe that the calorific value of the samples as a whole did not have much variation. The value of the gross and lower calorific value of the mixtures was higher than that of wood chips, which shows the positive effect of adding BSG to wood. It is worth mentioning that between BSG and Assay 1 there was no significant statistical difference at a level of 5%, this fact signals that the mixture in Assay 1 among all tests was the one that presented the best energy efficiency, with GCV = 20.05 MJ kg^{-1} and LCV = 17.71 MJ kg^{-1}.

Thus, taking into account all the experiments carried out and the parameters determined, the mixture of 80% of BSG with 20% of wood chips from Assay 1, was the one that presented the best set of results for the application of BSG as solid biomass in a direct combustion process in a boiler of a cogeneration system, with a low ash content (~ 0.39%), high volatile material (~ 97.35%) and high lower calorific power (~ 17.71 MJ kg^{-1}), inherent parameters of good fuel.

3.7 ASH COMPOSITION ANALYSIS

The results obtained for the EDS analysis of the ashes from Assay 1 are shown in Table 5.

TABLE 5 - INORGANIC COMPOSITION OF THE MIXTURE BETWEEN BSG AND WOOD CHIPS.

Sample	Oxide (wt% of ash)						
	Al_2O_3	Na_2O	MgO	K_2O	SiO_2	CaO	P_2O_5
Assay 1*	10.61	1.35	1.22	6.62	19.40	9.08	1.16

*Assay 1: 80% of BSG and 20% of wood chips.

As previously mentioned, it is important to have information about the composition of the ashes, as it provides us with important information about possible negative effects that may occur inside the boiler in a cogeneration system, such as for example fouling, corrosion and slagging.

The presence of alkali and alkali earth metals such as Na, K, Mg and Ca in the composition of the fuel ash can be a factor that causes oxidative corrosion process on the surface of the boiler, since during the combustion of the biomass, chlorine can be released in the form of HCl or Cl_2 and react with alkali metals to form volatile alkali chloride in the gas phase [21, 65]. In addition, the vast majority of alkali metals in gaseous form are deposited and condensate on the surface of the boiler at a lower temperature. Thus, they trap solid particles in the flue gas, which leads to serious corrosion, fouling and slagging, implying losses along with the heating exchanger inside the boiler, causing a loss in the energetic efficiency in cogeneration systems [21, 66].

However, as seen in Table 5, the ash from the burning of the mixture in this study does not contain chlorine in any amount, which leads us to believe that the fact mentioned above, will hardly occur, also emphasizing that the mass fraction of alkali type metals it does not exceed 15% of the total ash mass.

Moreover, the simultaneous burning of BSG with wood chips produced high levels of Si and Al in the ashes, 19.40 and 10.61%, respectively. In general, most alkali metals exist in the form of low reactivity aluminosilicates with a high melting point, which makes the content of chlorine and viscosity of the ash deposition lower, which means that the corrosion by ash deposition is slowed down [67-68].

3.8 ECONOMICAL EVALUATION

As illustrated in the previous topics, the use of BSG as a fuel for the boiler in a cogeneration system has extremely positive impacts for the brewing industry, such as the use of its main waste for electrical energy generation, reducing the cost of

processing this waste, once that it will be used within the plant itself, reducing costs with the usual boiler fuel, i.e. wood chips, and consequently decreasing the global cost of the energy industry. Since BSG is produced in large quantities at a minimum price and generates the same amount of energy, as the fuel that it previously had a cost, whether economic or environmental.

In this sense, an economic study was carried out to evaluate the impact of the use of the mixture between BSG and wood chips (Assay 1, Table 1) under the costs of steam and energy generation in an industrial cogeneration system. For this, Equations 4 and 5 adapted from Hugot [69] and the considerations made and presented in Table 6 were used.

$$\eta = \frac{m_v h_v - m_w h_w}{m_F H_F} \quad (4) \qquad m_F = \frac{m_v - (h_v - h_w)}{\eta H_F} \quad (5)$$

where: η (%) is the boiler efficiency, m_v (kg h^{-1}) mass flow rate of steam, h_v (3,423.10 KJ kg^{-1}) steam enthalpy, m_w (kg h^{-1}) mass flow rate of water, h_w (335.08 KJ kg^{-1}) water enthalpy, m_F (kg h^{-1}) mass flow rate of fuel, H_F (KJ kg^{-1}) fuel lower calorific value.

TABLE 6 - ASSUMPTIONS FOR THE DIMENSIONING OF STEAM PRODUCTION IN THE COGENERATION SYSTEM.

Input	Amount	Unit
Steam generate	1,000	Kg h^{-1}
Steam temperature	500	ºC
Water temperature	80	
Steam pressure	60	bar
LCV of Wood chips	14.17	MJ kg^{-1}
LCV of Assay 1	17071	
Operational days	270	days $year^{-1}$
Active operating	20	h day^{-1}
Steam use for heating	250	Kg h^{-1}
Isentropic efficiency of the steam turbine	60	%

In possession of the data of the considerations and using Equation 4, an efficiency value for the boiler of approximately η = 80% was obtained, this value is close to that found in the literature when a cogeneration system using biomass as fuel was used [70-72]. Then, the amount of fuel needed to produce 1,000 kg h^{-1} of steam was determined using Equation 5.When wood chips were used, approximately 243 kg h^{-1} of fuel was required, whereas for the mixture of Assay 1 was used approximately 218 kg h^{-1} of fuel, a reduction around of 10% in the total volume of fuel.

However, of the 218 kg h^{-1} of fuel needed to produce 1,000 kg h^{-1} of steam, only 20% of the mass was wood chips, which is around 44 kg h^{-1}, so the reduction was approximately 82% in the use of wood chips, which is an expressive value if we take

into account that the wood chips come from the exploitation of eucalyptus through the cutting of trees and their consequent processing, this reduction represents a positive carbon balance for the environment, since the deforestation will be slowed down, maintaining a balance between the local fauna and flora.

From an economic point of view, the balance of costs and profits for the use of BSG to generate steam through a cogeneration system is shown in Table 7.

TABLE 7 - ECONOMICAL BALANCE FOR THE PRODUCTION OF STEAM USING BSG AS FUEL FOR BOILER DURING A DAY.

	System	Fuel	Quantity (kg day^{-1})	Unit cost (USD kg^{-1})	Total cost (USD day^{-1})
Scenario A	Conventional	100% Wood chips	4,860	3.50	17,010
Scenario B	Mixture	20% Wood chips	880		3,080
		80% BSG	3,480	none	-

Observing Table 7, to meet the production demand of 20,000 kg day^{-1} of steam, 4,860 kg h^{-1} of wood chips will be necessary for a system that uses only this fuel, which generates a daily cost of approximately USD 17,010.00. While for a system that uses a mixture of wood chips and BSG in a ratio of 1:4, the same demand can be met with just 880 kg h^{-1} of wood chips, which would generate a cost of USD 3,080.00, a reduction of approximately USD 13,930.00 in fuel costs daily and annual savings of approximately 3.8 million US dollars.

If we take into account that of the 20,000 kg day^{-1} of steam produced, 5,000 kg day^{-1} was used in the form of steam to generate heat and the remaining 15,000 kg day^{-1} were used to run a turbine with an efficiency of 60%, approximately 149 kWh day^{-1} of electricity would be generated, which can be used for internal supply to the industry or sold to the electricity grid as surplus.

It is worth mentioning that all values for all variables were assumed in order to illustrate the significant reduction in the amount of wood chips used and also in fuel costs. The data in Table 6 can be adapted to the particular situations of each industry and consequently the values can vary.

4 CONCLUSIONS

The determination of the physical, chemical and energetic parameters for the brewers' spent grain, aiming the use in an energy cogeneration system was carried out. The analyzes were carried out taking into account the eucalyptus wood chip as a

control sample and a means of comparison, since there are few studies that address the use of BSG as a fuel for cogeneration.

According to the results presented, the BSG showed a moisture content of 77.86%, ash content of 0.52%, volatile material 95.94%, fixed carbon of 3.57%, the mean particle size of 0.28 mm, a density of 113 kg m^3 and a lower calorific value of 17.84 MJ kg^{-1}. This group of characteristics pointed out that BSG can be used as a fuel for direct combustion in a boiler in a cogeneration system.

Tests were carried out combining different proportions of BSG and wood chips in order to study whether the mixture of these fuels would bring beneficial results for the generation of energy and its influence on the cogeneration system. It was observed that the proportion between 80% of BSG and 20% of wood chips showed satisfactory results to be used as boiler fuel instead of using only wood chips and/or BSG, such as a low amount of ash, approximately 0.39%, high content of volatile material 97.35% and a high lower calorific value of approximately 17.71 MJ kg^{-1}.

Combined with these characteristics, the ash from the burning of the mixture between BSG and wood chips, generated a residue that has a low concentration of alkali metals and a high concentration of aluminosilicate species, both of which cause fouling, corrosion and slagging processes inside the boiler to be slowed down, thus increasing the useful life of the system and its energy efficiency.

Finally, from a technical and economic point of view, the concomitant use of wood chips and BSG in the proportion of 1:4, promoted a reduction of 82% in the use of wood. In addition to having the potential to generate 20 ton day^{-1} of steam and approximately 149 kWh day^{-1} of electricity, saving approximately 3.8 million US dollars annually.

REFERENCES

[1] F. Nocente, F. Taddei, E. Galassi, L. Gazza, Upcycling of brewers' spent grain by production of dry pasta with higher nutritional potential, LWT. 114 (2019) 108421. https://doi.org/10.1016/j.lwt.2019.108421.

[2] S. Saba, G. Zara, A. Bianco, M. Garau, M. Bononi, M. Deroma, A. Pais, M. Budroni, Comparative analysis of vermicompost quality produced from brewers' spent grain and cow manure by the red earthworm Eisenia fetida, Bioresource Technol. 293 (2019) 122019. https://doi.org/10.1016/j.biortech.2019.122019.

[3] C. Xiros, P. Christakopoulos, Biotechnological Potential of Brewers Spent Grain and its Recent Applications, Waste Biomass Valori. 3 (2012) 213–232. https://doi.org/10.1007/s12649-012-9108-8.

[4] K.M. Lynch, E.J. Steffen, E.K. Arendt, Brewers' spent grain: a review with an emphasis on food and health, J I Brewing. 122 (2016) 553–568. https://doi.org/10.1002/jib.363.

[5] Ministério da Agricultura, Pecuária e Abastecimento, Anuário da Cerveja, MAPA, Brasil, 2019. https://www.gov.br/agricultura/pt-br/assuntos/inspecao/produtos-vegetal/publicacoes/anuario-da-cerveja-2019 (accessed February 2020).

[6] Barth-Haas Group, The Barth Report, Joh. Barth & Sohn GmbH & Co KG, Nuremberg, 2019. https://www.barthhaas.com/fileadmin/user_upload/news/2019-07-23/barthreport20182019en.pdf (accessed February 2020).

[7] J. Buffington, The Economic Potential of Brewer's Spent Grain (BSG) as a Biomass Feedstock, Adv Chem Engin Sci. 04 (2014) 308–318. https://doi.org/10.4236/aces.2014.43034.

[8] M. Gupta, N. Abu-Ghannam, E. Gallaghar, Barley for Brewing: Characteristic Changes during Malting, Brewing and Applications of its By-Products, Compr Rev Food Sci F. 9 (2010) 318–328. https://doi.org/10.1111/j.1541-4337.2010.00112.x.

[9] M.E. Himmel, Biomass recalcitrance: deconstructing the plant cell wall for bioenergy, Blackwell Pub, Oxford, 2008.

[10] S.I. Mussatto, G. Dragone, I.C. Roberto, Brewers' spent grain: generation, characteristics and potential applications, J Cereal Sci. 43 (2006) 1–14. https://doi.org/10.1016/j.jcs.2005.06.001.

[11] V. Stojceska, P. Ainsworth, A. Plunkett, S. İbanogˇlu, The recycling of brewer's processing by-product into ready-to-eat snacks using extrusion technology, J Cereal Sci. 47 (2008) 469–479. https://doi.org/10.1016/j.jcs.2007.05.016.

[12] S. Öztürk, Ö. Özboy, İ. Cavidoğlu, H. Köksel, Effects of Brewer's Spent Grain on the Quality and Dietary Fibre Content of Cookies, J I Brewing. 108 (2002) 23–27. https://doi.org/10.1002/j.2050-0416.2002.tb00116.x.

[13] A. Gómez, J. Zubizarreta, M. Rodrigues, C. Dopazo, N. Fueyo, An estimation of the energy potential of agro-industrial residues in Spain, Resour Conserv Recy. 54 (2010) 972–984. https://doi.org/10.1016/j.resconrec.2010.02.004.

[14] S.B. da Silva, M.D.C. Arantes, J.K.B. de Andrade, C.R. Andrade, A. de C.O. Carneiro, T. de P. Protásio, Influence of physical and chemical compositions on the properties and energy use of lignocellulosic biomass pellets in Brazil, Renew Energ. 147 (2020) 1870–1879. https://doi.org/10.1016/j.renene.2019.09.131.

[15] S. Nishiguchi, T. Tabata, Assessment of social, economic, and environmental aspects of woody biomass energy utilization: Direct burning and wood pellets, Renew Sust Energ Rev. 57 (2016) 1279–1286. https://doi.org/10.1016/j.rser.2015.12.213.

[16] T.L. Deboni, F.J. Simioni, M.A. Brand, G.P. Lopes, Evolution of the quality of forest biomass for energy generation in a cogeneration plant, Renew Energ. 135 (2019) 1291–1302. https://doi.org/10.1016/j.renene.2018.09.039.

[17] V.V. Kosov, V.A. Sinelshchikov, G.A. Sytchev, V.M. Zaichenko, Effect of torrefaction on properties of solid granulated fuel of different biomass types, High Temp+. 52 (2014) 907–912. https://doi.org/10.1134/s0018151x14060170.

[18] H. Li, Q. Chen, X. Zhang, K.N. Finney, V.N. Sharifi, J. Swithenbank, Evaluation of a biomass drying process using waste heat from process industries: A case study, Appl Therm Eng. 35 (2012) 71–80. https://doi.org/10.1016/j.applthermaleng.2011.10.009.

[19] G. Bonassa, L.T. Schneider, V.B. Canever, P.A. Cremonez, E.P. Frigo, J. Dieter, J.G. Teleken, Scenarios and prospects of solid biofuel use in Brazil, Renew Sust Energ Rev. 82 (2018) 2365–2378. https://doi.org/10.1016/j.rser.2017.08.075.

[20] P.C. Lenço, D.A. Ramirez-Quintero, W.A. Bizzo, Characterization of sugarcane bagasse particles separated by elutriation for energy generation, Renew Energ. 161 (2020) 712–721. https://doi.org/10.1016/j.renene.2020.06.046.

[21] J.M.O. Camargo, J.M. Gallego-Ríos, A.M.P. Neto, G.C. Antonio, M. Modesto, J.T.C. Leite, Characterization of sugarcane straw and bagasse from dry cleaning system of sugarcane for cogeneration system, Renew Energ. 158 (2020) 500–508. https://doi.org/10.1016/j.renene.2020.05.107.

[22] T. Abbas, M. Issa, A. Ilinca, Biomass Cogeneration Technologies: A Review, J Sustain Bio Sys. 10 (2020) 1–15. https://doi.org/10.4236/jsbs.2020.101001.

[23] Q. Liu, S.C. Chmely, N. Abdoulmoumine, Biomass Treatment Strategies for Thermochemical Conversion, Energ Fuel. 31 (2017) 3525–3536. https://doi.org/10.1021/acs.energyfuels.7b00258.

[24] Z. Hameed, M. Aslam, Z. Khan, K. Maqsood, A.E. Atabani, M. Ghauri, M.S. Khurram, M. Rehan, A.-S. Nizami, Gasification of municipal solid waste blends with biomass for energy production and resources recovery: Current status, hybrid technologies and innovative prospects, Renew Sust Energ Rev. 136 (2021) 110375. https://doi.org/10.1016/j.rser.2020.110375.

[25] C. Yin, Development in biomass preparation for suspension firing towards higher biomass shares and better boiler performance and fuel rangeability, Energy. 196 (2020) 117129. https://doi.org/10.1016/j.energy.2020.117129.

[26] Y. Xie, Z. Lu, C. Ma, Z. Xu, Y. Tang, S. Ouyang, R. Wang, Y. Zhou, High-performance gas–electricity cogeneration using a direct carbon solid oxide fuel cell fueled by biochar derived from camellia oleifera shells, Int J Hydrogen Ener. 45 (2020) 29322–29330. https://doi.org/10.1016/j.ijhydene.2020.07.214.

[27] Y. Guo, Z. Yu, G. Li, H. Zhao, Performance assessment and optimization of an integrated solid oxide fuel cell-gas turbine cogeneration system, Int J Hydrogen Ener. 45 (2020) 17702–17716. https://doi.org/10.1016/j.ijhydene.2020.04.210.

[28] G. Song, L. Zhao, H. Zhao, J. Xiao, H. Wang, S. Guo, Design and Assessment of a Novel Cogeneration Process of Synthetic Natural Gas and Char via Biomass Pyrolysis-Coupled Hydrothermal Gasification, Ind Eng Chem Res. 59 (2020) 22205–22214. https://doi.org/10.1021/acs.iecr.0c04504.

[29] F. Sorgulu, I. Dincer, Development and assessment of a biomass-based cogeneration system with desalination, Appl Therm Eng. 185 (2021) 116432. https://doi.org/10.1016/j.applthermaleng.2020.116432.

[30] K. Sartor, S. Quoilin, P. Dewallef, Simulation and optimization of a CHP biomass plant and district heating network, Appl Energ. 130 (2014) 474–483. https://doi.org/10.1016/j.apenergy.2014.01.097.

[31] R. Roushenas, A.R. Razmi, M. Soltani, M. Torabi, M.B. Dusseault, J. Nathwani, Thermo-environmental analysis of a novel cogeneration system based on solid oxide

fuel cell (SOFC) and compressed air energy storage (CAES) coupled with turbocharger, Appl Therm Eng. 181 (2020) 115978. https://doi.org/10.1016/j.applthermaleng.2020.115978.

[32] A. Liñán-Montes, S.M. de la Parra-Arciniega, M.T. Garza-González, R.B. García-Reyes, E. Soto-Regalado, F.J. Cerino-Córdova, Characterization and thermal analysis of agave bagasse and malt spent grain, J Therm Anal Calorim. 115 (2013) 751–758. https://doi.org/10.1007/s10973-013-3321-y.

[33] L.G. Cordeiro, Â.A. El-Aouar, C.V.B. de Araújo, Energetic characterization of malt bagasse by calorimetry and thermal analysis, J Therm Anal Calorim. 112 (2012) 713–717. https://doi.org/10.1007/s10973-012-2630-x.

[34] J. Zhang, Q. Wang, Sustainable mechanisms of biochar derived from brewers' spent grain and sewage sludge for ammonia–nitrogen capture, J Clean Prod. 112 (2016) 3927–3934. https://doi.org/10.1016/j.jclepro.2015.07.096.

[35] L.D.M.S. Borel, T.S. Lira, J.A. Ribeiro, C.H. Ataíde, M.A.S. Barrozo, Pyrolysis of brewer's spent grain: Kinetic study and products identification, Ind Crop Prod. 121 (2018) 388–395. https://doi.org/10.1016/j.indcrop.2018.05.051.

[36] A. Weger, R. Jung, F. Stenzel, A. Hornung, Optimized Energetic Usage of Brewers' Spent Grains, Chem Eng Technol. 40 (2016) 306–312. https://doi.org/10.1002/ceat.201600186.

[37] S.B. Kang, H.Y. Oh, J.J. Kim, K.S. Choi, Characteristics of spent coffee ground as a fuel and combustion test in a small boiler (6.5 kW), Renew Energ. 113 (2017) 1208–1214. https://doi.org/10.1016/j.renene.2017.06.092.

[38] American Society For Testing And Materials, ASTM D5865: Standard Test Method for Gross Calorific Value of Coal and Coke. West Conshohocken, 2019.

[39] K.C. Fagnani, H.J. Alves, L.E.N. Castro, S.S. Kunh, L.M.S. Colpini, An alternative for the energetic exploitation of sludge generated in the physico-chemical effluent treatment from poultry slaughter and processing in Brazilian industries, J Environ Chem Eng. 7 (2019) 102996. https://doi.org/10.1016/j.jece.2019.102996.

[40] American Society For Testing And Materials, ASTM D4749-87: Standard Test Method for Performing the Sieve Analysis of Coal and Designating Coal Size. West Conshohocken, 2019.

[41] A.S. Foust, Principles of unit operations, Wiley, New York A.O, 1980.

[42] Daizo Kunii, Octave Levenspiel, Fluidization engineering, Elsevier; Butterworth-Heinemann, Amsterdam ; Heidelberg, 2012.

[43] P. Poullet, J.J. Muñoz-Perez, G. Poortvliet, J. Mera, A. Contreras, P. Lopez, Influence of Different Sieving Methods on Estimation of Sand Size Parameters, Water. 11 (2019) 879. https://doi.org/10.3390/w11050879.

[44] M. Alfi, M. Barrufet, J. Killough, Effect of pore sizes on composition distribution and enhance recovery from liquid shale—Molecular sieving in low permeability reservoirs, Fuel. 235 (2019) 1555–1564. https://doi.org/10.1016/j.fuel.2018.08.063.

[45] American Society For Testing And Materials, ASTM E873-62: Standard Test Method for Bulk Density of Densified Particulate Biomass Fuels. West Conshohocken, 2019.

[46] American Society For Testing And Materials, ASTM D792: Standard Test Methods for Density and Specific Gravity (Relative Density) of Plastics by Displacement. West Conshohocken, 2019.

[47] American Society For Testing And Materials, ASTM C1039: Standard Test Methods for Apparent Porosity, Apparent Specific Gravity, and Bulk Density of Graphite Electrodes. West Conshohocken, 2019.

[48] American Society For Testing And Materials, ASTM E870: Standard Test Methods for Analysis of Wood Fuels. West Conshohocken, 2019.

[49] A.A.C.E. Association for the Advancement of Cost Engineering International, Conducting Technical and Economic Evaluations - As Applied for the Process and Utility Industries, AACE recommended practices and standards, ACE International, 1990. .

[50] G. Sperandio, T. Amoriello, K. Carbone, M. Fedrizzi, A. Monteleone, S. Tarangioli, M. Pagano, Increasing the Value of Spent Grain from Craft Microbreweries for Energy Purposes, Chem Engineer Trans. 58 (2017) 487–492. https://doi.org/10.3303/CET1758082.

[51] K. Formela, A. Hejna, Ł. Zedler, M. Przybysz, J. Ryl, M.R. Saeb, Ł. Piszczyk, Structural, thermal and physico-mechanical properties of polyurethane/brewers' spent grain composite foams modified with ground tire rubber, Ind Crop Prod. 108 (2017) 844–852. https://doi.org/10.1016/j.indcrop.2017.07.047.

[52] A.S.N. Mahmood, J.G. Brammer, A. Hornung, A. Steele, S. Poulston, The intermediate pyrolysis and catalytic steam reforming of Brewers spent grain, J Anal Appl Pyrol. 103 (2013) 328–342. https://doi.org/10.1016/j.jaap.2012.09.009.

[53] B.M. Jenkins, L.L. Baxter, T.R. Miles, T.R. Miles, Combustion properties of biomass, Fuel Process Technol. 54 (1998) 17–46. https://doi.org/10.1016/s0378-3820(97)00059-3.

[54] Moh. Jufri, H. Hendaryati, Moch.F. Saugi, Daryono, The Influence of Cast Ring Diameter toward Bagasse Biopellet Heat Value, Moisture, and Ash Content, J Phys Conf Ser. 1477 (2020) 052031. https://doi.org/10.1088/1742-6596/1477/5/052031.

[55] Ya.S. Balaeva, Yu.S. Kaftan, D.V. Miroshnichenko, E.I. Kotliarov, Influence of Coal Properties on the Gross Calorific Value and Moisture-Holding Capacity, Coke Chem. 61 (2018) 4–11. https://doi.org/10.3103/s1068364x18010039.

[56] S. Ikram, L. Huang, H. Zhang, J. Wang, M. Yin, Composition and Nutrient Value Proposition of Brewers Spent Grain, J Food Sci. 82 (2017) 2232–2242. https://doi.org/10.1111/1750-3841.13794.

[57] A. Lorente, J. Remón, M. Salgado, A.J. Huertas-Alonso, P. Sánchez-Verdú, A. Moreno, J.H. Clark, Sustainable Production of Solid Biofuels and Biomaterials by Microwave-Assisted, Hydrothermal Carbonization (MA-HTC) of Brewers' Spent Grain (BSG), ACS Sustain Chem Eng. 8 (2020) 18982–18991. https://doi.org/10.1021/acssuschemeng.0c06853.

[58] M. Dudek, K. Świechowski, P. Manczarski, J. Koziel, A. Białowiec, The Effect of Biochar Addition on the Biogas Production Kinetics from the Anaerobic Digestion of Brewers' Spent Grain, Energies. 12 (2019) 1518. https://doi.org/10.3390/en12081518.

[59] F.P. Incropera, Fundamentals of heat and mass transfer., John Wiley, Hoboken, Nj, 2007.

[60] R.A. Jordan, R. Baldassin Junior, L.A.B. Cortez, A.V.A. Motomiya, Granulometric characterization of polydispersed biomass by the mechanical sieving method, Engen. Agri. 36 (2016) 102–113. https://doi.org/10.1590/1809-4430-eng.agric.v36n1p102-113/2016.

[61] A. Hejna, M. Barczewski, K. Skórczewska, J. Szulc, B. Chmielnicki, J. Korol, K. Formela, Sustainable upcycling of brewers' spent grain by thermo-mechanical treatment in twin-screw extruder, J Clean Prod. 285 (2021) 124839. https://doi.org/10.1016/j.jclepro.2020.124839.

[62] E. Virmond, R.F. De Sena, W. Albrecht, C.A. Althoff, R.F.P.M. Moreira, H.J. José, Characterisation of agroindustrial solid residues as biofuels and potential application in thermochemical processes, Waste Manage. 32 (2012) 1952–1961. https://doi.org/10.1016/j.wasman.2012.05.014.

[63] D. Zgureva, S. Boycheva, D. Behunová, M. Václavíková, Smart- and Zero-Energy Utilization of Coal Ash from Thermal Power Plants in the Context of Circular Economy and Related to Soil Recovery, J Environ Eng. 146 (2020) 04020081. https://doi.org/10.1061/(asce)ee.1943-7870.0001752.

[64] C. Baek, J. Seo, M. Choi, J. Cho, J. Ahn, K. Cho, Utilization of CFBC Fly Ash as a Binder to Produce In-Furnace Desulfurization Sorbent, Sustain. 10 (2018) 4854. https://doi.org/10.3390/su10124854.

[65] P.A. Jensen, F.J. Frandsen, K. Dam-Johansen, B. Sander, Experimental Investigation of the Transformation and Release to Gas Phase of Potassium and Chlorine during Straw Pyrolysis, Energ Fuel. 14 (2000) 1280–1285. https://doi.org/10.1021/ef000104v.

[66] Y. Wang, Y. Sun, L. Jiang, L. Liu, Y. Li, Characteristics of Corrosion Related to Ash Deposition on Boiler Heating Surface during Cofiring of Coal and Biomass, J Chem-NY. 2020 (2020) 1–9. https://doi.org/10.1155/2020/1692598.

[67] Y. Liu, W. Fan, X. Wu, X. Zhang, ChlorineInduced HighTemperature Corrosion of Boiler Steels Combusting Sha Erhu Coal Compared to Biomass, Energ Fuel. 32 (2018) 4237–4247. https://doi.org/10.1021/acs.energyfuels.7b03143.

[68] Y. Wang, X. Wang, M. Wang, H. Tan, Formation of Sulfide Deposits and HighTemperature Corrosion Behavior at Fireside in a CoalFired Boiler, Energ Fuel. 34 (2020) 13849–13861. https://doi.org/10.1021/acs.energyfuels.0c02634.

[69] E. Hugot, Handbook of cane sugar engineering. 2. ed, Elsevier, Amsterdam, 1972.

[70] G. Carraro, V. Bori, A. Lazzaretto, G. Toniato, P. Danieli, Experimental investigation of an innovative biomass-fired micro-ORC system for cogeneration applications, Renew Energ. 161 (2020) 1226–1243. https://doi.org/10.1016/j.renene.2020.07.012.

[71] Q. Wang, W. Wu, Z. He, Thermodynamic analysis and optimization of a novel organic Rankine cycle-based micro-scale cogeneration system using biomass fuel, Energ Convers Manage. 198 (2019) 111803. https://doi.org/10.1016/j.enconman.2019.111803.

[72] A. Wienese, Boilers, boiler fuel and boiler efficiency, Proc S Afr Sug Technol Ass. 75 (2001) 275–281.

CHAPTER III

Use of residual ashes from biomass burning process from brewer industry in production of activated carbons for adsorption processes

ABSTRACT

In this work activated carbons were synthesized from residual ashes of brewers spent grains burning process and were used for indigo carmine dye adsorption. The ashes were chemical activated using three types of reagents, HNO_3, H_3PO_4 and KOH and the structure, morphology and surface of the adsorbents were characterized by different techniques. The adsorbent synthesized with H_3PO_4 displayed the best performance in removing dye molecules in 10 mg L^{-1} solution, with a removal rate of approximately 98% when using a concentration of 0.5 g L^{-1} in a particle size of 0.088 mm. The surface area of the ashes enlarged from 120.3 to 605.1 m^2 g^{-1} when H_3PO_4 was used as an activator, producing a high quality adsorbent, with an excellent cost benefit, being it possible to be produced for a price of 9.35 USD kg^{-1}, and it can be reused up to four times. The Redlich-Peterson isotherm model provided a better fit to the experimental data for indigo carmine dye adsorption on the adsorbent, and the maximum adsorption capacity was approximately 100 mg g^{-1} according to the Langmuir model. The kinetic study showed that the adsorption process occurred in two stages and the pseudo-first order kinetic model better described both. The thermodynamic parameters involved in the adsorption mechanism, showed that it was a spontaneous and favorable process, and due to its endothermic nature, an increase in temperature leads to an increase in the amount of indigo carmine dye molecules adsorbed.

Keywords: Indigo carmine, green synthesis, malt bagasse, food dye, food waste, beer production.

Manuscript elaborated and formatted according to the guidelines of scientific publication, submitted to the journal *Chemical Engineering Journal*. Available at: <http://bit.ly/chemengjournal>

1 INTRODUCTION

Residual ash is formed by the process of burning fuel in boilers, during the burning process the produced ash falls onto the bottom of the boiler, called the ashtray, these ashes are classified as bottom ash, part of the ashes produced are also carried by air in the process and end up getting trapped in the boiler filters, these ashes are classified as fly ash [1-2]. Between the years 2017 to 2018, countries like India, China, United States and Germany, produced approximately 350 million tons of residual ash, and the estimate is that worldwide it has exceeded 700 million tons [1, 3].

Usually the residual ashes from the burning process are used on an industrial scale for the production of construction materials, such as portland cement and refractory bricks, however the unused parts of this waste end up being stored in an area of the industry, or disposed of as garbage, which can lead to the degradation of the local soil and create a possible risk for ground water bodies [4-6].

Studies in the literature have investigated the use of these residual ashes for the production of zeolitic material [7-8]. However, the cost of the process and the difficulty in synthesizing a material with a well-defined structure makes this use very little explored [9-10]. Alternative uses for these ashes such as the production of adsorbent materials, especially activated carbons, end up being a viable alternative to be explored, since these materials are produced at a low cost and have favorable characteristics for the production of an adsorbent. [11-12].

Overall, these residual ashes have the characteristics necessary to serve as a good adsorbent, such as a high concentration of minerals, especially carbon, silicon and aluminum and high volatile content, which helps generate a rich pore structure [13-14]. This means that extremely efficient and low cost adsorbent materials can be obtained, once the raw material is a residue and can easily be turned into an adsorbent material [15].

Carbon based materials can be activated through various methods and techniques, such as chemical activation with nitric acid, phosphoric acid, potassium hydroxide, potassium carbonate or physical activation with steam, carbon dioxide, ozone and others [16-22]. Before choosing an activation method, some factors require special attention, such as the cost and time spent to synthesize the material, the necessary equipment, the degree of difficulty of the synthesis, the type of reagent used and its toxicity and especially the characteristics of the material produced [13, 23].

Observing these factors, chemical activation becomes a viable alternative, since they produce materials with a high micropore content and high surface area, which can be used for the adsorption of high molecular weight species, such as azo dyes. In addition, most reagents have low toxicity, activation occurs in a low reaction time and in a low temperature around 300-400 ºC, which optimizes the synthesis process and reduces energy and personnel costs. Besides, the reagents needed are most often inexpensive, which reduces the global cost of the process [13, 19, 24-26].

For the treatment of liquid industrial effluents, usually primary treatments are used, such as coagulation, flocculation and sedimentation, these treatments are classic and highly studied by the literature [11, 27-28]. However, they demand high areas for construction, their use is directed to high volumes of effluent and consequently uses high amounts of material to perform the treatment of the effluent and generate high volumes of sludge that need further treatment [29-31]. In addition, they are often unable to remove the molecules responsible for giving color to the effluents, such as dye molecules, which makes other treatments steps necessary, elevating the time and cost of the process [32-33].

The adsorption process is an alternative to traditional methods since it has demonstrated to be efficient, simple to operate, with a low operational cost, zero sludge production, no chemical requirement and extremely competent in discoloration processes, in addition to being able to reuse the industrial waste in form of activated carbon [32, 34-35].

The adsorption of industrial effluents, especially from the food industry, has been studied in the literature in recent years and the results are in most cases more satisfactory than other processes, which makes adsorption using activated carbon an emerging technology that the industry may start to adopt for the treatment of its liquid waste [11, 32, 36].

Thus, the aim of this study was the synthesis and characterization of activated carbons obtained from residual ashes of brewers spent grains (BSG) burning process and application in ad sorptive processes of food dye Indigo Carmine.

2 MATERIALS AND METHODS

2.1 RAW MATERIALS PREPARATION

The material used for the preparation of the adsorbents came from the use of biomass produced by the brewing industry, brewers' spent grains, during the production of lager beer, in the north region of the state of Paraná, Brazil, the BSG were used as fuel to generate steam in a boiler where the biomass was burned mixed with woodchip and the residue generated by the burning process, bottom ash, was used as raw material for the production of the adsorbents. The process of obtaining the ashes is shown in Fig. 1.

FIGURE 1 - SCHEME FOR OBTAINING THE RESIDUAL ASHES USED IN THE PRODUCTION OF THE ADSORBENTS.

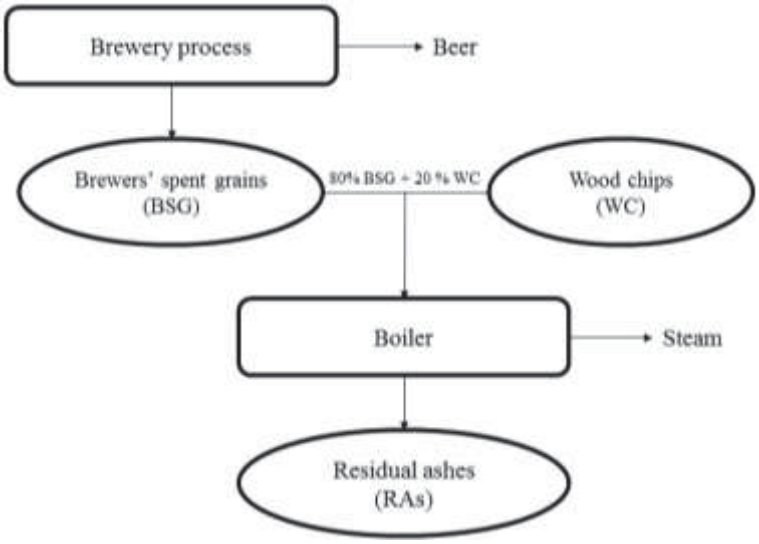

Once the ashes were obtained, a sample of the material was used to evaluate its adsorptive capacity and its morphological, structural and surface characteristics.

2.2 ACTIVATED CARBON PREPARATION

The residual ashes were chemical activated using three methods to obtain the activated carbon: (a) activation with potassium hydroxide (KOH), (b) phosphoric acid (H_3PO_4) and (c) nitric acid (HNO_3).

The activation using KOH was adapted from Lua and Yang [37], 20 g of ashes were mixed with the same proportion of solid KOH (P.A), mechanically agitated for 30

minutes and left to rest for 8 h to complete the impregnation process. After that, the material was dried in the oven at 110 ºC for 12 h. Then, the sample was carbonized at 400 ºC for 3 h with a temperature ramp of 5 ºC min^{-1}. At last, the sample was washed with HCl solution (0.1 mol L^{-1}) until pH = 7 was reached, to remove excessive liquid, the sample was dried in an oven at 105 ºC for approximately 4 h or until it got completely dry.

The activation using H_3PO_4 was adapted from Patnukao and Pavasant [38], firstly, 20 g of ashes were mixed with H_3PO_4 solution (85% m/v) in a proportion of 1:1 (w/v), then the mixture was agitated for 5 min and left to rest for 8 h. Then, the material was washed with approximately 150 mL of distilled water to remove the excessive acid and dried at 110 ºC for 12h. Thereupon, the sample was carbonized at 400 ºC for 3 h with a temperature ramp of 5 ºC min^{-1}. Lastly, the sample was washed with $NaHCO_3$ solution (2% m/v) until pH = 7 was reached, the sample was dried in an oven at 105 ºC for approximately 4 h.

The activation using HNO_3 was adapted from Rios et al. [39], 20 g of ashes were treated with 100 mL of concentrated HNO_3 (P.A) under reflux at 80 ºC for 6h. After reflux, the material was washed with heated distilled water to remove the excessive acid until approximately pH = 7, to remove excessive liquid the sample was dried at 105 ºC for 6 h. Then, the sample was carbonized at 400 ºC for 3 h with a temperature ramp of 10 ºC min^{-1}.

The adsorbents obtained were stored in vacuum packages at room temperature and labeled according to the activation method: Residual ashes (RAs), KOH (KOH), HNO_3 (HNO_3) and H_3PO_4 (PO_4).

2.3 ACTIVATED CARBON CHARACTERIZATION

The morphology was observed on scanning electron microscopy with energy dispersive spectroscopy (VEGA3 - TESCAN) using double-sided carbon tape and metallized with a thin layer of gold (5 nm, 35 mA). The N_2 adsorption/desorption isotherms were measured on a sorption analyzer (NOVA 2000e - Quantachrome Instruments). The surface area, pore volume and pore diameter were calculated from the Brunauer-Emmertt-Teller (BET) method, and pore size distributions were calculated with the Barret-Joyner-Hallenda (BJH) method. The materials structures were studied by Fourier transform infrared spectroscopy measuring diffuse reflectance

from 4,000-10,000 cm^{-1} (BRUKER - TENSOR 37). The surface charge distribution was determined by the point of zero charge (PZC) [11].

2.4 ADSORPTION EXPERIMENTS

2.4.1 Preliminary tests

Preliminary adsorption assays were performed to evaluate the adsorptive capacity of the materials in the removal of Indigo carmine (IC) dye (Fig. 2) in aqueous solutions, varying some parameters such as, activation method, particle size and concentration of the adsorbent.

FIGURE 2 - INDIGO CARMINE DYE STRUCTURE.

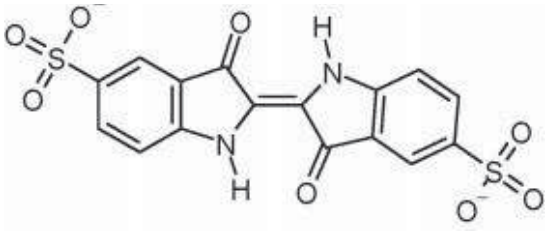

(m. wt. = 466.36 g mol^{-1}; λ_{max} = 609.5 nm)

In the activation method test, it has been evaluated the effect of the different methods of activation on the adsorptive capacity of the materials, in addition to comparing the synthesized materials with commercial activated carbons (Synth, particle size 4μm and 5 mm) used in adsorption reaction in industries. The effluent volume was 50 mL, adsorbent concentration (C_{ads}) was 1 g L^{-1}, dye concentration at 10 mg L^{-1}, pH of a solution at 7.2 and reaction time (t_{rea}) of 12 h, these parameters were constant during all tests.

With the material that obtained the highest percentage of removal of the dye in solution during the test of the activation methods, a granulometric test was carried out to evaluate the effect of the different particle sizes on the adsorptive performance of the materials, the particle diameter evaluated varied between 0.088-0.168 mm.

Lastly, with the other parameters determined, the concentration of the adsorbent was varied in order to find which value would have the greatest significance in removing the dye from the solution, so the values were varied between 0.5-10 g L^{-1}.

All tests were performed in an orbital shaker (TE-4200 Tecnal) at room temperature of 25 ºC. The adsorptive capacity of the material was evaluated by removing the dye molecules present in the solution by the adsorbent, according to

Equation 1, using an UV spectrophotometer (model EEQ-9006, Astral Scientific) at the maximum wavelength of the dye at 609.5 nm to determine concentrations.

$$R = \left(\frac{C_0 - C}{C_0}\right) 100 \quad (1)$$

where: R (%) is the percentage of removal of the IC dye from the solution by the adsorbent, C_0 (mg L^{-1}) is the initial concentration, C (mg L^{-1}) is the final solution concentration.

2.4.2 Adsorption kinetics

In order to determine the equilibrium time (t_e) for the adsorption assays with the IC dye, a kinetic study was performed using 50 mL of dye solution at 10 mg L^{-1}, pH of solution at 7.2 and the adsorbent that obtained the best results during the preliminary tests. Aliquots were collected in the first 1, 5, 10, 15 minutes, and then collected every 15 minutes until equilibrium time. The amount of dye adsorbed (q_t) in the adsorbent phase was determined using Equation 2.

$$q_t = \left(\frac{C_0 - C_t}{m}\right) V \quad (2)$$

where: q_t (mg g^{-1}) is the quantity of IC dye adsorbed at time t, C_t (mg L^{-1}) is the time t concentration, m (g) is the mass of adsorbent, V (L) is the volume of the solution of the IC dye.

Then, the theoretical value of the amount of IC dye adsorbed on the equilibrium (q_e) was determined using four kinetic models, the pseudo-first order, pseudo-second order, Avrami and Elovich models and then compared with the experimental value obtained of amount of IC dye adsorbed in equilibrium (q_{eExp}). Furthermore, the diffusion mechanism of the IC dye in the adsorbent was investigated using the intra-particle diffusion model, all equations are presented in Table 1.

TABLE 1 - KINETIC MODELS USED IN THE EXPERIMENT.

Model	Equation	Equation number	References
Pseudo-first order	$q_t = q_e(1-e^{-k_1 t})$	(3)	[40]
Pseudo-second order	$q_t = \frac{k_2 q_e^{\,2} t}{1+(k_2 q_e t)}$	(4)	[41]
	$h = k_2 q_e^{\,2}$	(5)	
Avrami	$q_t = q_e(1-e^{(-k_A t)^{n_A}})$	(6)	[42]
Elovich	$q_t = \frac{1}{\beta} \ln(\alpha\ \beta\ t)$	(7)	[43]

Intra-particle diffusion	$q_t = \left(k_{ip}\, t^{\frac{1}{2}}\right) + C$	(8)	[44]

where: q_e (mg g^{-1}) is the quantity of IC dye adsorbed at equilibrium; k_1 (min^{-1}) pseudo-first-order kinetic constant; t (min) reaction time; k_2 (g mg^{-1} min^{-1}) pseudo-second-order kinetic constant; h (mg g^{-1} min^{-1}) initial adsorption rate; k_A (min^{-nt}) avrami kinetic constant; n_A exponent avrami of time; β (g mg^{-1}) desorption constant; α (mg g^{-1} min^{-1}) initial adsorptive rate; k_{ip} (mg g^{-1} $min^{-0.5}$) intraparticle diffusion rate constant; C (mg L^{-1}) dye initial concentration.

2.4.3 Adsorption isotherms

It has been studied the adsorption equilibrium mechanism between the concentration of dye molecules (C_e) present in the liquid phase (solution), with the concentration of dye molecules (q_e) present on the surface of the solid phase (adsorbent), through adsorption isotherms and the influence of temperature on the maximum absorbent capacity of the materials. Experimental isotherm data were collected at different temperatures of 288, 298, 308 and 318 K and then adjusted using four models, Langmuir, Freundlich, Redlich-Peterson and Temkin, all equations are shown in Table 2.

TABLE 2 - ISOTHERMS USED IN THE EXPERIMENT.

Model	Equation	Equation number	References
Langmuir	$q_e = \frac{q_m\, k_L\, C_e}{1 + (k_L\, C_e)}$	(9)	[45]
	$R_L = \frac{1}{1 + (K_L C_0)}$	(10)	
Freundlich	$q_e = k_F \left(C_e^{\frac{1}{n}}\right)$	(11)	[46]
Redlich-Peterson	$q_e = \frac{k_R\, C_e}{1 + \left(a_R\, C_e^{\,b_R}\right)}$	(12)	[47]
Temkin	$q_e = B \ln (k_T\, C_e)$	(13)	[48]
	$B = \frac{R\, T}{b\, t}$	(14)	

where: k_L (L mg^{-1}) is Langmuir isotherm constant; q_m (mg g^{-1}) maximum monolayer adsorption; R_L (dimensionless) separation factor; C_0 (mg L^{-1}) initial dye concentration; k_F (mg g^{-1}) Freundlich isotherm constant; n (dimensionless) adsorption intensity; k_R (L g^{-1})/a_R (L $mg^{-(1/b)}$)/b_R (dimensionless) Redlich-Peterson isotherm constants; B (J mol^{-1}) adsorption heat constant; k_T (L mg^{-1}) Temkin isotherm constant; R (8.314 J mol^{-1} K^{-1}) ideal gas constant; T (K) temperature; b (dimensionless) constant related to the intensity of the adsorption.

2.4.4 Thermodynamic study

A thermodynamic study was carried out in order to improve the understanding regarding the energetic changes involved during the adsorption process at different temperatures. Enthalpy (ΔHº), entropy (ΔSº), free energy of adsorption (ΔGº) and

activation energy (E_a) were calculated for a better understanding of the effects of the parameters under the interaction mechanism between adsorbent and adsorbate involved in the adsorption process. The equations of Van't Hoff, Gibbs–Helmholtz and Arrhenius were used to determine the parameters mentioned above, and they are shown in Table 3.

TABLE 3 - THERMODYNAMIC EQUATIONS USED IN THE EXPERIMENT.

Model	Equation	Equation number	References
Van't Hoff	$\ln(k) = \frac{\Delta S^o}{R} - \frac{\Delta H^o}{R\,T}$	(15)	[49]
Gibbs-Helmholtz	$\Delta G^o = \Delta H^o - T\,\Delta S^o$	(16)	
Arrhenius	$\ln(k') = \ln A - \frac{E_a}{R\,T}$	(17)	

where: k (L mg^{-1}) is isotherm constant with better R^2; ΔS^o (J mol^{-1} K^{-1}) adsorption entropy; ΔH^o (J mol^{-1}) adsorption enthalpy; ΔG^o (J mol^{-1}) free energy of adsorption; k' (min^{-1}) kinetic constant with better R^2; A (dimensionless) pre-exponential factor; E_a (kJ mol^{-1}) activation energy.

2.4.5 Batch test

After the adsorption tests, the parameters evaluated that obtained the best adsorptive performance were adopted for batch tests. In order to maximize even more the removal of the IC dye of the aqueous solution, a 2^2 complete factorial design was carried to assess the influence of the parameter inherent to the solution on the adsorptive capacity of the activated carbons. The variables studied are shown in Table 4.

TABLE 4 - CONTROL VARIABLES CONSIDERED IN 2^2 FACTORIAL DESIGN.

Variable	Axial point ($-\sqrt{2}$)	Low Level (-1)	Central point (0)	High Level (+1)	Axial point ($+\sqrt{2}$)
pH	3	4	7	10	11
Reaction Temperature	16	20	30	40	44

2.4.6 Reuse test

In order to assess the useful life of the adsorbents and their recycling capacity, a reuse test was carried out with the adsorbent that have behaved in the best way during the adsorption tests.

2.4.7 Cost analysis

A cost analysis of the adsorbent synthesis was performed, based on the methodology of the Association for the Advancement of Cost Engineering [50]. Assumptions for scaled-up production costs comparisons were made from the information presented in this study and considering only the processing of residual ash to activated carbon.

2.5 CHARACTERIZATION OF ADSORBENTS AFTER ADSORPTION PROCESS

In order to evaluate the effect of the adsorption process on the morphology and surface of the material after the adsorption tests, the activated carbon was once again characterized by SEM and N_2 adsorption/desorption isotherms with BET analyzes.

2.6 STATISTICAL ANALYSIS

The results were expressed as mean ± standard deviation. The factorial design statistical analysis was performed to assess the effect of factors under the response variable and the interaction was tested statically by ANOVA at a significance level of 0.05, and for the mean comparison, it was performed the Tukey test. In addition, the response variable was optimized using the SIMPLEX method.

3 RESULTS AND DISCUSSION

3.1 ACTIVATED CARBON CHARACTERIZATION

Fig. 3 shows the SEM images obtained for the adsorbents.

FIGURE 3 - SEM IMAGES FOR THE ADSORBENTS AT 500X MAGNIFICATION.

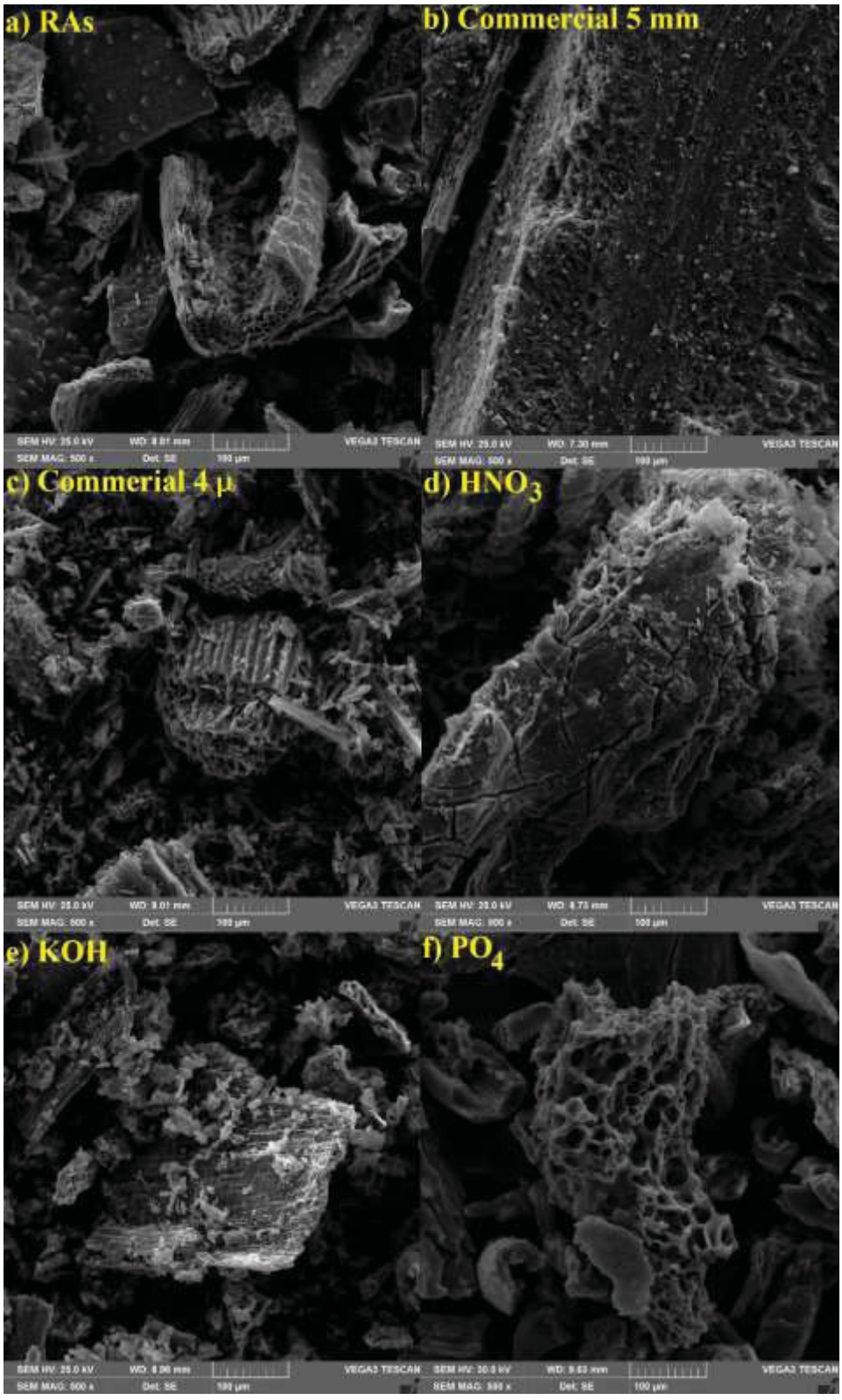

In Fig. 3, it was possible to observe that all the materials presented a rugged surface with laminar and granular particles. The RAs, commercials and the PO_4

showed a high distribution of pores on the surface, characteristic of materials with excellent adsorptive capacity as shown in previous literature [11, 51]. However, the surfaces of materials activated with KOH and HNO_3 do not have pores on their surface, probably due to the type of activation that the material was submitted [37, 52].

In Fig. 3 d), some crack in the structure from the aggregation state of the material can be observed, these cracks may be the result of the thermal process that the adsorbent activated with HNO_3 has undergone which may have caused a collapse in the structure, generating these flaws [37, 53].

The EDS analysis allowed the determination of the elemental composition of the adsorbents is shown in Table 5.

TABLE 5 - EDS ANALYSIS.

Adsorbent	**Element (%)**				
	C	**O**	**Si**	**N**	**P**
Commercial 5 mm	86.35	13.23	0.42	-	-
Commercial 4µ	89.06	10.78	0.16	-	-
RAs	77.41	20.95	0.55	-	1.09
HNO_3	32.53	50.55	8.43	8.49	-
KOH	61.27	35.82	2.91	-	-
PO_4	54.47	30.72	1.74	-	13.07

In general, carbon was the major element in the composition of adsorbents, indicating that the materials were carbonized throughout the synthesis process; the high carbon content can also be an indication that the material has the adsorptive capacity [11]. The presence of oxygen was also expected, since the carbonization of the materials was done in the presence of air. Silicon and phosphor come from the inherent composition of the ash source, since barley and brewers' spent grains are rich in this mineral [54]. The presence of nitrogen comes from the reagent used during synthesis, as well as the high phosphorous value in the PO_4 sample.

Fig. 4 shows the N_2 adsorption-desorption isotherms for the adsorbents obtained.

FIGURE 4 - N_2 ADSORPTION-DESORPTION ISOTHERMS.

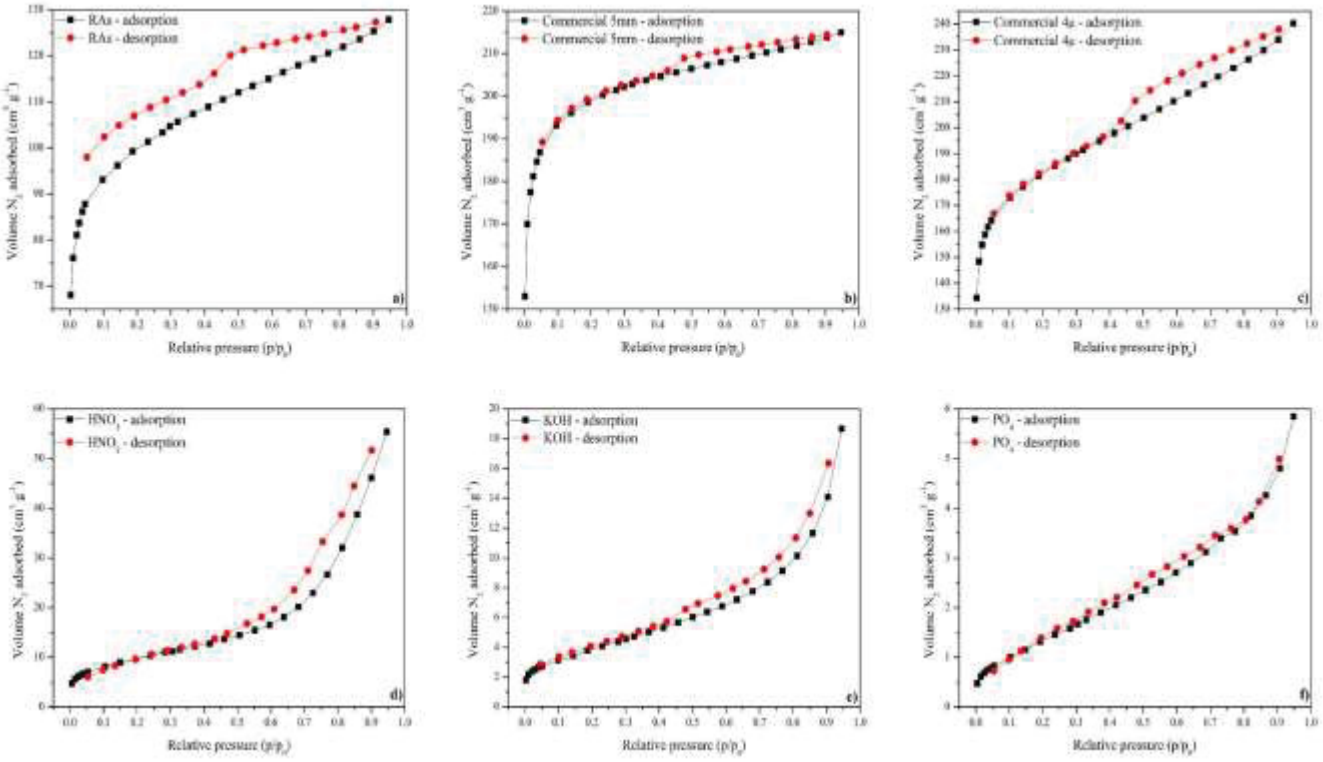

In Fig. 4 a), b) and c) the isotherms resembled the Type I, a typical characteristic of microporous materials, while the isotherms in Fig. 4 d), e) and f) resembled the Type II, characteristic of microporous and mesoporous materials [55-56]. This shift in the isotherm format occurred after the activation of the material, where the volume of N_2 adsorbed decreased, probably due to the interaction between the base material and chemical/thermal reactions that occurred during the activation process, modifying the surface structure of the materials, especially the shape and depth of the pores. Authors like Benedetti et al., Su et al. and Song et al., reported similar behavior regarding the shift in isotherm format and adsorptive volume [57-59].

The pore distribution for the adsorbent are shown in Fig. 5, it was possible to observe that the pore size distribution is concentrated in the range of approximately 1.8 nm, a range considered as micropore and commonly found in works that used activated carbon as adsorbent [14, 60-61].

FIGURE 5 - BJH PORE SIZE DISTRIBUTION ANALYSIS

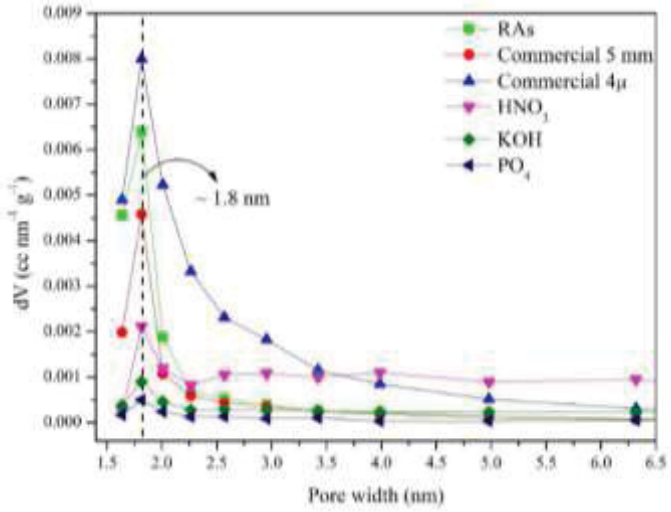

Table 6 shows the BET surface areas (S_o), mean pore diameter (d_p) and pore volumes (V_p) of the different adsorbents analyzed in this study.

TABLE 6 - TEXTURAL PROPERTIES OF THE ADSORBENTS.

Adsorbent	S_o (m^2 g^{-1})	V_p (cm^3 g^{-1})	d_p (nm)
Commercial 5 mm	587.5	0.33	1.10
Commercial 4μ	519.7	0.37	1.30
RAs	120.3	0.20	1.25
HNO_3	133.7	0.09	2.88
KOH	124.8	0.05	2.52
PO_4	605.1	0.01	2.01

It was possible to observe, that all surface area values increased after the process of activation of the residual ash, for example, the activation process using H_3PO_4 promoted an increase of almost six times higher, this increase on the surface area after the activations shows that the methods are chosen, somehow managed to improve the surface characteristics of the base material.

It is also worth mentioning that the PO_4 adsorbent obtained a higher value of surface area than the commercial adsorbents used as a control, which shows that this synthesis method is effective and can generate high quality adsorbent materials.

By observing the pore diameter values, it was possible to determine that the commercial materials and the RAs sample had a pore diameter characteristic of micropore material ($d_p < 2$ nm), while the other samples had slightly higher values, falling in the mesoporous materials range ($2 \leq d_p \leq 50$ nm), these results corroborate

with those obtained in the isotherms of Fig. 4. The values obtained in this study are similar to those found in the literature and are shown in Table 7.

TABLE 7 - LITERATURE RESULTS COMPARISON OF ACTIVATED CARBONS FROM BIOMASS.

Precursor	BET surface area (m^2 g^{-1})	Chemical activator	Activation Temperature (ºC)	Reference
Residual ash	605.1	H_3PO_4	400	This study
Macadamia nut	598.0	$ZnCl_2$	Microwave	[62]
P. oceanica fibers	502.9	KOH	600	[63]
Coffee grounds	640.0	H_3PO_4	600	[64]
Rice husk residue	585.0	H_3PO_4	400	[65]

Fig. 6 shows the FTIR spectra for the adsorbents obtained.

FIGURE 6 - NEAR INFRARED SPECTRUMS (NIR) OF THE ADSORBENTS AND SECOND DERIVATIVE.

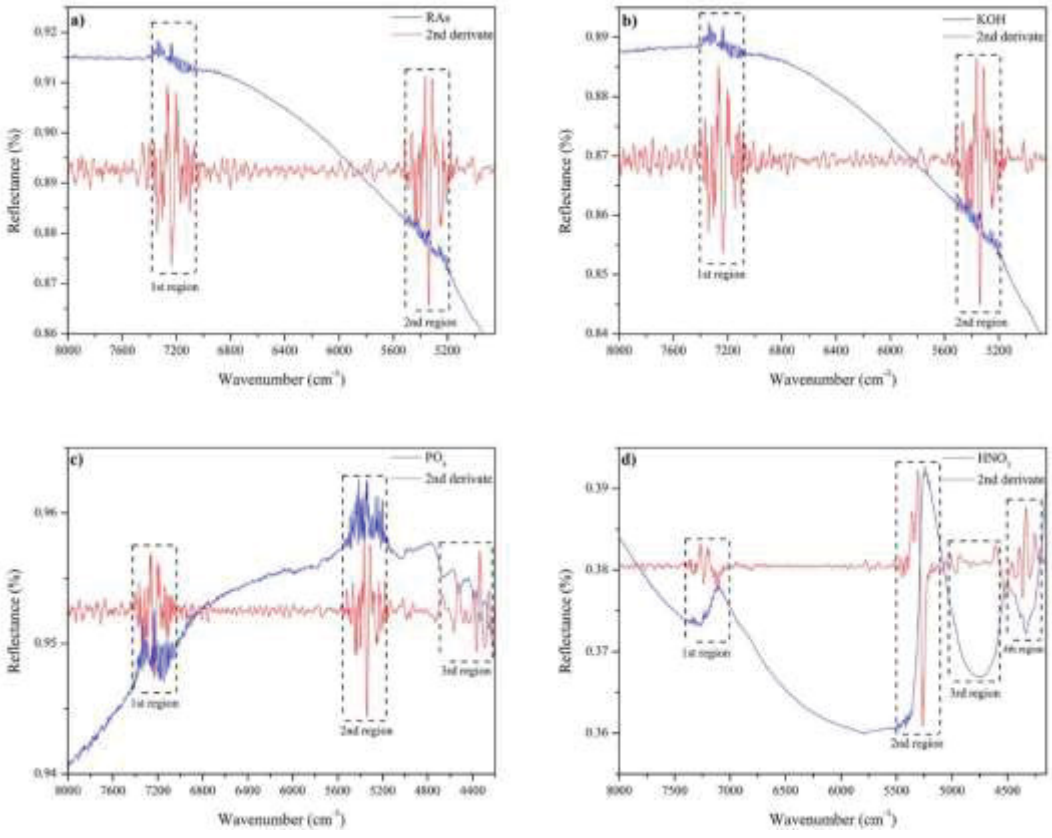

In Fig. 6 a) and b) the spectrum was divided into two regions, where there were expressive bands between 7,400 and 7,065 cm^{-1} (1^{st} region) with a maximum at about 7,231 cm^{-1} is characteristic of the first stretching overtone of hydrogen-bonded hydroxyl groups (O-H) (carboxyls, phenols or alcohols) and linked to the water adsorbed in the

activated carbon [17, 66]. The second region, with bands between 5,500 and 5,100 cm^{-1} with a maximum at about 5,410 cm^{-1} is characteristic of the second stretching of carbonyl groups (C=O) of ketones, aldehydes or carboxyl groups [67].

In Fig. 6 c) the spectrum was divided into three regions, the first and second regions are similar to the ones in Fig. 6 a) and b), however the third region with bands between 4,710 and 4,210 cm^{-1} with a maximum at about 4,333 cm^{-1} is characteristic of the combination between C-H + C-H groups (methyl, methylene or methine), which indicates the presence of a carbon structure in the material [68].

While in Fig. 6 d) the spectrum was divided into four regions, again the first and second regions are similar to the ones in Fig. 6 a) and b), the third region with bands between 5,040 and 4,560 cm^{-1}, with a maximum at about 4,756 cm^{-1} is characteristic of the combination band of N-H (amine, amide or nitroderivate), the presence of nitrogen groups comes from the synthesis with HNO_3 [68-69]. The fourth region is similar to the third region of Fig. 6 c).

The results of the PZC analysis are shown in Fig. 7, IC dye solution pH = 7.2 at a concentration of 10 mg L^{-1}.

FIGURE 7 - PZC ANALYSIS.

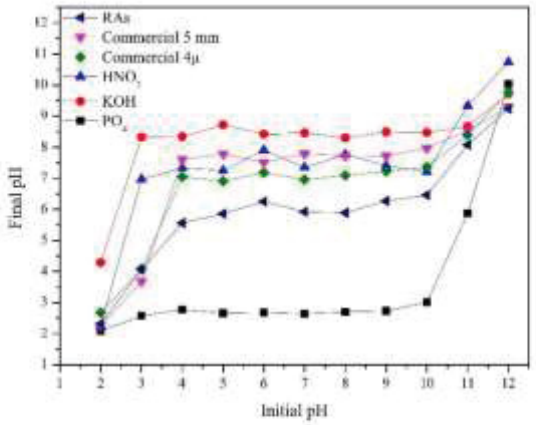

Adsorbent	pH_{PZC}
Commercial 5 mm	7.73
Commercial 4µ	7.11
RAs	6.03
HNO_3	7.46
KOH	8.47
PO_4	2.68

The point of zero charge, evaluates the behavior of the surface of the adsorbent, it may suggest the inclination of the surface of a material as to its acidity or basicity, indicating that the material is negatively charged when the pH_{PZC} is higher

than the pH of the solution or positively charged when the pH_{PZC} is lower than the pH of the solution [11].

It was possible to observe in Fig. 7 that the adsorbent presented different values of pH_{PZC}, consequently different surface charges, for Commercial 5 mm, HNO_3 and KOH the pH_{PZC} it was higher than the pH of the solution, which indicates that the surface is negatively charged, in that way causing cations to be adsorbed to the material surface to balance the negative charges.

While the other activated carbon presented a pH_{PZC} lower than the pH of the solution, which indicates that the surface is positively charged and leads to the attraction of negatively charged species, it is known that dye molecules present free electrons in their structure, so there is a tendency to have a negative charge, contributing to the adsorption process [70].

3.2 ADSORPTION EXPERIMENTS

3.2.1 Preliminary tests

Fig. 8 shows the results of the preliminary tests.

FIGURE 8 - PRELIMINARY TEST RESULTS: A) ACTIVATION METHOD; B) PARTICLE SIZE AND C) ADSORBENT CONCENTRATION.
(PARAMETERS: C_0 = 10 mg L^{-1}, C_{ads} = 1 g L^{-1}, t_{rea} = 12 h, V = 50 mL, pH = 7.2, T = 25 ºC)

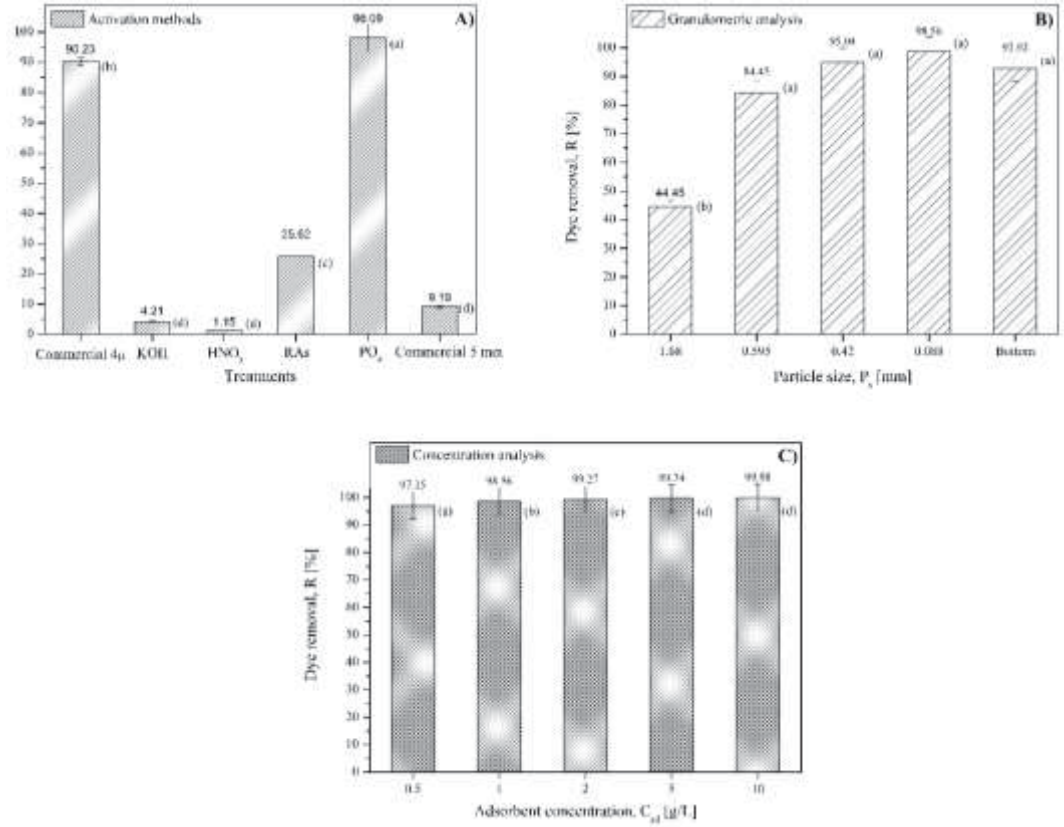

Results are averages of three repetitions with deviation standard estimates. Same lower case letters do not differ between tests ($p \leq 0.05$) [ANOVA and Tukey test].

In Fig. 8 a), it was possible to observe that the activation method had an influence on the removing value of IC dye from the solution. Commercial 4µ and H_3PO_4 were the samples that had the highest removal values, 90.23 and 98.09 %, respectively. This great performance is linked to the characteristics of the material, such as high surface area, high pore distribution and positive surface charge; all of these parameters make the materials to be great adsorbents.

However, the other materials presented unsatisfactory results, with less than 25% of IC dye removal. Commercial 5 mm, KOH and HNO_3 had the lowest removal values, 9.19, 4.21 and 1.15 %, respectively. This low discoloration rate is due to the surface charge of these materials, it presents a charge equal to the effluent, which ends up causing the charges to be repelled and consequently hamper the adsorptive process, even with other favorable characteristics such as the presence of pores and high surface area.

With the results obtained in the activation method test of Fig. 8 a), the adsorbent activated with H_3PO_4 was chosen as the study material and from this moment on, all tests were performed with it.

Fig. 8 b) shows the results obtained in the granulometric test of the PO_4 adsorbent, it was possible to observe that the particle size influenced the removal of the IC dye from the solution. The test with 0.595, 0.42, 0.088 mm and bottom, showed no statistical difference between the samples at a 5% level of significance, therefore, the granulometry that presented the highest discoloration value, 0.088 mm, was chosen.

In Fig. 8 c) all chosen PO_4 concentration showed discoloration higher than 97% for the IC dye solution, with the intention of using the least amount of adsorbent in order to save material and money, it was chosen to use the adsorbent concentration of 0.5 g L^{-1}, since 97.15% of dye removal is a value considered high and commonly found in the literature [26, 51].

With the preliminary tests done, the best parameters of each test were adopted from here for all the assays in this study. Summing up, chemical activation with H_3PO_4, in particle size of 0.088 mm and in the concentration of 0.5 g L^{-1}, obtained the best removal results for the IC dye solution at 10 mg L^{-1}.

3.2.2 Adsorption kinetics

Fig. 9 shows the results of the adsorption kinetics obtained for the tests with IC dye using the kinetic models and in Table 8 the parameters obtained during the data adjustment.

FIGURE 9 - ADSORPTION KINETIC FOR IC DYE SOLUTION.
(PARAMETERS: C_0 = 10 mg L^{-1}, C_{ads} = 0.5 g L^{-1}, V = 50 mL, pH = 7.2, T = 25 ºC)

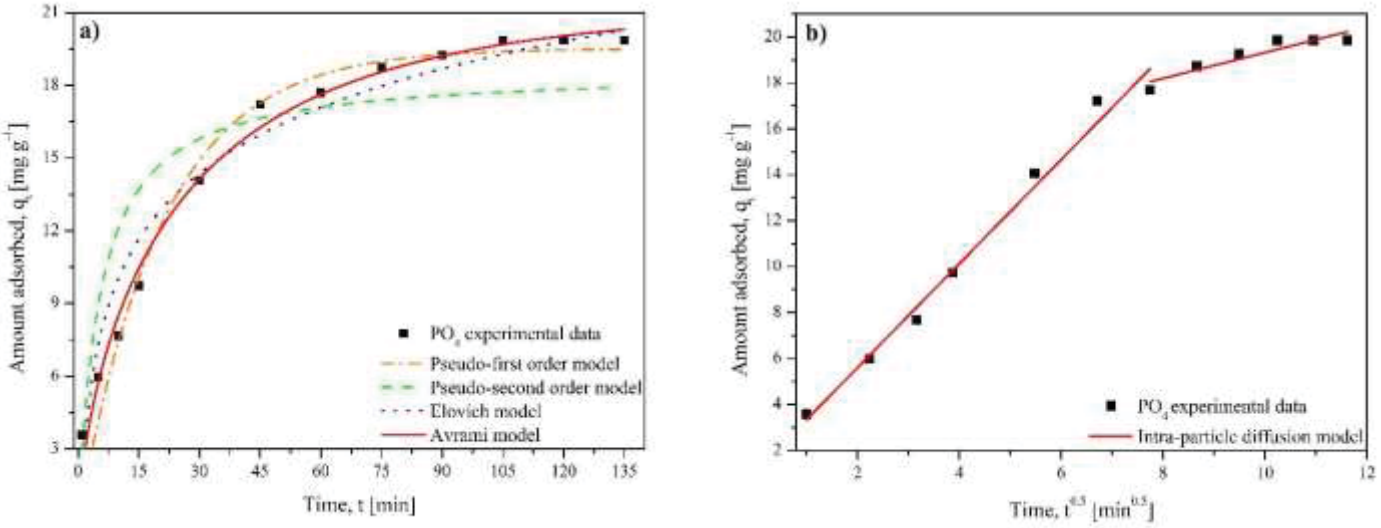

TABLE 8 - KINETIC PARAMETERS OF THE EXPERIMENT.

C_0	q_{eExp}	Pseudo-first order				Pseudo-second order				
		k_1	q_e	R^2	RMSE	k_2	q_e	h	R^2	RMSE
		0.05	19.51	0.98	0.001	0.01	18.62	3.47	0.82	0.002
		Elovich				Avrami				
		β	α	R^2	RMSE	k_A	q_e	n_A	R^2	RMSE
10	19.85	0.25	5.07	0.94	0.001	0.04	20.27	0.69	0.96	0.007
		Intra-particle diffusion[1]				Intra-particle diffusion[2]				
		k_{ip}	C	R^2	RMSE	k_{ip}	C	R^2	RMSE	
		2.27	1.07	0.98	0.007	0.56	13.71	0.83	0.003	

It can be observed in Fig. 9 a), that the kinetics of the dye was quick in the initial stage of the adsorptive process, where approximately 50% of the total dye in the solution was adsorbed in the first 15 min and from time, t_e = 105 min the adsorptive equilibrium was reached with the quantity of IC dye adsorbed, q_e = 19.85 mg g^{-1}.

The pseudo-first order model (eq. 3) was noted to be more suitable for the adsorption data according to the relatively high correlation coefficient (R^2 > 0.98) shown in Table 8, also, the kinetic rate was the highest with k_1 = 0.05 min^{-1}. In addition, the q_e values obtained theoretically by the pseudo-first, pseudo-second (eq. 4) and

Avrami (eq. 6) models, deviated from the experimental value by 1.7, 6.6 and 2.1%, respectively, which shows that the models fit well with the data, providing a reliable estimative.

The intra-particle diffusion model (eq. 8) for the adsorption of IC dye molecules on the PO_4 adsorbent, is given in Fig. 9 b), and illustrates that more than one process was involved in the adsorption process. The first stage (rapid removal, k_{ip} = 2.27 min^{-1}) could be attributed to boundary layer diffusion, where the dye molecules present in the liquid phase are transported to the solid surface of the adsorbent by external mass transfer factors and the following equilibrium stage (slow removal, k_{ip} = 0.56 min^{-1}) could be ascribed to the diffusion of IC dye molecules into the pores of the adsorbent [71-72]. In Fig. 10, it was possible to observe how the discoloration process occurred throughout the kinetic assays.

FIGURE 10 - ADSORPTION KINETIC FOR IC DYE SOLUTION AT 10 MG L^{-1}.

3.2.3 Adsorption isotherm

Fig. 11 shows the results of the adsorption isotherm obtained for the tests with IC dye using the equilibrium models and in Table 9 the parameters obtained during the data adjustment.

FIGURE 11 - ADSORPTION ISOTHERM FOR IC DYE SOLUTION.
(PARAMETERS: C_{ads} = 0.5 g L^{-1}, t_{eq} = 105 min, V = 50 mL, pH = 7.2)

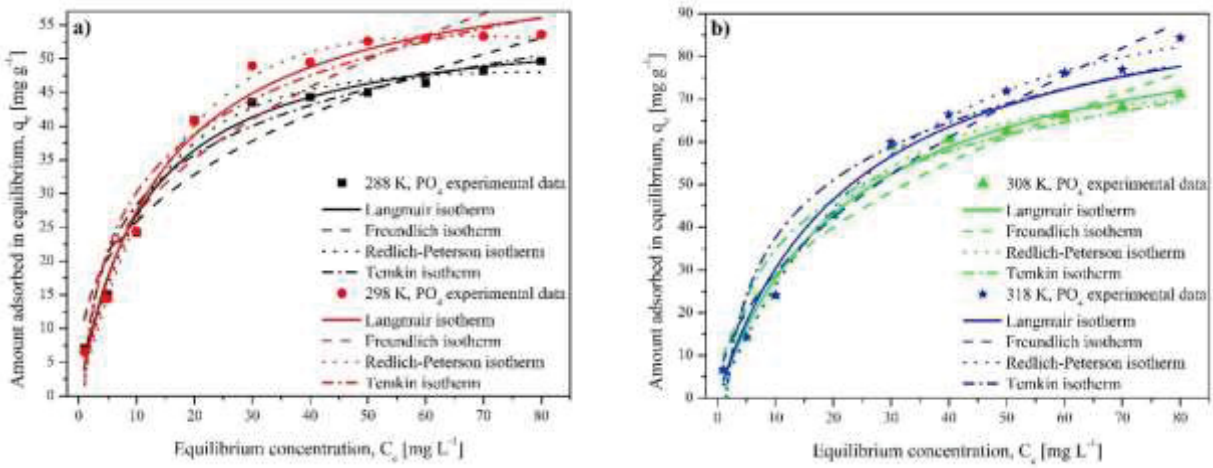

TABLE 9 - ISOTHERM PARAMETERS OF THE EXPERIMENT.

T (K)	Langmuir					Freundlich			
	q_m	k_L	R_L	R^2	RMSE	k_F	n	R^2	RMSE
288	56.47	0.09	0.92	0.97	0.02	11.63	2.89	0.90	0.04
298	65.78	0.07	0.93	0.98	0.02	11.23	2.62	0.91	0.05
308	92.46	0.04	0.96	0.98	0.03	9.95	2.15	0.94	0.05
318	100.00	0.04	0.96	0.97	0.05	8.64	1.89	0.97	0.05
T (K)	**Redlich-Peterson**					**Temkin**			
	k_R	a_R	b_R	R^2	RMSE	B	k_T	R^2	RMSE
288	3.92	0.03	1.17	0.98	0.02	10.63	1.44	0.94	0.03
298	3.21	0.01	1.34	0.99	0.01	12.46	1.13	0.93	0.04
308	3.17	0.01	1.27	0.99	0.02	16.63	0.81	0.92	0.06
318	3.04	0.01	1.20	0.99	0.02	19.48	0.69	0.91	0.08

In Fig. 11 it is possible to observe that all the equilibrium curves followed the same trend. While the initial dye concentration increased, the amount of dye molecules adsorbed in the material surface also increased, followed by a plateau formation, from the concentration of 40 mg L^{-1} onwards, representing a monolayer formation on the adsorbent surface. In addition, the isotherms presented a concave shape, this suggests they are favorable; that is, there is a great affinity between adsorbent and adsorbate [72-73].

Observing the isotherms, it resembles type H isotherms according to Giles et al. [74], in this type of isotherm, the solute (dye molecules) has such high affinity with the adsorbent that in dilute solution, in this case 10 mg L^{-1}, it is completely adsorbed and the initial part of the isotherm is vertical. Usually the adsorbed species are large

units, i.e., azo dyes, cyanine dyes, polymeric molecules, in this study it is the Indigo carmine food dye.

In Table 9, when observing the values of the correlation coefficient (R^2) and the square-root-mean error (RMSE), it was possible to note that the Redlich-Peterson model (eq. 12) was better adjusted to the equilibrium experimental data with $R^2 > 0.98$ and RMSE < 0.02.

It is also important to remark that the Langmuir model (eq. 9 and 10) presents important parameters on the equilibrium reaction mechanism, such as the maximum amount of adsorbate in monolayer, which for temperatures of 288, 298, 308 and 318 K, q_m was equal to 56.47, 65.78, 92.46 and 100 mg g^{-1}, respectively. In addition, the separation factor, R_L, for all temperatures studied was minor than one, which indicates that the adsorptive process was favorable. Adsorption intensity factor, n, of the Freundlich isotherm (eq. 11) also indicates whether the adsorption is favorable for n > 1 or not for n < 1. When observing Table 9, for all studied temperatures, the value of n was higher than one, indicating that the adsorption of IC dye on activated carbon PO_4 was a favorable process [75].

To test the statistical strength of the Langmuir model and its ability to predict the values of maximum amount of adsorbate in monolayer, a test with the IC dye solution at 100 mg L^{-1} and a reaction temperature of 35 ºC was performed and the deviation from the experimental value with the theoretical value of 92.46 mg g^{-1} obtained in Table 9, was evaluated.

FIGURE 12 - ADSORPTION KINETIC TEST EXPERIMENT FOR IC DYE.
(PARAMETERS: C_0 = 100 mg L^{-1}, C_{ads} = 0.5 g L^{-1}, V = 50 mL, pH = 7.2, T = 35 ºC)

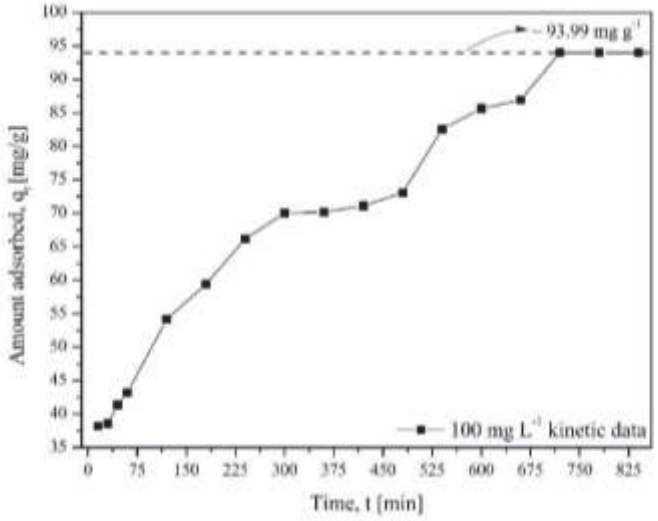

In Fig. 12, it was possible to observe that the adsorptive equilibrium for the IC dye solution at 100 mg L^{-1}, was obtained after 720 min and with the quantity of dye molecules adsorbed of 93.99 mg g^{-1}. This value deviated approximately 1.6% from the theoretical value obtained by the Langmuir model in Table 9, when the temperature was 35ºC. This indicates that the Langmuir model can predict with precision the maximum monolayer adsorption values in the studied temperature range.

3.2.4 Thermodynamic study

Fig. 13 and Table 10 show the results of the thermodynamic study obtained for the adsorption tests with IC dye solution.

FIGURE 13 - THERMODYNAMIC EXPERIMENT FOR IC DYE ADSORPTION PROCESS.
(Parameters: C_0 = 10 mg L^{-1}, C_{ads} = 0.5 g L^{-1}, t_{eq} = 105 min, V = 50 mL, pH = 7.2)

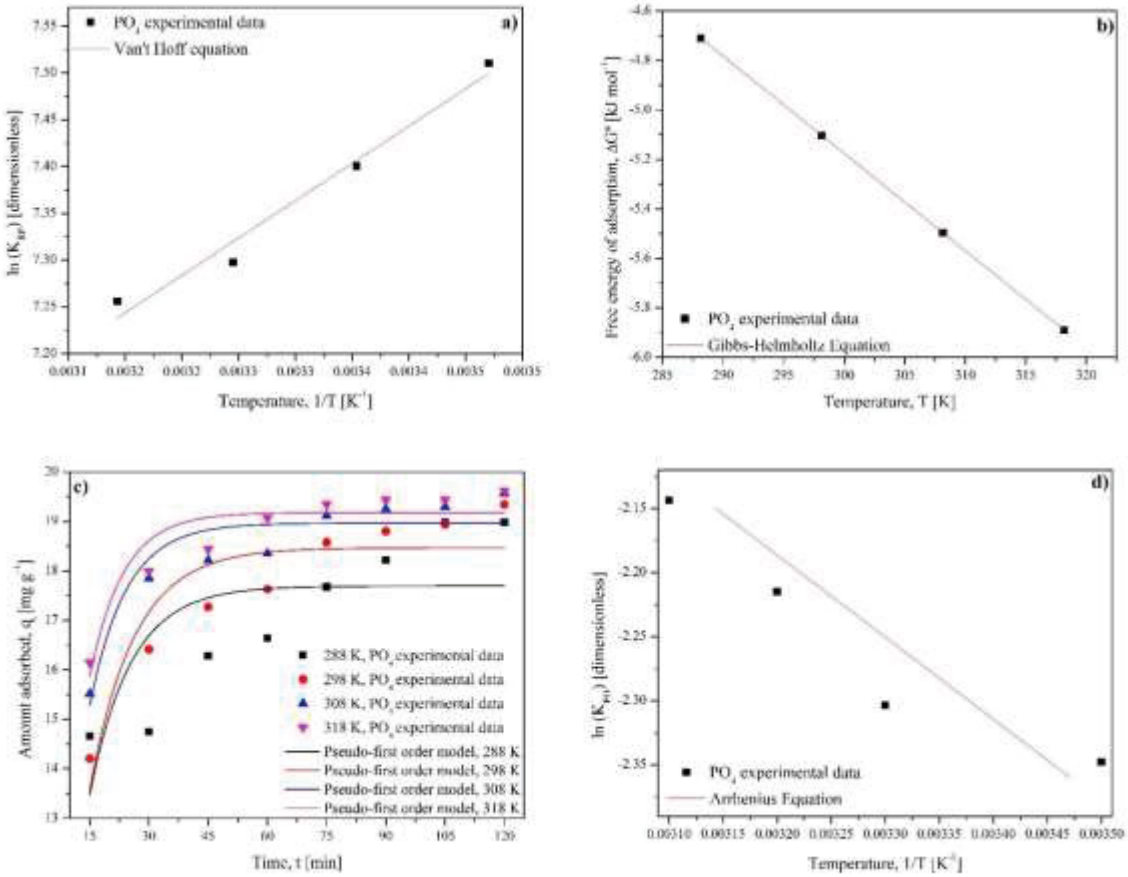

TABLE 10 - THERMODYNAMIC PARAMETERS OF THE EXPERIMENT.

T (K)	Ea (kJ mol^{-1})	ΔSº (kJ mol^{-1} K^{-1})	ΔHº (kJ mol^{-1})	ΔG (kJ mol^{-1})
288	5.31	0.04	6.63	-4.71
298				-5.10
308				-5.50
318				-5.89

Fig. 13 a) shows the Van't Hoff plot for the adsorption of the IC dye onto PO_4 activated carbon, once the Redlich-Peterson model fitted the isotherm data in the best way, the values of the k_{RP} constant were used in the Van't Hoff equation (eq. 15) to determine ΔSº and ΔHº and their values are shown in Table 10, 0.04 kJ mol^{-1} K^{-1} and 6.63 kJ mol^{-1}, respectively.

The positive value of ΔHº indicates that the process is endothermic, being justified by the fact that when the temperature is increased, the amount of adsorbate adsorbed by the adsorbent increases as well, respecting the Le Chatelier's principle of chemical equilibrium disturbance [76].

Also, ΔHº smaller than 40 kJ mol^{-1} suggests that a physisorption process is dominant; while the positive value of ΔSº suggests an increase in the degrees of freedom (randomness) at the solid-solution interface during the adsorption of IC dye onto PO_4 activated carbon [49].

Fig. 13 b) shows the Gibbs-Helmholtz plot (eq. 16) for the adsorption process in different temperatures, and the values of ΔGº are summarized in Table 10. The negative values of free energy indicate that the adsorption process was spontaneous and thermodynamically favorable, the higher the value of ΔGº the greater is the driving force of adsorption, resulting in a higher adsorption capacity. For the physisorption process, the ΔGº range is between -20 and 0 kJ mol^{-1}, which includes the values that came from this study and corroborates with the information obtained with ΔHº [49-76].

The pseudo-first order model was the one that obtained the higher R^2 in the kinetics test, so the same test was carried out; however, with varying reaction temperatures. The results are shown in Fig. 13 c) and the rate constant were expressed as a function of temperature by the Arrhenius equation (eq. 17) in Fig. 13 d) and the slope is the activation energy, E_a.

The activation energy of this study was E_a = 5.31 kJ mol^{-1} (Table 10), usually physisorption processes have activation energy in the range of 5-40 kJ mol^{-1}. Lazaridis and Asouhidou [77] stated that in an adsorption process with E_a lower than 25-30 kJ mol^{-1}, the diffusion process is the governing mechanism in the adsorption of the liquid

phase molecules on the surface of the solid phase, corroborating with the results obtained from the intra-particle diffusion model (eq. 8) shown in Table 8.

Therefore, ΔH^o, ΔG^o and E_a all suggested that the nature of the physisorption process of IC dye molecules onto PO_4 activated carbon surface. Khadhri et al. and Harrache et al. [78-79], when studying the adsorption of the Indigo Carmine dye on activated carbon they also concluded that the adsorptive process is mainly physical, endothermic and spontaneous.

3.2.5 Batch test

The results of the statistical analysis of batch tests are shown in Table 11 and Fig. 14.

TABLE 11 - ANOVA RESULTS FOR THE QUADRATIC MODEL OF RESPONSE SURFACE.

Source	DF	Sum of squares	Mean square	F value	p-value
pH	1	55.84	55.84	14.65	0.012
pH^2	1	19.77	19.77	5.18	0.072
Reaction Temperature	1	1.42	1.42	0.37	0.569
Reaction Temperature^2	1	7.35	7.35	1.93	0.224
Residual	5	19.06	3.81		
Total	9	96.88			
		R^2 = 0.8032	R^2_{adj} = 0.6458		
Fitted function		$z = 1.861 + 2.354\ x - 0.231\ x^2 + 0.803\ y - 0.0127\ y^2$			(18)

where: z (mg g^{-1}) is the amount of dye adsorbed; x (dimensionless) is pH; y (ºC) is reaction temperature.

FIGURE 14 - STATISTICAL ANALYSIS OF THE EXPERIMENT.
(PARAMETERS: C_0 = 10 mg L^{-1}, C_{ads} = 0.5 g L^{-1}, t_{eq} = 105 min, V = 50 mL)

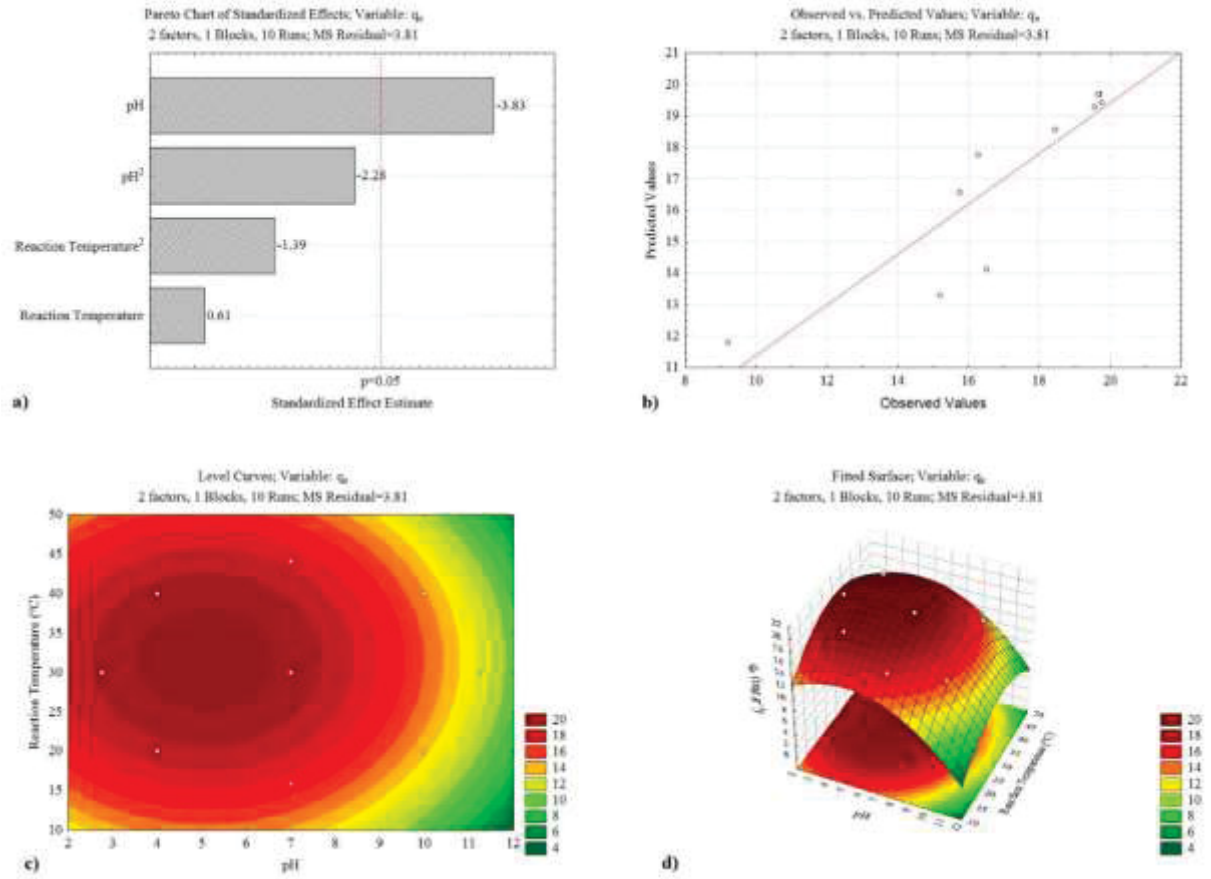

It was possible to evaluate how the factors interfered in the response variable by observing the Pareto chart in Fig. 14 a), where the factor x (pH) had a significant statistical effect on the quantity of dye adsorbed (q_e) in a significance level of 5%. This result can also be observed in the Anova table (Table 11), where the variable pH was the only one that had a p-value < 0.05. The residual error of the experiment was $\sqrt{3.81}$ = 1.95 (see the value in column 4, row 6 in Table 11).

In Fig. 14 b) the plot between the predicted and observed values is shown, it was possible to observe that the regression model better adjusted the data with the higher numerical value, in the region of $q_e \geq 18$ mg g^{-1}, where there is a greater concentration of data. However, when calculating the RMSE of the data, the value was approximately 1.01, which indicates that in a global context the model adjusted the experimental data satisfactorily, even with a value of R^2 = 0.8032 (Table 11).

Fig. 14 c) presents the level curves obtained in the statistical analysis, the burgundy region showed the highest values for the variable response, q_e, when the value of the x axis (pH) was between 3 and 7 and the value of the y axis (Reaction

temperature) was between 20 and 40 ºC, it shows that the best adsorptive capacity occurs in an acid reaction medium and in mild temperatures.

Moreover, Fig. 14 d) shows the response surface obtained for the factorial design; the graph has a downward-facing concavity that resembles a curve of a second-degree equation. As well as the level curves, the burgundy region showed the highest values for the quantity of indigo carmine dye adsorbed.

A second-order response surface model (Table 11, eq. 18) was obtained by using the quadratic main effects model. To optimize the factorial design and maximize the value of the variable response, q_e, the model obtained was subjected to SIMPLEX method analysis, to determine what is the optimum value of the factors, pH and reaction temperature that generate the highest quantity of indigo carmine dye adsorbed.

The calculations were performed using the solver tool in Excel®. The restrictions used in the software were the levels imposed by the factorial design, $1 \leq pH \leq 12$ and $10 \leq$ Temperature ≤ 55 ºC and the objective was the response variable itself. The optimization results were pH = 5.1 and reaction temperature = 31.6 ºC, in these experimental conditions the maximum value of $q_e = 20.5$ mg g^{-1}.

3.2.6 Reuse test

Based on all the experimental results obtained in the study, the best parameters of each variable were used to perform the reuse tests and the results are shown in Fig. 15.

FIGURE 15 - REUSABILITY TEST FOR THE IC DYE SOLUTION.
(PARAMETERS: C_0 = 10 mg L^{-1}, C_{ads} = 0.5 g L^{-1}, t_{eq} = 105 min, V = 50 mL, pH = 5, T = 32 ºC)

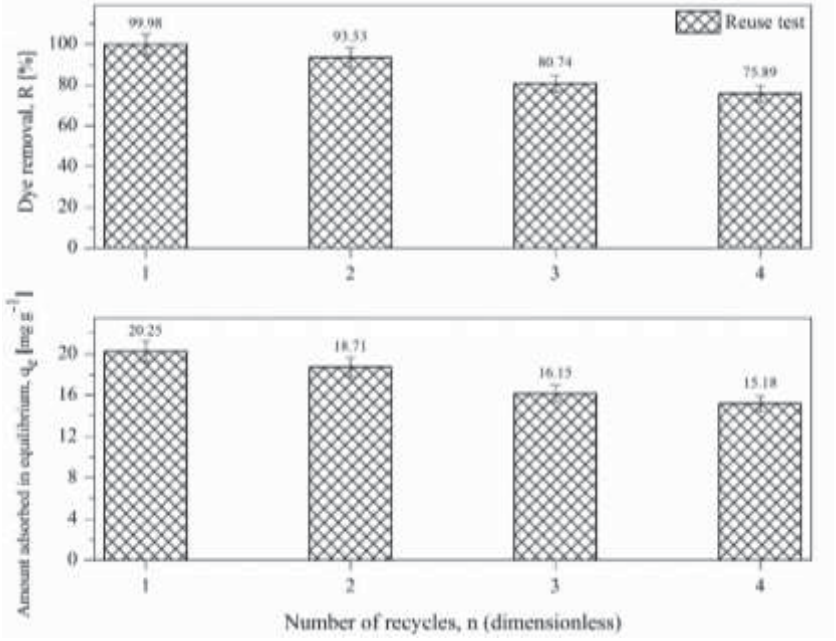

Even after four cycles, the dye removal was approximately 76%, which indicates that the activated carbon PO_4 is a possible reusable adsorbent. It is also worth mentioning that, after the first cycle, the amount of dye adsorbed was q_e = 20.25 mg g^{-1}, this value is close to the value found during the optimization of the adsorption data of the previous topic (q_e = 20.50 mg g^{-1}), showing a deviation of approximately 1.22%. The values obtained in this study are similar to those found in the literature and are shown in Table 12.

TABLE 12 - COMPARISON OF THE RESULTS OF THE REUSE TEST WITH RESULTS FROM THE LITERATURE USING ACTIVATED CARBON FROM BIOMASS.

Precursor	Adsorbate	Numbers of recycle	Final removal (%)	Reference
Residual ash	Indigo carmine dye	4	75.89	This study
Coconut shell	Malachite green dye	5	89.12	[80]
Date palm pits	Methylene blue dye	4	74.80	[81]
Waste tea residue	Acid blue 25 dye	3	92.86	[82]

3.2.7 Cost analysis

The recycling of any adsorbent is important in industries, once it decreases the costs with material during the wastewater treatment stage. In view of this fact, a cost analysis was carried out for the synthesis of PO_4 activated carbon.

The equipments were selected to meet the necessities of the synthesis described in topic 2.2, quotations were made in the state of Parana, Brazil and all the assumptions used are for a large industry that generates nearly 1,000 kg of residual ash per day. Inputs and operating time parameters are listed in Table 13.

TABLE 13 - ASSUMPTIONS FOR SCALED-UP PRODUCTION OF ACTIVATED CARBON.

Input	Amount	Unit
Residual ash	1,000	Kg day^{-1}
H_3PO_4	1,700	
$NaHCO_3$	1,500	
Water usage	200	m^3 dia^{-1}
Electricity usage	80,000	kWh
PO_4 yield	60	%
Operational days	270	days $year^{-1}$
Active operating	20	h day^{-1}

The scaled-up occurred linearly from laboratory processes and thus may include some error in the amounts of materials needed to produce the adsorbents. The values in Table 13 are an estimation of production costs, a large number of industries have their own methods for the activated carbon production, but these data are not available for the public. The analysis did not delve into characteristics such as logistical, personnel, building and equipment costs, since most of these variables depend on the country of production and considering that these expenses are present in the global budget of the industry, not taking into account the creation of a new industry for the synthesis of this material.

Cost estimates were based on a synthesis yield of approximately 60% and an input of residual ash of 1,000 kg day^{-1}, thus the daily output of PO_4 activated carbon would be around 600 kg day^{-1}. Another assumption is that 80% of the H_3PO_4 can be recovered during the washing step, concentrated and reused once, the same occurs for the $NaHCO_3$, but with a recovery rate of 20% at the end of the neutralization step. In the interest of saving costs, as well as in the bench scale synthesis, it was considered that during the carbonization stage the oven would be supplied by ambient air.

Table 14 shows the costs estimated for production of the PO_4 activated carbon.

TABLE 14 - PRODUCTION COSTS ESTIMATED FOR PO_4 ACTIVATED CARBON.

Input	**Cost**
Residual ash	none
H_3PO_4	2,350 USD day^{-1}
$NaHCO_3$	1,450 USD day^{-1}
Water usage	360 USD day^{-1}
Electricity usage	1,450 USD day^{-1}
Variable	**Total**
Operational cost	5,610 USD day^{-1}
Production rate	600 kg day^{-1}
Unit production cost	9.35 USD kg^{-1}

Based on the daily production of 1,000 kg of residual ash and an operational cost of 5,610.00 USD, PO_4 activated carbon would cost approximately 9.35 USD per kg. This value is higher concerning other values of activated carbon production found in the literature, such as, 2.89 USD kg^{-1} for pecan shells activated with phosphoric acid [83] or 2.82 USD kg^{-1} for almond shells activated with phosphoric acid [84]. However, none of these studies presented industrial applications for the obtained adsorbents and their process yield.

The adsorbent in our study is capable of treating approximately 5,500 L of IC dye solution with 1 kg of material considering four reuse cycles. If compared with the commercial 4-µm activated carbon used during this study, the price of the kg of this adsorbent is approximately 13 USD kg^{-1} (Synth®), approximately 40% more expensive than activated carbon synthesized with H_3PO_4, reinforcing that the obtained adsorbent presents a beneficial cost for application in an industrial environment in the treatment of effluents step.

3.3 CHARACTERIZATION AFTER ADSORPTION PROCESS

Table 15 shows the BET surface areas (S_o), mean pore diameter (d_p) and pore volumes (V_p) for the PO_4 activated carbon after the adsorption process in the equilibrium time.

TABLE 15 - TEXTURAL PROPERTIES OF THE PO_4 ACTIVATED CARBON AFTER ADSORPTION PROCESS.

Adsorbent	**S_o (m^2 g^{-1})**	**V_p (cm^3 g^{-1})**	**d_p (nm)**
before	605.1	0.01	2.01
after	297.8	0.17	1.17

All the studied parameters (Table 15) had a reduction in their values after the adsorption process. The reason for this is that during the adsorptive process, the number of active sites of the adsorbent tends to decrease with the reaction time, since the dye molecules adhere to the surface of the material. This makes a smaller number of pores available for the N_2 used in the adsorption/desorption measures can percolate the material, thus causing the equipment to accuse a lower value in the readings, which makes sense, since the adsorbate molecules are attached to the surface of the material.

Fig. 16 shows the N_2 adsorption-desorption isotherms and the SEM images for the PO_4 activated carbon after the adsorption process in the equilibrium time.

FIGURE 16 - N_2 ADSORPTION-DESORPTION ISOTHERMS AND SEM IMAGES AT MAGNIFICATION OF 500X OF PO_4 ACTIVATION CARBON AFTER ADSORPTION PROCESS.

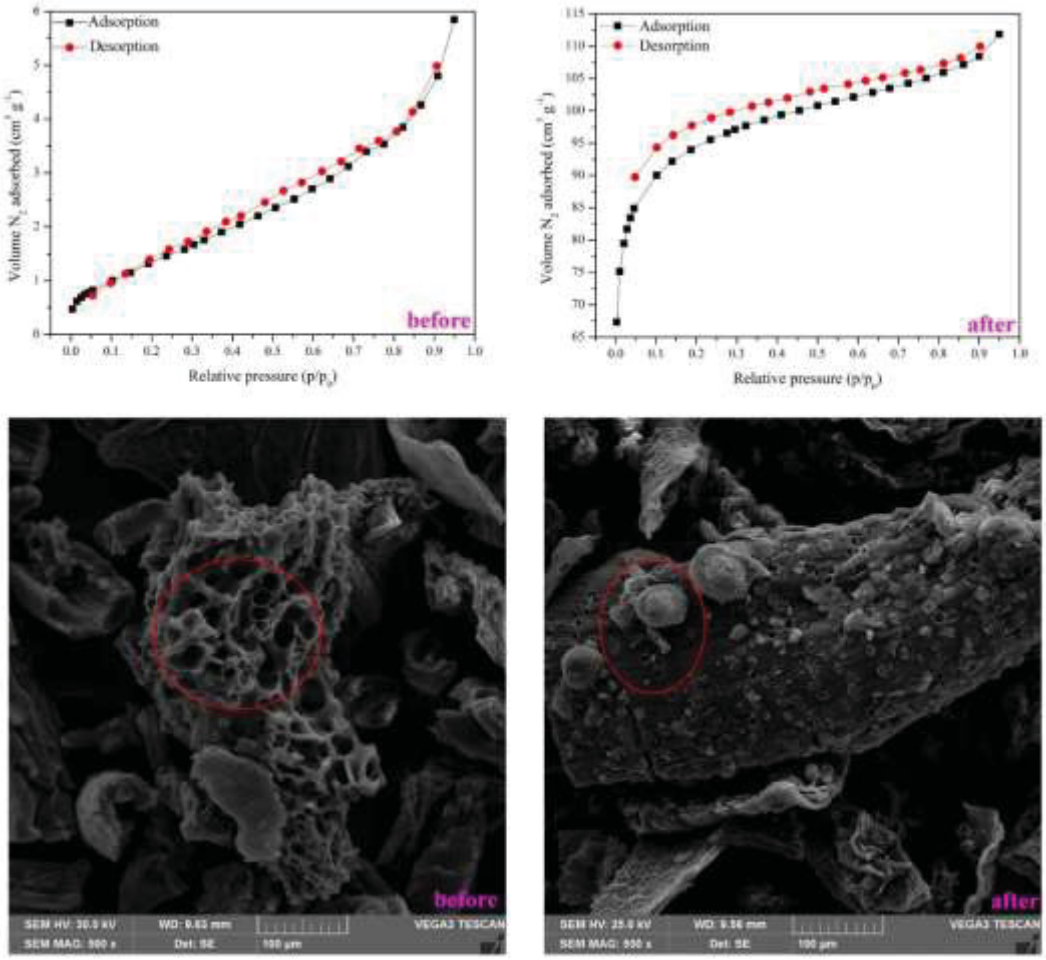

It was possible to observe that the N_2 adsorption/desorption isotherm had a change in its shape, starting as an isotherm that resembles a type II , characteristic of microporous and mesoporous material, and then morphed into a type I isotherm,

characteristic of microporous material, according to the IUPAC classification [55]. This change of shape is inherent to the alterations observed in Table 15, when observing the mean pore diameter values, before the adsorption process the material appeared to have a mixture of mesopores and micropores in the structure and after the adsorption only micropores.

This decrease in the presence of mesopores in the material structure happens due to the preference for the dye molecules to be adsorbed in larger pores, due to the size-exclusion effect, where molecules with high molecular mass, as is the case of dyes, preferentially adhere to mesopores rather than micropores [85].

Observing the SEM images in Fig. 16, it was possible to notice that before the adsorptive process, the material had high pore dispersion on the surface, while after the adsorption process dye molecules could be found to be adsorbed on the surface of the material, confirming the removal of the IC dye from the aqueous solution.

Fig. 17 shows the SEM images for the PO_4 activated carbon during the kinetic experiment.

FIGURE 17 - SEM IMAGES AT MAGNIFICATION OF 1,000X OF PO_4 ADSORBENT DURING THE KINETIC EXPERIMENT.

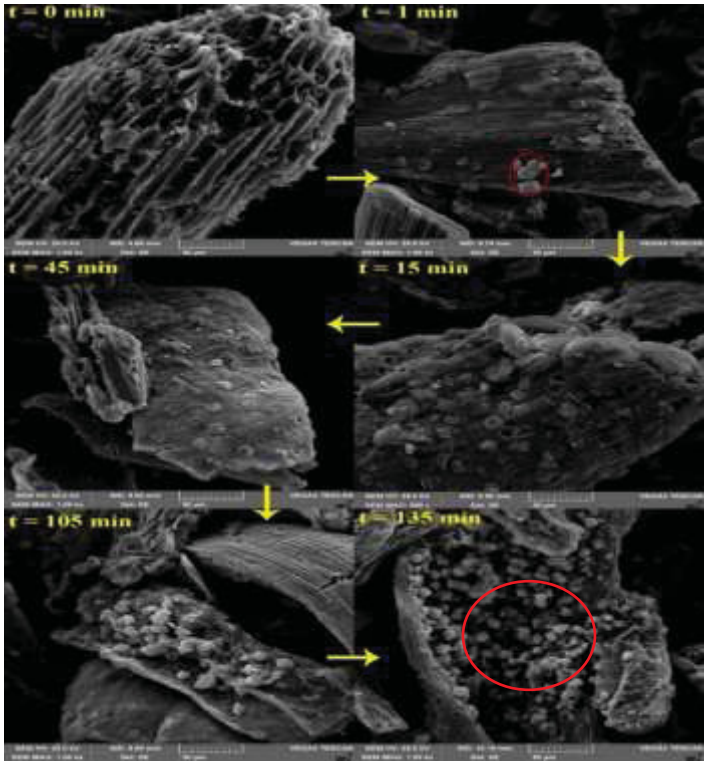

It was possible to notice that over time more and more molecules of adsorbate were being adhered to the surface of the adsorbent during the kinetic tests, until

equilibrium time (t_e = 105 min), where all the dye was removed from the liquid phase and transferred to the surface of the solid phase of the PO_4 activated carbon.

Fig. 18 shows the SEM images for the PO_4 activated carbon during the reuse test.

FIGURE 18 - SEM IMAGES AT MAGNIFICATION OF 2,500X OF PO_4 ADSORBENT DURING THE REUSE EXPERIMENT.

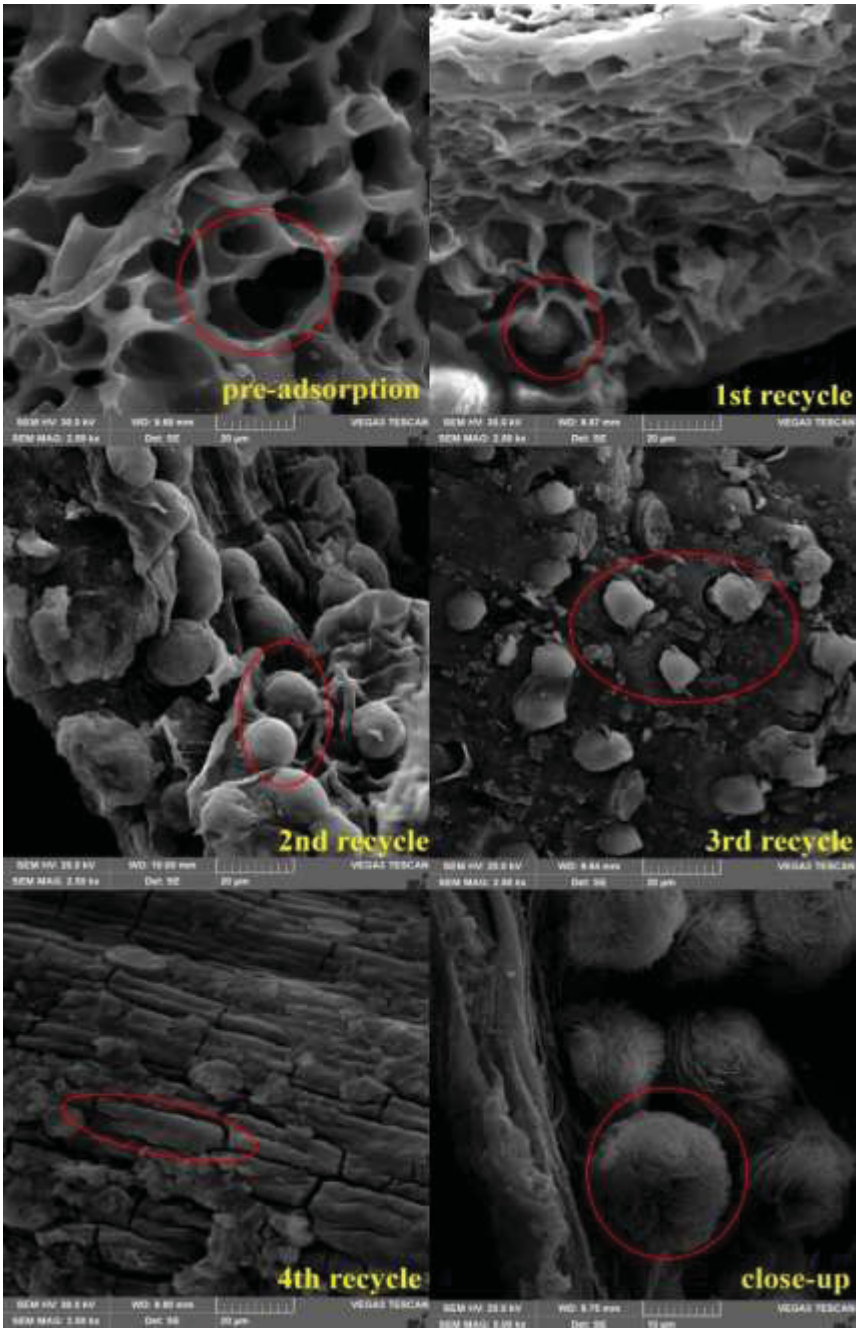

It was possible notice that before the adsorptive process, the material had a high distribution of pores on the surface, during the first recycling, some dye molecules

started to adhere to the adsorbent surface and in consecutive reuses the amount increased, until the last recycling, when a large part of the pores on the surface of the material was occupied by molecules of the liquid phase, causing the amount of IC dye adsorbed to be lesser than in the previous cycle.

In addition, out of curiosity, a SEM image was added with a close-up on a dye molecule, in order to illustrate the shape of these adsorbates on a microscopic scale, these molecules have a circular shape with a kind of hair on the surface, resembling a hairball.

4 CONCLUSIONS

It can be concluded that three types of residual ash based activated carbons were prepared using different methods of chemical activation. Through characterization analysis, all materials changed the initial characteristics of the raw material and somehow influenced its adsorptive capacity. The PO_4 activated carbon, presented the best performance in the preliminary adsorption tests, where approximately 98% of the dye molecules were removed from the solution. Having this fact in mind, it was chosen as the studied adsorbent. The surface area of the RAs increased from 120.3 to 605.1 $m^2\ g^{-1}$ when H_3PO_4 was used as an activator, which shows that this synthesis method produced a high quality adsorbent, with an excellent cost benefit, being it possible to be produced at a price of 9.35 USD kg^{-1}, a lower price than the commercial activated carbon and can be reused up to four times, being a promising candidate for application in an industrial environment.

The Redlich-Peterson isotherm model provided a better fit to the experimental data for IC dye adsorption on the PO_4 adsorbent and the maximum adsorption capacity was approximately 100 mg g^{-1} according to the Langmuir model. The kinetic study showed that the adsorption process occurred in two stages and the pseudo-first order kinetic model better described both. The thermodynamic parameters involved in the adsorption mechanism, showed that it was a spontaneous and favorable process, and due to its endothermic nature, an increase in temperature leads to an increase in the amount IC dye molecules adsorbed.

REFERENCES

[1] K. Hui, C. Chao, S. Kot, Removal of mixed heavy metal ions in wastewater by zeolite 4A and residual products from recycled coal fly ash, J. Hazard Mater. 127 (2005) 89–101. https://doi.org/10.1016/j.jhazmat.2005.06.027.

[2] F. Canpolat, K. Yılmaz, M.M. Köse, M. Sümer, M.A. Yurdusev, Use of zeolite, coal bottom ash and fly ash as replacement materials in cement production, Cement Concrete Res. 34 (2004) 731–735. https://doi.org/10.1016/s0008-8846(03)00063-2.

[3] A. Rastogi, V. Kumar Paul, A Critical Review of the Potential for Fly Ash Utilisation in Construction-Specific Applications in India, Environ. Res. Eng. Manag. 76 (2020) 65–75. https://doi.org/10.5755/j01.erem.76.2.25166.

[4] D. Zgureva, V. Stoyanova, A. Shoumkova, S. Boycheva, G. Avdeev, Quasi Natural Approach for Crystallization of Zeolites from Different Fly Ashes and Their Application as Adsorbent Media for Malachite Green Removal from Polluted Waters, Crystals. 10 (2020) 1064. https://doi.org/10.3390/cryst10111064.

[5] D. Zgureva, S. Boycheva, D. Behunová, M. Václavíková, Smart- and Zero-Energy Utilization of Coal Ash from Thermal Power Plants in the Context of Circular Economy and Related to Soil Recovery, J. Environ. Eng. 146 (2020) 04020081. https://doi.org/10.1061/(asce)ee.1943-7870.0001752.

[6] C. Baek, J. Seo, M. Choi, J. Cho, J. Ahn, K. Cho, Utilization of CFBC Fly Ash as a Binder to Produce In-Furnace Desulfurization Sorbent, Sustainability. 10 (2018) 4854. https://doi.org/10.3390/su10124854.

[7] S. Bukhari, S. Rohani, Continuous Flow Synthesis of Zeolite-A from Coal Fly Ash Utilizing Microwave Irradiation with Recycled Liquid Stream, Am. J. Environ. Sci. 13 (2017) 233–244. https://doi.org/10.3844/ajessp.2017.233.244.

[8] W. Feng, Z. Wan, J. Daniels, Z. Li, G. Xiao, J. Yu, D. Xu, H. Guo, D. Zhang, E.F. May, G. (Kevin) Li, Synthesis of high quality zeolites from coal fly ash: Mobility of hazardous elements and environmental applications, J. Clean. Prod. 202 (2018) 390–400. https://doi.org/10.1016/j.jclepro.2018.08.140.

[9] J. Andrés, A. Valero, A. Medinaceli, A. Alastuey, X. Querol, N. Moreno, A. Soler, C. Ibáñez, Synthesis of high ion exchange zeolites from coal fly ash, Geol. Acta. 5 (2007) 47–55.

[10] S. Varandani, P. Prabhu, Zeolite A from Fly ash: Synthesis and Characterization, Int. J. Chem. 533 (2016) 313–323.

[11] L.E.N. Castro, J.V.F. Santos, K.C. Fagnani, H.J. Alves, L.M.S. Colpini, Evaluation of the effect of different treatment methods on sugarcane vinasse remediation, J. Environ. Sci. Heal. B. 54 (2019) 791–800. https://doi.org/10.1080/03601234.2019.1669981.

[12] J.F. Nure, N.T. Shibeshi, S.L. Asfaw, W. Audenaert, S.W.H.V. Hulle, COD and colour removal from molasses spent wash using activated carbon produced from bagasse fly ash of Matahara sugar factory, Oromiya region, Ethiopia, Water SA. 43 (2017) 470–479. https://doi.org/10.4314/wsa.v43i3.12.

[13] M.B. Ahmed, M.A. Hasan Johir, J.L. Zhou, H.H. Ngo, L.D. Nghiem, C. Richardson, M.A. Moni, M.R. Bryant, Activated carbon preparation from biomass feedstock: Clean production and carbon dioxide adsorption, J. Clean. Prod. 225

(2019) 405–413. https://doi.org/10.1016/j.jclepro.2019.03.342.

[14] M.J. Prauchner, F. Rodríguez-Reinoso, Chemical versus physical activation of coconut shell: A comparative study, Micropor. Mesopor. Mat. 152 (2012) 163–171. https://doi.org/10.1016/j.micromeso.2011.11.040.

[15] T. Guimarães, A.P. de Carvalho Teixeira, A.F. de Oliveira, R.P. Lopes, Biochars obtained from arabica coffee husks by a pyrolysis process: characterization and application in Fe(ii) removal in aqueous systems, New J. Chem. 44 (2020) 3310–3322. https://doi.org/10.1039/c9nj04144c.

[16] Ç. Öter, Ö. Selçuk Zorer, Adsorption behaviours of Th(IV) and U(VI) using nitric acid (HNO3) modified activated carbon: equilibrium, thermodynamic and kinetic studies, Int. J. Environ. An. Ch. (2019) 1–16. https://doi.org/10.1080/03067319.2019.1691184.

[17] A.H. Jawad, R. Abd Rashid, K. Ismail, S. Sabar, High surface area mesoporous activated carbon developed from coconut leaf by chemical activation with H3PO4 for adsorption of methylene blue, Desalin. Water Treat. 74 (2017) 326–335. https://doi.org/10.5004/dwt.2017.20571.

[18] T.M. Darweesh, M.J. Ahmed, Batch and fixed bed adsorption of levofloxacin on granular activated carbon from date (Phoenix dactylifera L.) stones by KOH chemical activation, Environ. Toxicol. Phar. 50 (2017) 159–166. https://doi.org/10.1016/j.etap.2017.02.005.

[19] H.N. Tran, S.-J. You, H.-P. Chao, Fast and efficient adsorption of methylene green 5 on activated carbon prepared from new chemical activation method, J. Environ. Manage. 188 (2017) 322–336. https://doi.org/10.1016/j.jenvman.2016.12.003.

[20] J.F. Vivo-Vilches, A.F. Pérez-Cadenas, F.J. Maldonado-Hódar, F. Carrasco-Marín, R.P.V. Faria, A.M. Ribeiro, A.F.P. Ferreira, A.E. Rodrigues, Biogas upgrading by selective adsorption onto CO 2 activated carbon from wood pellets, J. Environ. Chem. Eng. 5 (2017) 1386–1393. https://doi.org/10.1016/j.jece.2017.02.015.

[21] S.S. Lam, M.H. Su, W.L. Nam, D.S. Thoo, C.M. Ng, R.K. Liew, P.N. Yuh Yek, N.L. Ma, D.V. Nguyen Vo, Microwave Pyrolysis with Steam Activation in Producing Activated Carbon for Removal of Herbicides in Agricultural Surface Water, Ind. Eng. Chem. Research. 58 (2018) 695–703. https://doi.org/10.1021/acs.iecr.8b03319.

[22] L. Chandana, K. Krushnamurty, D. Suryakala, Ch. Subrahmanyam, Low-cost adsorbent derived from the coconut shell for the removal of hexavalent chromium from aqueous medium, Mater. Today-Proc. (2019). https://doi.org/10.1016/j.matpr.2019.04.205.

[23] M. Li, R. Xiao, Preparation of a dual Pore Structure Activated Carbon from Rice Husk Char as an Adsorbent for CO2 Capture, Fuel Process. Technol. 186 (2019) 35–39. https://doi.org/10.1016/j.fuproc.2018.12.015.

[24] J.A. Maciá-Agulló, B.C. Moore, D. Cazorla-Amorós, A. Linares-Solano, Activation of coal tar pitch carbon fibres: Physical activation vs. chemical activation, Carbon. 42 (2004) 1367–1370. https://doi.org/10.1016/j.carbon.2004.01.013.

[25] O. Üner, Ü. Geçgel, Y. Bayrak, Preparation and characterization of mesoporous activated carbons from waste watermelon rind by using the chemical activation method with zinc chloride, Arab. J. Chem. 12 (2019) 3621–3627. https://doi.org/10.1016/j.arabjc.2015.12.004.

[26] L.E.N. de Castro, E.C. Meurer, H.J. Alves, M.A.R. dos Santos, E. de C. Vasques, L.M.S. Colpini, Photocatalytic Degradation of Textile dye Orange-122 Via Electrospray Mass Spectrometry, Braz. Arch. Biol. Tech. 63 (2020). https://doi.org/10.1590/1678-4324-2020180573.

[27] K.C. Fagnani, H.J. Alves, L.E.N. de Castro, S.S. Kunh, L.M.S. Colpini, An alternative for the energetic exploitation of sludge generated in the physico-chemical effluent treatment from poultry slaughter and processing in Brazilian industries, J. Environ. Chem. Eng. 7 (2019) 102996. https://doi.org/10.1016/j.jece.2019.102996.

[28] A.L. Ahmad, S. Sumathi, B.H. Hameed, Coagulation of residue oil and suspended solid in palm oil mill effluent by chitosan, alum and PAC, Chem. Eng. J. 118 (2006) 99–105. https://doi.org/10.1016/j.cej.2006.02.001.

[29] M.A. Aboulhassan, S. Souabi, A. Yaacoubi, M. Baudu, Improvement of paint effluents coagulation using natural and synthetic coagulant aids, J. Hazard Mater. 138 (2006) 40–45. https://doi.org/10.1016/j.jhazmat.2006.05.040.

[30] V. Golob, A. Vinder, M. Simonic, Efficiency of the coagulation/flocculation method for the treatment of dyebath effluents, Dyes Pigments. 67 (2005) 93–97. https://doi.org/10.1016/j.dyepig.2004.11.003.

[31] M. Chowdhury, M.G. Mostafa, T.K. Biswas, A.K. Saha, Treatment of leather industrial effluents by filtration and coagulation processes, Wat. Reso. Ind. 3 (2013) 11–22. https://doi.org/10.1016/j.wri.2013.05.002.

[32] W. Qasim, A.V. Mane, Characterization and treatment of selected food industrial effluents by coagulation and adsorption techniques, Wat. Reso. Ind. 4 (2013) 1–12. https://doi.org/10.1016/j.wri.2013.09.005.

[33] C. Allegre, M. Maisseu, F. Charbit, P. Moulin, Coagulation–flocculation–decantation of dye house effluents: concentrated effluents, J. Hazard Mater. 116 (2004) 57–64. https://doi.org/10.1016/j.jhazmat.2004.07.005.

[34] G.L. Dotto, G. McKay, Current scenario and challenges in adsorption for water treatment, J. Environ. Chem. Eng. 8 (2020) 103988. https://doi.org/10.1016/j.jece.2020.103988.

[35] S. Barakan, V. Aghazadeh, The advantages of clay mineral modification methods for enhancing adsorption efficiency in wastewater treatment: a review, Environ. Sci. Pollut. R. 28 (2020) 2572–2599. https://doi.org/10.1007/s11356-020-10985-9.

[36] N.S. Azmi, K.F.Md. Yunos, Wastewater Treatment of Palm Oil Mill Effluent (POME) by Ultrafiltration Membrane Separation Technique Coupled with Adsorption Treatment as Pre-treatment, Agric. Agric. Sci. Proc. 2 (2014) 257–264. https://doi.org/10.1016/j.aaspro.2014.11.037.

[37] A.C. Lua, T. Yang, Effect of activation temperature on the textural and chemical properties of potassium hydroxide activated carbon prepared from pistachio-nut shell, J. Colloid Interf. Sci. 274 (2004) 594–601. https://doi.org/10.1016/j.jcis.2003.10.001.

[38] P. Patnukao, P. Pavasant, Activated carbon from Eucalyptus camaldulensis Dehn bark using phosphoric acid activation, Bioresource Technol. 99 (2008) 8540–8543. https://doi.org/10.1016/j.biortech.2006.10.049.

[39] R.R.A. Rios, D.E. Alves, I. Dalmázio, S.F.V. Bento, C.L. Donnici, R.M. Lago, Tailoring activated carbon by surface chemical modification with O, S, and N containing molecules, Mater. Res. 6 (2003) 129–135. https://doi.org/10.1590/s1516-

14392003000200004.

[40] S. Lagergreen, Zur Theorie der sogenannten Adsorption gelöster Stoffe, Z. Chem. 24 (1898) 1–39. https://doi.org/10.1007/bf01501332.

[41] Y.S. Ho, G. McKay, Sorption of dye from aqueous solution by peat, Chem. Eng. J. 70 (1998) 115–124. https://doi.org/10.1016/s0923-0467(98)00076-1.

[42] A.R. Cestari, E.F.S. Vieira, E.C.N. Lopes, R.G. da Silva, Kinetics and equilibrium parameters of Hg(II) adsorption on silica-dithizone, J. Colloid Interf. Sci. 272 (2004) 271–276. https://doi.org/10.1016/j.jcis.2003.09.019.

[43] M.J.D. Low, Kinetics of Chemisorption of Gases on Solids. Chem. Rev. 60 (1960) 267–312. https://doi.org/10.1021/cr60205a003.

[44] D.M. Ruthven, Principles of adsorption and adsorption processes, Wiley, New York, 1984.

[45] I. Langmuir, The constitution and fundamental properties of solids and liquids. part i. solids., J. Am. Chem. Soc. 38 (1916) 2221–2295. https://doi.org/10.1021/ja02268a002.

[46] H.M.F. Freundlich, Over the absorption in solution., J. Phys. Chem-US. 57 (1906) 385–470.

[47] O. Redlich, D.L. Peterson, A Useful Adsorption Isotherm, J. Phys. Chem-US. 63 (1959) 1024–1024. https://doi.org/10.1021/j150576a611.

[48] M.I. Temkin, V.P. Pyzhev, Kinetics of ammonia synthesis over a promoted iron catalyst, Zh. Fiz. Khim. 7 (1939) 851–867.

[49] B.H. Hameed, A.A. Ahmad, N. Aziz, Isotherms, kinetics and thermodynamics of acid dye adsorption on activated palm ash, Chem. Eng. J. 133 (2007) 195–203. https://doi.org/10.1016/j.cej.2007.01.032.

[50] AACE. Association for the Advancement of Cost Engineering International, Conducting Technical and Economic Evaluations - As Applied for the Process and Utility Industries, AACE recommended practices and standards, ACE International, 1990.

[51] Q. Han, J. Wang, B.A. Goodman, J. Xie, Z. Liu, High adsorption of methylene blue by activated carbon prepared from phosphoric acid treated eucalyptus residue, Powder Technol. 366 (2020) 239–248. https://doi.org/10.1016/j.powtec.2020.02.013.

[52] Y.K. Allo, Sudarmono, O. Togibasa, Synthesis and Characterization of Activated Carbon from Sago Waste (Metroxylon sagu) with ZnCl2 Activation and HNO3 Modification, J. Idn. Chem. Soc. 2 (2019) 48. https://doi.org/10.34311/jics.2019.02.1.48.

[53] G.V.S. Sarma, K.S. Rani, K.S. Chandra, B.K. Babu, K.V. Ramesh, Potential removal of phenol using modified laterite adsorbent, Indian J. Biochem. Bio. 57 (2020) 613–619.

[54] K. K.M, N. Abdullah, A. P., Brewery Spent Grain: Chemical Characteristics and utilization as an Enzyme Substrate, Malay. J. Sci. 29 (2010) 41–51. https://doi.org/10.22452/mjs.vol29no1.7.

[55] K.S.W. Sing, Reporting physisorption data for gas/solid systems with special reference to the determination of surface area and porosity (Provisional), Pure Appl. Chem. 54 (1982) 2201–2218. https://doi.org/10.1351/pac198254112201.

[56] Z. ALOthman, A Review: Fundamental Aspects of Silicate Mesoporous Materials, Materials. 5 (2012) 2874–2902. https://doi.org/10.3390/ma5122874.

[57] V. Benedetti, F. Patuzzi, M. Baratieri, Characterization of char from biomass gasification and its similarities with activated carbon in adsorption applications, Appl. Energ. 227 (2018) 92–99. https://doi.org/10.1016/j.apenergy.2017.08.076.

[58] X.-L. Su, J.-R. Chen, G.-P. Zheng, J.-H. Yang, X.-X. Guan, P. Liu, X.-C. Zheng, Three-dimensional porous activated carbon derived from loofah sponge biomass for supercapacitor applications, Appl. Surf. Sci. 436 (2018) 327–336. https://doi.org/10.1016/j.apsusc.2017.11.249.

[59] M. Song, W. Zhang, Y. Chen, J. Luo, J.C. Crittenden, The preparation and performance of lignin-based activated carbon fiber adsorbents for treating gaseous streams, Front. Chem. Sci. Eng. 11 (2017) 328–337. https://doi.org/10.1007/s11705-017-1646-y.

[60] R. Bardestani, G.S. Patience, S. Kaliaguine, Experimental methods in chemical engineering: specific surface area and pore size distribution measurements—BET, BJH, and DFT, Can. J. Chem. Eng. 97 (2019) 2781–2791. https://doi.org/10.1002/cjce.23632.

[61] Md.A. Islam, S. Sabar, A. Benhouria, W.A. Khanday, M. Asif, B.H. Hameed, Nanoporous activated carbon prepared from karanj (Pongamia pinnata) fruit hulls for methylene blue adsorption, J. Taiwan Inst. Chem. E. 74 (2017) 96–104. https://doi.org/10.1016/j.jtice.2017.01.016.

[62] O. Pezoti Junior, A.L. Cazetta, R.C. Gomes, É.O. Barizão, I.P.A.F. Souza, A.C. Martins, T. Asefa, V.C. Almeida, Synthesis of ZnCl2-activated carbon from macadamia nut endocarp (Macadamia integrifolia) by microwave-assisted pyrolysis: Optimization using RSM and methylene blue adsorption, J. Anal. Appl. Pyrol. 105 (2014) 166–176. https://doi.org/10.1016/j.jaap.2013.10.015.

[63] M.C. Ncibi, R. Ranguin, M.J. Pintor, V. Jeanne-Rose, M. Sillanpää, S. Gaspard, Preparation and characterization of chemically activated carbons derived from Mediterranean Posidonia oceanica (L.) fibres, J. Anal. Appl. Pyrol. 109 (2014) 205–214. https://doi.org/10.1016/j.jaap.2014.06.010.

[64] A. Namane, A. Mekarzia, K. Benrachedi, N. Belhanechebensemra, A. Hellal, Determination of the adsorption capacity of activated carbon made from coffee grounds by chemical activation with ZnCl and HPO, J. Hazard Mater. 119 (2005) 189–194. https://doi.org/10.1016/j.jhazmat.2004.12.006.

[65] Y. Luo, D. Li, Y. Chen, X. Sun, Q. Cao, X. Liu, The performance of phosphoric acid in the preparation of activated carbon-containing phosphorus species from rice husk residue, J. Mater. Sci. 54 (2018) 5008–5021. https://doi.org/10.1007/s10853-018-03220-x.

[66] M.D. Pavlović, A.V. Buntić, K.R. Mihajlovski, S.S. Šiler-Marinković, D.G. Antonović, Ž. Radovanović, S.I. Dimitrijević-Branković, Rapid cationic dye adsorption on polyphenol-extracted coffee grounds—A response surface methodology approach, J. Taiwan Inst. Chem. E. 45 (2014) 1691–1699. https://doi.org/10.1016/j.jtice.2013.12.018.

[67] M. Benadjemia, L. Millière, L. Reinert, N. Benderdouche, L. Duclaux, Preparation, characterization and Methylene Blue adsorption of phosphoric acid activated carbons from globe artichoke leaves, Fuel Process. Technol. 92 (2011)

1203–1212. https://doi.org/10.1016/j.fuproc.2011.01.014.

[68] Z. Xiaobo, Z. Jiewen, M.J.W. Povey, M. Holmes, M. Hanpin, Variables selection methods in near-infrared spectroscopy, Anal. Chim. Acta. 667 (2010) 14–32. https://doi.org/10.1016/j.aca.2010.03.048.

[69] A.B.D. Nandiyanto, R. Oktiani, R. Ragadhita, How to Read and Interpret FTIR Spectroscope of Organic Material, Indones. J. Sci. Technol. 4 (2019) 97–118. https://doi.org/10.17509/ijost.v4i1.15806.

[70] S.Y. Lee, H.E. Shim, J.E. Yang, Y.J. Choi, J. Jeon, Continuous Flow Removal of Anionic Dyes in Water by Chitosan-Functionalized Iron Oxide Nanoparticles Incorporated in a Dextran Gel Column, Nanomaterials. 9 (2019) 1164. https://doi.org/10.3390/nano9081164.

[71] W. Chen, X. Zhang, M. Mamadiev, Z. Wang, Sorption of perfluorooctane sulfonate and perfluorooctanoate on polyacrylonitrile fiber-derived activated carbon fibers: in comparison with activated carbon, RSC Advances. 7 (2017) 927–938. https://doi.org/10.1039/c6ra25230c.

[72] F. Manzotti, O.A.A. dos Santos, Evaluation of removal and adsorption of different herbicides on commercial organophilic clay, Chem. Eng. Commun.. 206 (2019) 1515–1532. https://doi.org/10.1080/00986445.2019.1601626.

[73] Warren Lee Mccabe, Julian Cleveland Smith, P. Harriott, Unit operations of chemical engineering., Mcgraw-Hill, Boston, 2005.

[74] C.H. Giles, T.H. MacEwan, S.N. Nakhwa, D. Smith, Studies in adsorption. Part XI. A system of classification of solution adsorption isotherms, and its use in diagnosis of adsorption mechanisms and in measurement of specific surface areas of solids, J. Chem. Soc. 111 (1960) 3973–3993. https://doi.org/10.1039/JR9600003973.

[75] T.A. Saleh, S.O. Adio, M. Asif, H. Dafalla, Statistical analysis of phenols adsorption on diethylenetriamine-modified activated carbon, J. Clean. Prod. 182 (2018) 960–968. https://doi.org/10.1016/j.jclepro.2018.01.242.

[76] C.-H. Wu, Adsorption of reactive dye onto carbon nanotubes: Equilibrium, kinetics and thermodynamics, J. Hazard Mater. 144 (2007) 93–100. https://doi.org/10.1016/j.jhazmat.2006.09.083.

[77] N.K. Lazaridis, D.D. Asouhidou, Kinetics of sorptive removal of chromium(VI) from aqueous solutions by calcined Mg–Al–CO3 hydrotalcite, Water Res.. 37 (2003) 2875–2882. https://doi.org/10.1016/s0043-1354(03)00119-2.

[78] N. Khadhri, M. El Khames Saad, M. ben Mosbah, Y. Moussaoui, Batch and continuous column adsorption of indigo carmine onto activated carbon derived from date palm petiole, J. Environ. Chem. Eng. 7 (2019) 102775. https://doi.org/10.1016/j.jece.2018.11.020.

[79] Z. Harrache, M. Abbas, T. Aksil, M. Trari, Thermodynamic and kinetics studies on adsorption of Indigo Carmine from aqueous solution by activated carbon, Microchem. J. 144 (2019) 180–189. https://doi.org/10.1016/j.microc.2018.09.004.

[80] S.A.H. Azaman, A. Afandi, B.H. Hameed, A.T.M. Din, Removal of Malachite Green from Aqueous Phase Using Coconut Shell Activated Carbon: Adsorption, Desorption, and Reusability Studies, J. Appl. Sci. Eng. 21 (2018) 317–330. https://doi.org/10.6180/jase.201809_21(3).0003.

[81] Mu. Naushad, A.A. Alqadami, Z.A. AlOthman, I.H. Alsohaimi, M.S. Algamdi, A.M.

Aldawsari, Adsorption kinetics, isotherm and reusability studies for the removal of cationic dye from aqueous medium using arginine modified activated carbon, J. Mol. Liq. 293 (2019) 111442. https://doi.org/10.1016/j.molliq.2019.111442.

[82] S.N. Jain, S.R. Tamboli, D.S. Sutar, S.R. Jadhav, J.V. Marathe, A.A. Shaikh, A.A. Prajapati, Batch and continuous studies for adsorption of anionic dye onto waste tea residue: Kinetic, equilibrium, breakthrough and reusability studies, J. Clean. Prod. 252 (2020) 119778. https://doi.org/10.1016/j.jclepro.2019.119778.

[83] C. Ng, W.E. Marshall, R.M. Rao, R.R. Bansode, J.N. Losso, Activated carbon from pecan shell: process description and economic analysis, Ind. Crop. Prod. 17 (2003) 209–217. https://doi.org/10.1016/s0926-6690(03)00002-5.

[84] C.A. Toles, W.E. Marshall, M.M. Johns, L.H. Wartelle, A. McAloon, Acid-activated carbons from almond shells: physical, chemical and adsorptive properties and estimated cost of production, Bioresource Technol. 71 (2000) 87–92. https://doi.org/10.1016/S0960-8524(99)00029-2.

[85] F. Liu, Z. Xu, H. Wan, Y. Wan, S. Zheng, D. Zhu, Enhanced adsorption of humic acids on ordered mesoporous carbon compared with microporous activated carbon, Environ. Toxicol. Chem. 30 (2011) 793–800. https://doi.org/10.1002/etc.450.

FINAL CONSIDERATIONS AND PROSPECTIVE FOR THE FUTURE

The research aim of the dissertation was successfully achieved. It was possible to use the residue of the brewing industry, brewers' spent grains, in the generation of clean technologies, such as the production of steam and electrical energy through a cogeneration system using solid biomass in the direct combustion in a boiler, with a saving of approximately 85% in the total volume of fuels, which represents approximately 3.8 million dollars annually. In addition, to the synthesis of activated carbon using the residual ash from this burning process and the application of the adsorbent material in the treatment of the Indigo Carmine food effluent, this adsorbent material can be produced at a value of approximately 9.35 dollars per kilogram and used to treat around 5500 L of effluent.

The use of a waste for the production of clean technologies that will be used for the treatment of other wastes or incorporated in some way back into the production process, should be the "gold standard" adopted by the industries in their waste management and production-operating mode. This makes it possible to achieve a circular economy, a circular system that employ reuse, remanufacturing and recycling to create a closed-loop system, minimizing the use of resource inputs and the creation of waste, pollution and carbon emissions.

Thus, the idea is that this work will serve as a guide for future research to be carried out in the area of wastewater treatment and in the production of clean technologies using residual waste, which can be used effectively in industrial environments helping the production chain to become more sustainable and more environmentally responsible.